2014

Characterization of bacterial RND efflux systems via transcriptional regulator CmeR and outer membrane channels CusC and MtrE

Hsiang-Ting Lei
Iowa State University

Characterization of bacterial RND efflux systems via transcriptional regulator CmeR and outer membrane channels CusC and MtrE

by

Hsiang-Ting (Angela) Lei

A dissertation submitted to the graduate faculty

in partial fulfillment of the requirements for the degree of

DOCTOR OF PHILOSOPHY

Major: Chemistry

Program of Study Committee
Edward W. Yu, Major Professor
Emily A. Smith
Ning Fang
Arthur Winter
Drena L. Dobbs

Iowa State University

Ames, Iowa

2014

TABLE OF CONTENTS

ABSTRACT

The problem of bacterial resistance has been recently brought to light due to the extra medical expenses and deaths involved in infections by resistant strains. Although there have been improvements in developing antimicrobials, the basic understanding of the mechanisms conferring resistance to Gram-negative bacteria is still needed to combat complex drug resistance. Among bacterial defense mechanisms, the efflux of antimicrobials by multi-drug and metal ion membrane pumps is the major concern in this dissertation. Particularly, the resistance-nodulation-cell division (RND) family has shown the power of bypassing the periplasm when pumping toxins and enhancing the efficacy of substrate extrusion. Drug resistance is also mediated at the genetic level by local repressors such as the TetR protein family. CmeR, a member of the TetR family from *Campylobactor jejuni*, represses the expression of the RND efflux pump CmeABC by binding at the promoter region of the *cmeABC* operon. CmeR has the ability to accommodate large amphiphiles. The crystal structures of the CmeR-bile acid complexes are presented to show the details of the ligand-binding tunnel at the C-terminal. In this dissertation, two other RND efflux systems, Cus and Mtr, are discussed. The importance of the first cysteine residue on the outer membrane protein CusC has been demonstrated by the crystal structures. The structures of the Cys1-mutated CusC suggest a possible route of the channel formation on the outer membrane prior to the assembly of the Cus efflux system. The efficient extrusion of antimicrobials requires an open state of the outer membrane channel in the RND efflux system. Recently, the crystal structure of MtrE, an outer membrane channel of the Mtr system from *Neisseria gonorrhoeae,* has also been solved. Due to the relaxed coiled-coils of the α-helical domain, the crystal structure of MtrE is found at its open state. The structural analysis of MtrE gives insights of a native open state of an outer membrane channel. In comparison with other outer membrane channels with known crystal structures, the structure of MtrE agrees with the transition theory hypothesized by the structure of TolC, the outer membrane channel of the AcrAB-TolC efflux system. In depth, the findings regarding RND-type efflux pumps and their transcriptional regulators should elucidate the mechanisms mediating drug resistance in bacteria at the atomic level.

CHAPTER 1. GENERAL INTRODUCTION

Antimicrobial resistance has been the focus of public health ever since the emergence of new resistance mechanisms outpaced development of new antibiotics. The spread of infectious diseases was once slowed down by the invention of broad-spectrum antibiotics in the golden era from 1940-1960 [1]. Soon after, people started to notice the relapse of the illness from chronic infections [2]. The mechanisms that allow bacteria to survive after therapeutic treatment by antibiotics are still under investigation. Gastroenteritis and gonorrhea are two of the most common infectious diseases in the world [3]. The pathogenic bacteria that cause these diseases include *Campylobacter jejuni*, *Escherichia coli* and *Neisseria gonorrhoeae*. Like other bacteria, they have the ability to persist in the presence of toxins and antibiotics [4], [5].

In order to be effective, the drug must reach the bacterial cells and accumulate to raise the intracellular concentration [6]. The studies of *E. coli* minicells led to the discovery of a membrane protein conferring resistance to tetracycline [7]. This protein was later identified as an inner membrane transporter. Indeed, the resistant cells have demonstrated the induction of active efflux pumps in response to antibiotics [8], [9]. The efflux systems in the cell membranes counteract the diffusion of the drugs to reduce the concentration in the cytosol. Interestingly, the efflux pumps are not only observed in prokaryotic organisms, but also in eukaryotic plant and mammalian cells [10].

At present, bacterial efflux systems are extensively characterized and classified into five major superfamilies: resistance-nodulation-cell division (RND), major facilitator (MF), small multidrug resistance (SMR), ATP-binding cassette (ABC) and multidrug and toxic

compound extrusion (MATE) [11]. RND efflux systems are found in all kingdoms of life, but are mainly involved in conferring drug resistance to bacteria [12]. The topology of most RND transporters characteristically shows 12 transmembrane segments (TMs) and 2 large loops protruding into the periplasmic region between TM1, TM2 and TM7, TM8. The water-soluble loops reside in the periplasmic region and form the well-structured periplasmic subdomains [11]. Among the identified RND transporters, seven out of eight in *E. coli*, two out of four in *C. jejuni* and one out of two in *N. gonorrhoeae* mediate multidrug or metal ion efflux through the bacterial membrane [13]–[15]. The RND efflux system is essential to multidrug resistance by directly exporting antibiotics to the extracellular space. With experimental evidence, the expression of the RND efflux proteins synergistically affects intrinsic antibiotic resistance of Gram-negative bacteria with the outer membrane [9].

A RND efflux system contains three parts: inner membrane efflux pump (IMP), the periplasmic membrane fusion protein (MFP) and the outer membrane channel protein (OMP). The polypeptide ratio of the components in the tripartite complex has been demonstrated to be 3:6:3 for CzcCBA, TolC-AcrAB and CusCBA [16]–[19]. Crystal structures of three more RND transporters have been published since the first structure of the RND efflux pump AcrB was revealed [20]–[22]. In the previous phylogenetic analysis of bacterial genome based on the amino acid sequences, HAE (hydrophobe/amphiphilic efflux pumps) and HME (heavy-metal efflux pumps) are two major clusters [23]. It is shown that these two subfamilies are found in gram-negative bacteria [24]. As a trimer, inner membrane pumps utilize the proton motive force to transfer a broad range of substrates such as antimicrobials, detergents, small toxic molecules and metal ions. The IMPs have shown the ability to take up substrates from both the periplasmic and cytoplasmic space [16], [25], [26].

To analyze the efficacy of IMPs, fluorescence quenching, which utilizes the liposome-reconstituted IMPs, has been performed for AcrB, CzcA and CusA [20], [27], [28]. Different from the multidrug transporters, the metal ion efflux pumps usually have a narrow range of substrates. The substrate specificity of the pump depends on the binding site, which consists of diverse residues such as asparagine, aspartic acid, glutamic acid and methionine [29]. The monovalent and divalent metal ion binding sites possess different coordination geometry to adopt the selectivity with various sets of residues [30]. On the other hand, HAE pumps have flexible binding pockets that are mainly hydrophobic. The large ligands often require additional stabilization by a few polar or charged residues together with the hydrophobic interactions in the binding cavity [31]. The pioneer investigations on the membrane efflux protein AcrB led to the proposed mechanism of stepwise substrate extrusion. In the active export of its substrates, the AcrB protomer turns into the access state, the binding state and the extrusion state in a rotational sequence between three protomers [16], [32], [33].

MFPs are elongated polypeptides that interact with both inner membrane pumps and outer membrane proteins in the periplasmic space. To date, four MFPs (MexA, AcrA, CusB and ZneB) involved in RND efflux systems have been investigated and have had crystal structures described in detail [34]–[37]. Among the four, MexA and AcrA are parts of the HAE-RND efflux systems MexAB-OprM and AcrAB-TolC, respectively. CusB and ZneB belong to the HME-RND efflux systems CusCBA and ZneCAB. MexA and AcrA have 62% identity and structurally resemble each other with the same linear arrangement of secondary domains [35]. The sickle-curved MFP is comprised of a β-barrel domain at one end, a central globular domain and an adjacent α-helical hairpin domain [34], [35]. CusB consists of three β-strand globular domains and one α-helical domain distinctively formed from three α-

helices where other MFPs only have two α-helices at the tip [36]. Proteolytic digestions have been used to prove the conformational flexibility of the MFP. In the case of AcrA, only the stable core structure was retained after digestion by thermolysin [35], indicating that the peptide chain has a great proteinase accessibility and flexible regions. The nature of MFPs to present themselves as multimers in the asymmetric units implies the availability of collaborative activities that require interactions between molecules. The interaction between MFP and IMP has been elucidated through the recent publication of the crystal structure of the CusBA complex [19]. The involvement of the first two globular domains of CusB with the IMP CusA includes charge-charge and charge-dipole interactions. It is also found that the three-methionine binding site of CusB in the lower β-barrel domain is likely posed at the cleft between periplasmic subdomains PC1 and PC2 of CusA. The proximity of random coils of CusB to this cleft could be supportive to the proposed mechanism that MFPs assist IMPs in substrate extrusion [19][38]. The presence of the MFP in the RND efflux systems has been considered indispensable for the extrusion of substrates [39].

To complete the transenvelope transport, a RND efflux system must organize the readily formed IMP-MFP complex to cooperate with the OMP [40], [41]. So far, five different OMPs of RND efflux systems have been structurally characterized. Unlike the restricted combination of the IMP and MFP, the working partner of the OMP could be substitutable; for instance, in the RND efflux system AcrAB-TolC and the ATP binding cassette (ABC) transporter MacAB-TolC [8][42]. TolC, the efflux component of AcrAB-TolC system, was the first OMP structure elucidated. Similar to other later structures of OMPs, the TolC channel is comprised of three protomers [43]. The twisted homotrimer creates a pore on the outer membrane of gram-negative bacterial cells. Each protomer has

three major domains: the transmembrane β-barrel domain, the extending α-helical domain and the equatorial domain. With each protomer contributing four β-strands and four pseudocontinuous helices, the trimeric channel is able to become a gigantic cannon possessing an internal volume in the range of 25000-45000 $Å^3$ [43]–[46]. The importance of TolC has been demonstrated in previous studies in not only the antimicrobial efflux systems, but also the large polypeptide transport systems [47]. The incomplete exit of substrates due to the absence of the OMP leads to increased drug susceptibility [48]. The direct association of TolC with the MFP AcrA and the IMP AcrB has been used to propose the extrusion model in which the conformational change of the adaptor protein MFP opens the periplasmic channel and connects the inner membrane pump and outer membrane channel [28]. Besides the AcrAB-TolC system, other RND efflux systems such as MtrCDE and CusCBA have similar proposed extrusion mechanisms [8], [19], [49], [50]. It was pointed out that the collaboration between the channel protein and adaptor protein is transient [47]. The rapid and repeated recruitment of outer membrane channels is expected. Evidence pertinent to the recruiting process initiated by the adaptor protein has been mentioned in recent publications [49], [51]. Through analysis of residues near the end of the periplasmic helices, the transition from the closed to the open state of the OMPs is proposed to coincide with the shift of two helices from the inward position to the outward position [52]. The electrostatic potential of the interior surface of the channel is usually negative [53]. However, because of the short association between the OMP and the efflux system, it is difficult to use the charged surface to selectively react with various classes of substrates. Thus, the selectivity may depend on other factors such as the width of the opening or the residues near the tip of the α-helical domain in the periplasmic region.

Transcriptional regulator proteins can control the expression of efflux systems in response to the environment. A typical transcriptional regulator of drug efflux pumps has a ligand binding domain and a DNA-binding domain. For the TetR family, the biologically functional form is a dimer that contains a helix-turn-helix (HTH) DNA-binding motif in each protomer. The profile of the TetR family exemplified by alignment has shown conserved residues in the region of two helices α2 and α3 at the N-terminal [54], [55]. The genes encoding several local repressors such as AcrR, MtrR, MexR and CmeR are found near their designated downstream operons encoding RND efflux systems [56]–[59]. With an inducer bound to the ligand binding sites of the repressor protein, the conformational change introduced in the HTH DNA-binding motif loosens the regulator protein from the operator and allows the transcription of the efflux transporter. This derepression process contributes to the intrinsic drug resistance in bacterial cells by allowing the expression of the proteins that pump out drugs [54]. The crystal structures of the regulator proteins, describing the DNA recognition and the change of conformation upon binding with the ligands, can help us understand the intrinsic drug resistance of Gram-negative bacteria.

Thesis Organization

Chapter 1 is the general introduction that provides the background information of the RND efflux systems, which mediate the bacterial drug resistance, and their adaptive regulation by transcriptional regulators.

Chapter 2 is a manuscript published in *Protein Science*. In this chapter, the ability of CmeR, the repressor of the *cmeABC* operon, to bind large amphiphiles has been explained by the crystal structures of the CmeR-bile acid complexes. The comparison between different sets of residues interacting with the two large bile salts is described. The interactions between ligands and the protein in the crystal structures can give rise to the importance of the charged residues near the hydrophobic binding tunnel in the ligand-binding domain.

In Chapter 3, the formation of the mature outer membrane channel CusC is discussed as published in *Journal of Molecular Biology*. Through the guidance of the first cysteine in the protein sequence, CusC protein molecules are likely to anchor onto the inner leaflet of the outer membrane before the subsequent folding of transmembrane β-barrel domain. The proposed mechanism is based on the discovery of the immature intermediate structures of CusC mutants.

Chapter 4 is a manuscript accepted in *PLoS One*. The newly found crystal structure of the outer membrane channel MtrE is the only reported open state without any alteration of the protein sequence [52]. The hypothesis of transitioning from closed state to open state during the active export of substrates can be supported by the existence of the open state conformation found from the native MtrE. Additional analysis has been made on the trace of the charged residues at the inter- and intra-protomer grooves of the α-helical domain, essential for collaboration with other components in the efflux assembly.

Chapter 5 is the conclusion and future directions. In this chapter, all the findings are summarized and organized by the theme of understanding the mechanism of the RND efflux systems. The work in this dissertation contributes to the field of bacterial multidrug efflux through the elucidation of the crystal structures of the proteins that are essential to the fully functional RND efflux complexes.

Reference

[1] Butler, M. & Cooper, M. Antibiotics in the clinical pipeline in 2011. *J. Antibiot.* **64**, 413-25 (2011).

[2] Blanchard, J. S. Molecular Mechanisms Of Drug Resistance In Tuberculosis. *Annu. Rev. Biochem.* **65**, 215-39 (1996).

[3] Centers for Disease Control and Prevention, U. S. Department of Health and Human Services, "Antibiotic resistance threats." (2013).

[4] Andersson, D. I. & Hughes, D. Antibiotic resistance and its cost: is it possible to reverse resistance? *Nat. Rev. Microbiol.* **8**, 260-71 (2010).

[5] Deguchi, T., Nakane, K., Yasuda, M. & Maeda, S. Emergence and spread of drug resistant *Neisseria gonorrhoeae*. *J. Urol.* **184**, 851-858 (2010).

[6] Nikaido, H. & Pagès, J.-M. Broad-specificity efflux pumps and their role in multidrug resistance of Gram-negative bacteria. *FEMS Microbiol. Rev.* **36**, 340–363 (2012).

[7] Levy, S. B. Active Efflux Mechanisms for Antimicrobial Resistance. *Antimicrob. Agents Chemother.* **36**, 695-703 (1992).

[8] Zgurskaya, H. I. & Nikaido, H. Multidrug resistance mechanisms: drug efflux across two membranes. *Mol. Microbiol.* **37**, 219-225 (2000).

[9] Nikaido, H. Multidrug resistance in bacteria. *Annu. Rev. Biochem.* **78**, 119-146 (2009).

[10] Tseng, T. T., Gratwick, K. S., Kollman, J., Park, D., Nies, D. H., Goffeau, A. & Saier, M. H. The RND permease superfamily: an ancient, ubiquitous and diverse family that includes human disease and development proteins. *J. Mol. Microbiol. Biotechnol.* **1**, 107–25 (1999).

[11] Saier, M. H., Paulsen, I. T., Sliwinski, M. K., Pao, S. S., Skurray, R. A. & Nikaido, H. Evolutionary origins of multidrug and drug-specific efflux pumps in bacteria. *FASEB J.* **12**, 265-274 (1998).

[12] Paulsen, I. T., Brown, M. H. & Skurray, R. A. Proton-dependent multidrug efflux systems. *Microbiol. Rev.* **60**, 575–608 (1996).

[13] Routh, M. D., Su, C.-C., Zhang, Q. & Yu, E. W. Structures of AcrR and CmeR: insight into the mechanisms of transcriptional repression and multi-drug recognition in the TetR family of regulators. *Biochim. Biophys. Acta* **1794,** 844-851 (2009).

[14] Jerse, A. E., Sharma, N. D., Simms, A. N., Emily, T., Snyder, L. A., Shafer, W. M. & Crow, E. T. A Gonococcal Efflux Pump System Enhances Bacterial Survival in a Female Mouse Model of Genital Tract Infection. *Infect. Immun.* **71**, 5576-5582 (2003).

[15] Nishino, K. & Yamaguchi, A. Analysis of a Complete Library of Putative Drug Transporter Genes in *Escherichia coli*. *J. Bacteriol.* **183**, 5803-5812 (2001).

[16] Misra, R. & Bavro, V. N. Assembly and transport mechanism of tripartite drug efflux systems. *Biochim. Biophys. Acta* **1794**, 817-825 (2009).

[17] Rensing, C., Pribyl, T., Nies, D. H. New Functions for the Three Subunits of the CzcCBA Cation-Proton Antiporter. *J. Bacteriol.* **179**, 6871–6879 (1997).

[18] Stegmeier, J. F., Polleichtner, G., Brandes, N., Hotz, C. & Andersen, C. Importance of the adaptor (membrane fusion) protein hairpin domain for the functionality of multidrug efflux pumps. *Biochemistry* **45,** 10303-10312 (2006).

[19] Su, C.-C., Long, F., Zimmermann, M. T., Rajashankar, K. R., Jernigan, R. L. & Yu, E. W. Crystal structure of the CusBA heavy-metal efflux complex of *Escherichia coli*. *Nature* **470**, 558–562 (2011).

[20] Long, F., Su, C.-C., Zimmermann, M. T., Boyken, S. E., Rajashankar, K. R., Jernigan, R. L. & Yu, E. W. Crystal structures of the CusA efflux pump suggest methionine-mediated metal transport. *Nature* **467**, 484–488 (2010).

[21] Sennhauser, G., Bukowska, M. A., Briand, C. & Grütter, M. G. Crystal structure of the multidrug exporter MexB from *Pseudomonas aeruginosa*. *J. Mol. Biol.* **389**, 134-145 (2009).

[22] Pak, J. E., Ekendé, E. N., Kifle, E. G., O'Connell, J. D., De Angelis, F., Tessema, M. B., Derfoufi, K.-M., Robles-Colmenares, Y., Robbins, R. A., Goormaghtigh, E., Vandenbussche, G. & Stroud, R. M. Structures of intermediate transport states of ZneA, a Zn(II)/proton antiporter. *Proc. Natl. Acad. Sci. U. S. A.* **110**, 18484–18489 (2013).

[23] Meguro, N., Kodama, Y., Gallegos, M. & Watanabe, K. Molecular Characterization of Resistance-Nodulation-Division Transporters from Solvent- and Drug-Resistant Bacteria in Petroleum-Contaminated Soil. *Appl. Environ. Microbiol.* **71**, 580–586 (2005).

[24] Perrin, E., Fondi, M., Papaleo, M. C., Maida, I., Buroni, S., Pasca, M. R., Riccardi, G. & Fani, R. Exploring the HME and HAE1 efflux systems in the genus *Burkholderia*. *BMC Evol. Biol.* **10**, 164 (2010).

[25] Kim, E.-H., Nies, D. H., McEvoy, M. M. & Rensing, C. Switch or funnel: how RND-type transport systems control periplasmic metal homeostasis. *J. Bacteriol.* **193**, 2381–2387 (2011).

[26] Aires, J. R. & Nikaido, H. Aminoglycosides Are Captured from both Periplasm and Cytoplasm by the AcrD Multidrug Efflux Transporter of *Escherichia coli*. *J. Bacteriol.* **187**, 1923–1929 (2005).

[27] Goldberg, M., Pribyl, T., Juhnke, S. & Nies, D. H. Energetics and Topology of CzcA , a Cation / Proton Antiporter of the Resistance-Nodulation-Cell Division Protein Family. *J. Biol. Chem.* **274**, 26065–26070 (1999).

[28] Zgurskaya, H. I. & Nikaido, H. Bypassing the periplasm: reconstitution of the AcrAB multidrug efflux pump of *Escherichia coli*. *Proc. Natl. Acad. Sci. U. S. A.* **96**, 7190–7195 (1999).

[29] Nies, D. H. Efflux-mediated heavy metal resistance in prokaryotes. *FEMS Microbiol. Rev.* **27**, 313–339 (2003).

[30] Ma, Z., Jacobsen, F. E. & Giedroc, D. P. Coordination chemistry of bacterial metal transport and sensing. *Chem. Rev.* **109**, 4644–4681 (2009).

[31] Yu, E. W., Aires, J. R. & Nikaido, H. AcrB Multidrug Efflux Pump of *Escherichia coli* : Composite Substrate-Binding Cavity of Exceptional Flexibility Generates Its Extremely Wide Substrate Specificity. *J. Bacteriol.* **185**, 5657–5664 (2003).

[32] Seeger, M. A., Schiefner, A., Eicher, T., Verrey, F., Diederichs, K. & Pos, K. M. Structural asymmetry of AcrB trimer suggests a peristaltic pump mechanism. *Science* **313**, 1295–1298 (2006).

[33] Murakami, S. Multidrug efflux transporter, AcrB--the pumping mechanism. *Curr. Opin. Struct. Biol.* **18**, 459–65 (2008).

[34] Akama, H., Matsuura, T., Kashiwagi, S., Yoneyama, H., Narita, S.-I., Tsukihara, T., Nakagawa, A. & Nakae, T. Crystal structure of the membrane fusion protein, MexA, of the multidrug transporter in *Pseudomonas aeruginosa*. *J. Biol. Chem.* **279**, 25939–25942 (2004).

[35] Mikolosko, J., Bobyk, K., Zgurskaya, H. I. & Ghosh, P. Conformational flexibility in the multidrug efflux system protein AcrA. *Structure* **14**, 577–587 (2006).

[36] Su, C.-C., Yang, F., Long, F., Reyon, D., Routh, M. D., Kuo, D. W., Mokhtari, A. K., Van Ornam, J. D., Rabe, K. L., Hoy, J. A., Lee, Y. J., Rajashankar, K. R. & Yu, E. W. Crystal structure of the membrane fusion protein CusB from *Escherichia coli*. *J. Mol. Biol.* **393**, 342–355 (2009).

[37] De Angelis, F., Lee, J. K., O'Connell, J. D., Miercke, L. J. W., Verschueren, K. H., Srinivasan, V., Bauvois, C., Govaerts, C., Robbins, R. A., Ruysschaert, J.-M., Stroud, R. M. & Vandenbussche, G. Metal-induced conformational changes in ZneB suggest an active role of membrane fusion proteins in efflux resistance systems. *Proc. Natl. Acad. Sci. U. S. A.* **107**, 11038–11043 (2010).

[38] Gerken, H. & Misra, R. Genetic evidence for functional interactions between TolC and AcrA proteins of a major antibiotic efflux pump of Escherichia coli. *Mol. Microbiol.* **54**, 620–631 (2004).

[39] Ge, Q., Yamada, Y. & Zgurskaya, H. The C-terminal domain of AcrA is essential for the assembly and function of the multidrug efflux pump AcrAB-TolC. *J. Bacteriol.* **191**, 4365–4371 (2009).

[40] Stone, B. J. & Miller, V. L. *Salmonella enteritidis* has a homologue of *tolC* that is required for virulence in BALB/c mice. *Mol. Microbiol.* **17**, 701–712 (1995).

[41] Bina, J. E. & Mekalanos, J. J. *Vibrio cholerae tolC* Is Required for Bile Resistance and Colonization. *Infect. Immun.* **69,** 4681–4685 (2001).

[42] Xu, Y., Song, S., Moeller, A., Kim, N., Piao, S., Sim, S.-H., Kang, M., Yu, W., Cho, H.-S., Chang, I., Lee, K. & Ha, N.-C. Functional implications of an intermeshing cogwheel-like interaction between TolC and MacA in the action of macrolide-specific efflux pump MacAB-TolC. *J. Biol. Chem.* **286**, 13541–13549 (2011).

[43] Koronakis, V., Sharff, A., Koronakis, E., Luisi, B. & Hughes, C. Crystal structure of the bacterial membrane protein TolC central to multidrug efflux and protein export. *Nature* **405**, 914–919 (2000).

[44] Akama, H., Kanemaki, M., Yoshimura, M., Tsukihara, T., Kashiwagi, T., Yoneyama, H., Narita, S., Nakagawa, A. & Nakae, T. Crystal structure of the drug discharge outer membrane protein, OprM, of *Pseudomonas aeruginosa*. *J. Biol. Chem.* **279**, 52816–52819 (2004).

[45] Federici, L., Du, D., Walas, F., Matsumura, H., Fernandez-Recio, J., McKeegan, K. S., Borges-Walmsley, M. I., Luisi, B. F. & Walmsley, A. R. The crystal structure of the outer membrane protein VceC from the bacterial pathogen *Vibrio cholerae* at 1.8 Å resolution. *J. Biol. Chem.* **280**, 15307–15314 (2005).

[46] Kulathila, R., Kulathila, R., Indic, M. & van den Berg, B. Crystal structure of *Escherichia coli* CusC, the outer membrane component of a heavy metal efflux pump. *PLoS One* **6**, 15610 (2011).

[47] Thanabalu, T., Koronakis, E., Hughes, C. & Koronakis, V. Substrate-induced assembly of a contiguous channel for protein export from *E . coli* : reversible bridging of an inner-membrane translocase to an outer membrane exit pore. *The EMBO Journal* **17**, 6487–6496 (1998).

[48] Franke, S., Grass, G., Rensing, C. & Nies, D. H. Molecular Analysis of the Copper-Transporting Efflux System CusCFBA of *Escherichia coli*.," *J. Bacteriol.* **185**, 3804–3812 (2003).

[49] Janganan, T. K., Zhang, L., Bavro, V. N., Matak-Vinkovic, D., Barrera, N. P., Burton, M. F., Steel, P. G., V Robinson, C., Borges-Walmsley, M. I. & Walmsley, A. R. Opening of the outer membrane protein channel in tripartite efflux pumps is induced by interaction with the membrane fusion partner. *J. Biol. Chem.* **286**, 5484–5493 (2011).

[50] Janganan, T. K., Bavro, V. N., Zhang, L., Matak-Vinkovic, D., Barrera, N. P., Venien-Bryan, C., V Robinson, C., Borges-Walmsley, M. I. & Walmsley, A. R. Evidence for the assembly of a bacterial tripartite multidrug pump with a stoichiometry of 3:6:3. *J. Biol. Chem.* **286**, 26900–26912 (2011).

[51] Tikhonova, E. B., Yamada, Y. & Zgurskaya, H. I. Sequential mechanism of assembly of multidrug efflux pump AcrAB-TolC. *Chem. Biol.* **18**, 454–463 (2011).

[52] Andersen, C., Koronakis, E., Bokma, E., Eswaran, J., Humphreys, D., Hughes, C. & Koronakis, V. Transition to the open state of the TolC periplasmic tunnel entrance. *Proc. Natl. Acad. Sci. U. S. A.* **99**, 11103–11108 (2002).

[53] Pei, X., Hinchliffe, P., Symmons, M. F., Koronakis, E., Benz, R. & Hughes, C. Structures of sequential open states in a symmetrical opening transition of the TolC exit duct. *Proc. Natl. Acad. Sci. U. S. A.* **108,** 5–10 (2011).

[54] Ramos, J. L., Martı, M., Molina-henares, A. J., Tera, W., Brennan, R. & Tobes, R. The TetR Family of Transcriptional Repressors. *Microbiol. Mol. Biol. Rev.* **69**, 326–356 (2005).

[55] Pabo C. O. & Sauer, R. T. Transcription factors: structural families and principles of DNA recognition. *Annu. Rev. Biochem.* **61**, 1053–1095 (1992).

[56] Grkovic, S., Brown, M. H. & Skurray, R. A. Regulation of Bacterial Drug Export Systems. *Microbiol. Mol. Biol. Rev.* **66**, 671-701 (2002).

[57] Ma, D., Alberti, M., Lynch, C., Nikaido, H. & Hearst, J. E. The local repressor AcrR plays a modulating role in the regulation of *acrAB* genes of *Escherichia coli* by global stress signals. *Mol. Microbiol.* **19**, 101–112 (1996).

[58] Lucas, C. E., Balthazar, J. T. & Hagman, K. E. The MtrR repressor binds the DNA sequence between the *mtrR* and *mtrC* genes of *Neisseria*. *J. Bacteriol*. **179**, 4123-4128 (1997).

[59] Lin, J., Akiba, M., Sahin, O. & Zhang, Q. CmeR Functions as a Transcriptional Repressor for the Multidrug Efflux Pump CmeABC in *Campylobacter jejuni*. *Antimicrob. Agents Chemother*. **49**, 1067-1075 (2005).

CHAPTER 2. CRYSTAL STRUCTURES OF CMER-BILE ACID COMPLEXES FROM *CAMPYLOBACTER JEJUNI*

A paper published in Protein Science, 2011, Vol 20: 712-723

Hsiang-Ting Lei, Zhangqi Shen, Priyanka Surana, Mathew D. Routh, Chih-Chia Su, Qijing Zhang, and Edward W. Yu

Abstract

The TetR family of transcription regulators are diverse proteins capable of sensing and responding to various structurally dissimilar antimicrobial agents. Upon detecting these agents, the regulators allow transcription of an appropriate array of resistance markers to counteract the deleterious compounds. *Campylobacter jejuni* CmeR is a pleiotropic regulator of multiple proteins, including the membrane-bound multidrug efflux transporter CmeABC. CmeR represses the expression of CmeABC and is induced by bile acids, which are substrates of the CmeABC tripartite pump. The multiligand-binding pocket of CmeR has been shown to be very extensive and consists of several positively charged and multiple aromatic amino acids. Here we describe the crystal structures of CmeR in complexes with the bile acids, taurocholate and cholate. Taurocholate and cholate are structurally related, differing by only the anionic charged group. However, these two ligands bind distinctly in the binding tunnel. Taurocholate spans the novel bile acid binding site adjacent to and without overlapping with the previously determined glycerol-binding site. The anionic aminoethanesulfonate group of taurocholate is neutralized by a charge-dipole interaction. Unlike taurocholate, cholate binds in an anti-parallel orientation but occupies the same bile acid- binding site. Its anionic pentanoate moiety makes a water-mediated hydrogen bond

with a cationic residue to neutralize the formal negative charge. These structures underscore the promiscuity of the multifaceted binding pocket of CmeR. The capacity of CmeR to recognize bile acids was confirmed using isothermal titration calorimetry and fluorescence polarization. The results revealed that the regulator binds these acids with dissociation constants in the micromolar region.

Introduction

The ability of bacteria to adapt and respond to diverse classes of toxic compounds allows these organisms to survive in a variety of harsh environments. *Campylobacter jejuni*, the leading bacterial cause of food-borne enteritis in humans, is able to flourish in the intestinal mucosa due to its rapid response to bile acid intrusion.[1,2] This Gram-negative enteric pathogen has become increasingly resistant to common anti- bacterial agents encountered during the course of an infection. The intrinsic and acquired resistance to these diverse classes of toxic chemicals is facilitated through the expression of multidrug resistant (MDR) efflux transporters. The MDR pumps are capable of effectively lowering the intracellular concentration, thus compromising the effectiveness of the antibacterial compounds. Based on the genomic sequence of *C. jejuni* NCTC 11168, this organism harbors 13 putative MDR transporters that belong to five different classes, including the ATP-binding cassette (ABC) superfamily, the resistance-nodula- tion-division (RND) family, the multidrug and toxic compound extrusion (MATE) family, the major facilitator (MF) superfamily, and the small multidrug resistance (SMR) family.[3,4] Currently, only two RND efflux transporters, CmeABC and CmeDEF, in *C. jejuni* have been functionally characterized.[5–8]

Among these five different families of transporters, members of the RND superfamily exhibit the broadest range of substrate specificity and are usually the primary contributor to the intrinsic multi- drug resistance associated with Gram-negative organisms.[9,10] CmeB, a prototypical RND family transporter, is the major efflux transporter in *C. jejuni*. This inner membrane efflux pump functions as a tripartite protein complex along with a periplasmic membrane fusion protein, CmeA, and an outer membrane channel, CmeC, to extrude deleterious compounds from the bacterial cell.[6] The CmeABC complex recognizes and protects *C. jejuni* from a diverse set of antibacterial compounds, including commonly used antibiotics, metal ions, and lipophilic compounds.[2,6–8,11] In addition, CmeABC plays a major role in conferring resistance to bile acids, which are ubiquitously present in the intestinal tract.[2,12] It has been reported that mutant strains of *C. jejuni* lacking a functional CmeABC are unable to colonize in the intestinal tract of chickens.[2] The essential role of CmeABC for the growth of *C. jejuni* in the intestinal mucosa highlights the importance of this efflux complex to the pathogenicity of the bacterium.

The expression of CmeABC is controlled by the transcriptional regulator CmeR, whose open reading frame is located immediately upstream of the cmeABC operon and is transcribed divergently.[13] Transcription of the cmeR gene gives rise to a 210 amino acid protein, which shares N-terminal sequence and structural similarities to members of the TetR family.[14,15] CmeR is a two-domain protein with an N-terminal DNA-binding motif and a C-terminal multiligand-binding domain. Experimental evidence suggests that the 16 base pair palindromic inverted repeat (IR) sequence, 5’ TGTAATAAATATTACA 3’, located between cmeR and cmeABC is the operator site for CmeR binding and transcriptional repression.[13] Bile acids induce the expression of cmeABC by inhibiting the binding of CmeR to this

operator.[12]

The crystal structure of CmeR revealed that CmeR exhibits a unique secondary structural feature among all known structures of the TetR family of regulators.[16] To date, CmeR is the only regulator in the TetR family that lacks the N-terminal helix-turn-helix DNA-binding motif, in which the recognition helix α3 is replaced by a random coil.[16,17] Along with this unique characteristic, a large center-to-center distance (54 Å as measured by the separation between Cα atoms of Y51 and Y51' from the other subunit) was observed between the two N-termini of the dimer, making it incompatible with the distance between two consecutive major grooves of B-DNA. Each monomer of CmeR consists of nine helices, and numbered with helix α3 being skipped to facilitate comparisons to other members of the TetR family. As a result, the N-terminal domain of CmeR comprises helices α1 and α2 along with this random coil (Fig. 1). The larger C-terminal domain is composed of helices α4-α10, forming a very large hydrophobic tunnel for substrate binding. This tunnel is about 20 Å long with a volume of approximately 1000 $Å^3$, which is distinctly larger than the binding pockets of many other members of the TetR family. Surprisingly, a fortuitous glycerol molecule was found to bind in the binding tunnel of each monomer.[16] Residues F99, F103, F137, S138, Y139, V163, C166, T167, and K170 are responsible for forming this glycerol-binding site. The structure also suggests that CmeR binds glycerol in a manner of 1:1 monomer-to-ligand molar ratio. The volume of the ligand-binding tunnel of CmeR is large enough to accommodate a few of the ligand molecules. Additional water molecules fill the portion of the large tunnel that is unoccupied by ligand. Thus, CmeR might be able to bind more than one drug molecule at a time, or possibly accommodate a significantly larger ligand that spans across the entire binding tunnel. This tunnel, possibly consisting of multiple binding sites for

different ligands, is rich in aromatic residues and contains four positively charged amino acids (three histidines and one lysine). Based on the structural information and the fact that bile acids induce transcription of cmeABC, we hypothesize that CmeR may utilize these positively charged residues to recognize negatively charged ligands, like bile acids. To elucidate how CmeR recognizes these large anionic ligands, we here report the crystal structures of CmeR in complexes with taurocholate (Tch) and cholate (Chd), respectively.

Results

Crystals of the bile acid bound complexes belonged to the space group $P2_12_12$, with the asymmetric unit being occupied by one CmeR molecule. The symmetry operators were used to identify the dimeric state of CmeR (Fig. 1). These bile acids were found to bind within the ligand-binding tunnel and interact with the regulator using a surprisingly novel binding site. However, the overall conformation of the bile acid bound CmeR structures are very similar to that of the CmeR-glycerol structure.

Structure of the CmeR-Taurocholate complex. The crystal structure of the CmeR-Tch complex (Fig. 1) was refined to 2.20 Å resolution with a final R_{work} of 22.2% and R_{free} of 28.4% (Table I), revealing that Tch binds within the ligand-binding tunnel in a position adjacent to the previously identified glycerol-binding site. The Tch binding site utilizes a distinct set of amino acids to accommodate the elongated structure of the bile acid, while leaving the glycerol-binding site unoccupied. The simulated annealing electron density omit map of this bound Tch is illustrated in Figure 2.

The four-ring system of the bound Tch is completely buried in the CmeR binding

tunnel, leaving its negatively charged 2-aminoethanesulfonate group in the 5β position oriented at the entry point and exposed to the solvent. This four-ring skeleton, mimicking the steroid backbone, consists of three hydroxyl groups located at the 3α, 7α, and 12α positions. The CmeR-Tch structure demonstrates that the 3α-hydroxyl group in the A ring makes a hydrogen bond with the positively charged residue H72 (Fig. 3). The C ring and the 12α-hydroxyl group of Tch; however, face directly toward helix α8 and subunit interface of the dimer. This orientation facilitates the interaction between the 12α-hydroxyl oxygen and H175' of the next subunit of CmeR, allowing them to form a second hydrogen bond to anchor the bound Tch. Interestingly, the repressor protein further anchors this bound bile acid molecule through a water-mediated hydrogen bond between K170 of helix α8 and the 7α-hydroxyl group of the B ring to secure the binding.

Perhaps, the most striking feature for Tch binding is found at the other end of the molecule which harbors the anionic, conjugated ethanesulfonate tail. Tch is bound in such a way that the long 2-aminoethanesulfonate moiety at the 5β position is extended slightly out of the binding tunnel exposed to the solvent, while still in close enough proximity to interact with residues forming the entrance of the tunnel. Within 5 Å of this negatively charged sulfonate group, there are no positively charged histidines, lysines or arginines available to neutralize the formal negative charge of this sulfonate moiety. Instead, this conjugated acidic tail is engaged to interact with the side chain carbamoyl nitrogen of residue Q134, thus forming an additional hydrogen bond to anchor the bound Tch.

Surprisingly, the large molecule of Tch does not occupy the entire volume of the tunnel. The four-ring backbone and the 2-aminoethanesulfonate tail of the bound Tch are not linear in shape, but rather curve upward and result in a concave conformation. Thus, the end-

to-end length of the molecule is significantly shorter than it was expected and only reaches 16.1 Å. In doing so, CmeR is able to accommodate and create a novel bile acid-binding pocket for Tch. This new binding pocket is distinct from the previously determined glycerol-binding site. The bound Tch only spans this Tch-binding site and several solvent molecules are found in the glycerol-binding pocket. Thus, it is very likely that the large ligand-binding tunnel of CmeR could accommodate a bile acid and a glycerol molecule simultaneously. As the binding tunnel of CmeR is mostly hydrophobic in nature, the bound Tch is also found to make extensive hydrophobic contacts with residues forming the wall of this tunnel. It is observed that at least 10 hydrophobic amino acids, including four aromatic residues (F103, F111, W129 and F137), that line the inside wall of the tunnel are involved in Tch binding (Table II).

Structure of the CmeR-Cholate complex. The crystal structure of the CmeR-Chd complex was refined to a resolution of 2.35 Å, resulting in R_{work} and R_{free} of 20.0% and 26.3%, respectively (Table I). This structure revealed that the binding mode for Chd, which differs from Tch by its 5β-cholanoate group, is very distinct. Figure 4 illustrates the simulated annealing electron density omit map of this bound Chd. Surprisingly, the bound Chd was found to orient in an opposite direction when compared with Tch. Thus, the bound Chd and Tch are antiparallel to each other. For Chd binding, Chd is completely buried within the hydrophobic tunnel in a way that its non-conjugated 5β-cholanoate tail is inserted into the end of the tunnel, leaving its four-ring steroid backbone anchored closer to the entrance. In this manner, the anionic pentanoate moiety of Chd directly interacts with the positively charged H174 of helix α9 through a water-mediated hydrogen bond to anchor this bile acid

(Fig. 5). Unlike Tch, in which its anionic ethanesulfoate group is stabilized by charge-dipole interaction, the structure of CmeR-Chd suggests that the negatively charged end of Chd is neutralized by this positively charged histidine residue via a water-mediated hydrogen bond. Important interactions have been found to establish at the 3α, 7α and 12α-hydroxyl groups of the four-ring system. The 3α and 7α-hydroxyl groups contribute two hydrogen bonds with C166 and H175', respectively, to stabilize the steroid backbone. However, the 12α-hydroxyl moiety participates to form two water-mediated hydrogen bonds with C69 and K170 to further secure the binding. The bound Chd molecule is significantly curved upward and exhibits a boat-like conformation. As a result, the end-to-end length of the molecule is only 11.5 Å. The curved Chd also makes interactions with 11 additional amino acids, including five aromatic residues (F103, F111, W129, F137 and Y139) that create the wall of the tunnel (Table II).

Overall, Chd and Tch share the same ligand-binding pocket. These bile acids do not span the entire tunnel, but rather bend into a concave structure. In this conformation, these bile acids occupy a novel distinct binding site that is not overlapped with the previously determined glycerol-binding site (Figs. 3 and 5). Based on the structures of CmeR-bile acid complexes, it is observed that the glycerol-binding site in the tunnel remains unoccupied upon bile acid binding. Instead, several solvent molecules are found in this glycerol site. Thus, it is very likely that the large ligand-binding tunnel of CmeR could accommodate a bile acid and a glycerol molecule simultaneously. Tch and Chd are structurally related, differing only by the anionic charged group. Nonetheless, these two bile acids bind distinctly in the binding tunnel. These distinct binding modes indeed underscore the promiscuity of the multifaceted binding pocket of CmeR.

CmeR-bile acid interactions. The binding affinity of each bile acid for the CmeR regulator was determined using isothermal titration calorimetry (ITC), which obtained dissociation constants, K_Ds, of 1.5 ± 0.1 μM for Tch and 2.5 ± 0.1 μM for Chd. In each case, the titration is characterized by a negative enthalpic contribution, which gives rise to a hyperbolic binding curve (Fig. 6). As expected, the thermodynamic parameters of binding of each bile acid to CmeR are similar, with Tch and Chd displaying enthalpic (ΔH) contributions of −59 ± 1 kcal/mol and −44 ± 4 kcal/mol, respectively. Similar entropic contributions have also been found through these titrations, with ΔS(Tch) = 8 cal mol deg^{-1} and ΔS(Chd) = 10 cal mol deg^{-1}. The stoichiometries of bile acid binding observed with ITC ranged from 0.9 to 1.0 (bile acid/CmeR monomer).

Figure 7(a) illustrates the binding isotherm of CmeR in the presence cholyl-lysyl-fluorescein (Clf, a fluorescein-labeled bile acid) using fluorescence polarization (FP). As presented in the figure, a simple hyperbolic curve was observed for the binding of Clf with a dissociation constant, K_D, of 50.2 ± 0.4 μM. A Hill plot of the data yielded a Hill coefficient of 1.07 ± 0.03 [Fig. 7(b)], suggesting a simple drug binding process with a stoichiometry of one CmeR monomer per Clf ligand. These results indeed are in good agreement with the crystal structure that each monomer of CmeR binds one bile acid in the binding tunnel.

Discussion

With the rising incidences of MDR strains of bacteria, it has become increasingly important to understand how individual proteins are able to recognize such diverse substrates. The crystal structures of the QacR multidrug binding protein in complex with its

respective ligands have provided many insights into the mechanism of multidrug binding,[18,19] but these reports have primarily involved positively charged compounds. The CmeR-bile acid complexes reveal how a TetR family protein specifically interacts with negatively charged ligands. To this point, the crystal structure of MarR-salicylate has provided evidence on how regulatory proteins recognize anionic compounds.[20] The negatively charged salicylate binds to MarR within a solvent exposed crevice, rather than a large pocket, and interacts with arginines to neutralize its formal charge. The binding crevice lacks the familiar aromatic residues that are critically important in other multidrug binding proteins. It is intriguing that the multidrug binding protein TtgR seems to utilize a different mechanism to recognize negatively charged antibiotics and plant antimicrobials.[21] The hydrophobic environment is provided in the ligand binding pocket at the C-terminal regulatory domain. In addition, a positively charged histidine and a polar asparagine are also found to involve in the binding. For CmeR, this regulator seems to share a similar mechanism with TtgR to recognize negatively charged bile acids. Within the multifaceted binding tunnel there are at least seven aromatic residues, five phenylalanines, one tyrosine and one tryptophan, lining the hydrophobic surface to accommodate staking interactions with the ligands. In addition, cationic amino acids are observed to involve in bile acid binding. In fact, within the binding tunnel of CmeR, there are four positively charged residues, including H72, K170, H174 and H1750 (Table II). These residues, which underscore the diversity of the CmeR binding tunnel, probably function to neutralize charges and accommodate the binding of anionic and neutral ligands. This phenomenon is clearly demonstrated in the structures of CmeR-Tch and CmeR-Chd, in which the negatively charged ligands are secured in the binding tunnel by several of these cationic residues. Surprisingly, the two elongated bile acids did not bind in

the same orientation inside the tunnel of CmeR, but were actually bound antiparallel to each other. Chd was bound in an orientation where its A ring was located close to the tunnel opening. However, the bound Tch molecule displayed a contrasting orientation, whereby the corresponding A ring was buried deeply inside the far end of the tunnel. Because of the difference in orientation, the conserved four-ring systems of Tch and Chd were found to bind in different environments. Intriguingly, only two positively charged residues are found to commonly used in the binding of Tch and Chd. Residues K170 and H175' form important hydrogen bonds to secure the steroid backbones of Tch and Chd. In the case of Tch, CmeR further anchors the steroid backbone of this ligand by using the positively charged H72 residue to form an additional hydrogen bond with the 3α-hydroxyl group. For Chd binding, the regulator chooses H174 to neutralize the anionic charge of the non-conjugated 5β-cholanoate tail of Chd. Tch and Chd are related in chemical structure and have identical charge. Both of these two bile acids are bound by the regulator in the micromolar region. The different binding modes of these two bile acids indeed highlight the promiscuity of the multiligand-binding tunnel of CmeR.

Previously, the crystal structure of CmeR was fortuitously resolved in complex with a glycerol molecule.[16] This structure suggested that at least two distinct binding sites existed within the tunnel. Indeed, one of these predicted binding sites was occupied by the bound glycerol. Interestingly, the CmeR-bile acid structures indicated that the large molecules of Chd and Tch did not span both predicted binding sites, but instead took the distinct second site and left the glycerol-binding site unoccupied (Fig. 8). In comparison with the Tch, Chd and glycerol-bound structures, it was found that these three complexes displayed almost an identical structure (with the center-to-centre distance of 54 Å). To bind the operator DNA,

this center-to-center distance has to be less than 40 Å because the distance between two consecutive major grooves of B-DNA is 34 Å. Thus, these structures are incompatible with the 16 bp IR operator and should correspond to the induced form of the CmeR regulator. On the basis of these crystal structures, it is possible that CmeR can accommodate a bile acid and a glycerol molecule at the same time (Fig. 8). Such a phenomenon has been previously observed with the crystal structure of QacR simultaneously bound to two ligands, proflavin and ethidium,[19] and has been predicted through biochemical analysis to occur in many other proteins, including AcrR,[22,23] TtgV[24] and MdfA.[25] It has also been reported that the QacR repressor can bind a single ligand in multiple positions,[26] possibly due to the multifaceted nature of this protein. Thus, there is a chance that the same ligand could interact with these promiscuous multidrug regulators in different orientations within the multifaceted binding pockets.

The plasticity and promiscuity of the multiligand-binding tunnel of CmeR were further underscored by these CmeR-ligand complex structures. As mentioned previously, glycerol and bile acids have distinct binding sites within the tunnel. In the glycerol-bound structure, the bile acid binding site was unoccupied and filled with water molecules. This empty site was surrounded with several hydrophobic residues, including F111, I115, F137 and Y139. When Tch occupied this bile acid site, which was observed from the CmeR-Tch structure, some of these residues were found to significantly change in position. For example, residues I115, F137 and Y139, which form the wall of the binding tunnel, appeared to shift outward and seemingly participated to expand the internal volume of this binding site, probably accommodating the large size of the bile acid (Fig. 9). Interestingly, residue K170, which was found to form a hydrogen bond with the bound bile acid, reoriented its side chain to

accommodate the ligand. Additional movements were also seen through the side chains of H72 and F111. These residues appeared to adjust their orientation to facilitate Tch binding (Fig. 9). It is worth noting that the formal negative charge of Tch was not neutralized by positively charged residues. Instead, electrostatic neutralization was achieved by interaction between the anionic Tch and the positive dipole of the side chain of Q134. Thus, charge-charge electrostatic interaction is not essential for binding negatively charged ligands. Similar drug-regulator interaction has been found in QacR, in which the QacR regulator neutralized one end of the positively charged pentamidine by using carbonyl and side chain oxygen atoms.[27] Interestingly, the bound Chd rather employed another mechanism to neutralize its formal negative charge, whereas the anionic pentanoate group was compensated by the formal positive charge of H174.

In summary, the ability of CmeR to bind two very similar bile acids in quite distinct manners highlighted the plasticity and promiscuity of the ligand-binding tunnel of this regulator. This plasticity is very likely applicable to other multiligand binding proteins, including the AcrR multidrug regulator. Further, neutralization of the negatively charged bile acids can take place using the proximal positively charge residues or the nearby polar groups. The proximal and distinct bile acid and glycerol-binding sites of CmeR highlights the capacity of this regulator, whereby the sizeable hydrophobic tunnel indeed consists of multiple mini-pockets to accommodate diverse ligands.

Materials And Methods

Preparation and crystallization of the CmeR-ligand complexes. Recombinant CmeR containing a 6xHis tag at the N-terminus was overexpressed in Escherichia coli strain JM109

using the pQE30 vector. The cloning, expression and purification procedures have been described previously.[16,28] The purified protein was extensively dialyzed against buffer containing 10 mM Na-phosphate pH 7.2 and 100 mM NaCl and concentrated to 10-15 mg/mL. Prior to crystallization trials, Tch or Chd was added to the protein solution at a final concentration of 2 mM and then incubated overnight at 4°C. The stock solution of Tch was prepared by dissolving the sodium salt of Tch (Sigma-Aldrich) in a buffer containing 10 mM Na-phosphate pH 7.2. The Chd solution was made by solubilizing cholate acid (Sigma-Aldrich) in 500 mM NaOH. The resulting solution was then adjusted to a pH of 7.2 with 10 mM Na-phosphate.

Crystals of the 6xHis CmeR were crystallized at room temperature using hanging-drop vapor diffusion as described.[16] Briefly, a 4-µl drop containing equal volume of protein solution and reservoir buffer (30% PEG 3350, 0.1 M Tris-HCl pH 8.5 and 0.16 M $MgCl_2$) was equilibrated against 500 µl of reservoir buffer. Crystals of apo-CmeR appeared within two weeks with typical dimensions of 0.2 × 0.2 × 0.2 mm. The CmeR-Tch and CmeR-Chd complex crystals were then prepared by incubating crystals of apo-CmeR in solution containing 30% PEG 3350, 0.1 M Tris-HCl pH 8.5, 0.16 M $MgCl_2$, and 10 mM Tch or Chd for 24 h at 25°C.

X-ray data collection, processing, and structural refinement. X-ray intensity data were collected at 100 K using beamline-24IDC at the Advanced Photon Source. Crystals of CmeR-Tch and CmeR-Chd were cryoprotected with a solution containing 32% PEG 3350, 0.1 M Tris-HCl pH 8.5, 0.16 M $MgCl_2$ and 10 mM of the corresponding bile acid (Tch or Chd). Diffraction data sets were processed with DENZO and scaled with SCALEPACK.[29]

Both the CmeR-Tch and CmeR-Chd crystals took the space group of $P2_12_12$ with unit cell dimensions that were isomorphous to the previously determined CmeR-glycerol complex (Table I).

The structures of the CmeR-Tch and CmeR-Chd complexes were determined using the PHENIX suite of programs for crystallographic computing.[30] The initial phases were calculated by molecular replacement as implemented in Phaser[31] using the previously determined CmeR-glycerol structure (2QCO) with the bound glycerol and water molecules removed as the starting model. Based on the simulated annealing electron density omit maps, the molecule of the corresponding taurocholate (PDB: tch) or cholate (PDB: chd) was manually added into the binding tunnel. Model building was performed using the program Coot.[32] Refinement of both structures was carried out using CNS[33] and PHENIX.[30] The final model was verified by inspection of the simulated annealing composite omit maps. The 2Fo-Fc simulated annealing electron density omit maps of the bound Tch and Chd are shown in Figures 2 and 4. In the final models of both Tch and Chd bound structures, 100% of the residues are within either the most favored or additional allowed regions of the Ramachandran plot analysis, as defined by the program PROCHECK.[34]

Isothermal titration calorimetry. We used ITC to examine the binding of Tch or Chd to the purified CmeR regulator. Measurements were performed on a VP-Microcalorimeter (MicroCal, Northampton, MA) at 25°C. Before titration, the protein was thoroughly dialyzed against buffer containing 10 mM Na-phosphate pH 7.2 and 100 mM NaCl. The protein concentration was determined using the Bradford assay. The protein sample was then adjusted to a final concentration of 20 μM. Ligand solution consisting of 0.5 mM Tch or Chd

in 10 mM Na-phosphate pH 7.2 and 100 mM NaCl was prepared as the titrant. The protein and ligand samples were degassed before they were loaded into the cell and syringe. Binding experiments were carried out with the protein solution (1.5 mL) in the cell and the ligand as the injectant. Ten microliter injections of the ligand solution were used for data collection. Injections occurred at intervals of 300 s, and the duration time of each injection was 10 s. Heat transfer (μcal/s) was measured as a function of elapsed time (s). The mean enthalpies measured from injection of the ligand in the buffer were subtracted from raw titration data before data analysis with ORIGIN software (MicroCal). Titration curves were fitted by a nonlinear least squares method to a function for the binding of a ligand to a macromolecule. Nonlinear regression fitting to the binding isotherm provided us with the equilibrium binding constant ($K_A = 1/K_D$) and enthalpy of binding (ΔH). Based on the values of K_A, the change in free energy (ΔG) and entropy (ΔS) were calculated with the equation: $\Delta G = -RT \ln K_A = \Delta H - T\Delta S$, where T is 273K and R is 1.9872 cal/K per mol. Calorimetry trials were also carried out in the absence of CmeR in the same experimental conditions. No change in heat was observed in the injections throughout the experiment.

Fluorescence polarization. FP was used to determine the bile acid binding affinity of CmeR. As Tch and Chd are not fluorescent chemicals, we used Clf (BD Biosciences, San Jose, CA) as a fluorescent ligand to perform this binding assay. The experiment was done using a ligand binding solution containing 10 mM Na-phosphate (pH 7.2), 100 mM NaCl and 1 μM Clf. The protein solution consisting of CmeR in 10 mM Na-phosphate (pH 7.2), 100 mM NaCl and 1 μM Clf was titrated into the ligand binding solution until the polarization (P) was unchanged. As this is a steady-state approach, fluorescence polarization measurement

was taken after a 5 min incubation for each corresponding concentration of the protein and bile acid to ensure that the binding has reached equilibrium. All measurements were performed at 25°C using a PerkinElmer LS55 spectrofluorometer equipped with a Hamamatsu R928 photomultiplier. The excitation and emission wavelengths were 480 and 517 nm. Fluorescence polarization signal (in ΔP) was measured at the emission wavelength. Each titration point recorded was an average of 15 measurements. Data were analyzed using the equation, $P = \{(P_{bound} - P_{free})[protein]/(K_D + [protein])\} + P_{free}$, where P is the polarization measured at a given total protein concentration, P_{free} is the initial polarization of free ligand, P_{bound} is the maximum polarization of specifically bound ligand, and [protein] is the protein concentration. The titration experiments were repeated for three times to obtain the average K_D value. Curve fitting was accomplished using the program ORIGIN (OriginLab Corporation, Northampton, MA).

Accession Numbers. Coordinates and structural factors have been deposited in the Protein Data Bank with accession numbers 3HGY (CmeR-taurocholate) and 3HGG (CmeR-cholate).

Acknowledgments. This work is based upon research conducted at the Northeastern Collaborative Access Team beamlines of the Advanced Photon Source, supported by award RR-15301 from the National Center for Research Resources at the National Institutes of Health. Use of the Advanced Photon Source is supported by the U.S. Department of Energy, Office of Basic Energy Sciences, under Contract No. DE-AC02-06CH11357.

References

1. Friedman CR, Neimann J, Wegener HC, Tauxe RV, Epidemiology of *Campylobacter jejuni* infections in the United States and other industrialized nations. In: Nachamkin I, Blaser MJ, Ed. (2000) *Campylobacter*. Washington DC: ASM Press, pp 121–138.

2. Lin J, Sahin O, Michel L O, Zhang Q (2003) Critical role of multidrug efflux pump CmeABC in bile resistance and in vivo colonization of *Campylobacter jejuni*. *Infect Immun* 71:4250–4259.

3. Parkhill J, Wren BW, Mungall K, Ketley JM, Churcher C, Basham D, Chillingworth T, Davies RM, Feltwell T, Holrovd S, Jagels K, Karlvshev AV, Moule S, Pallen MJ, Penn CW, Quail MA, Raiandream MA, Rutherford KM, van Vliet AH, Whitehead S, Barrell BG (2000) The genome sequence of the food-borne pathogen *Campylobacter jejuni* reveals hypervariable sequences. *Nature* 403:665–668.

4. Lin J, Akiba M, Zhang Q, Multidrug efflux systems in *Campylobacter*. In: Ketley, JM, Konkel, ME, Ed. (2005) *Campylobacter*: *Molecular and Cell Biology*. Norfolk: Horizon Bioscience, pp 205–218.

5. Akiba M, Lin J, Barton YW, Zhang QJ (2006) Interaction of CmeABC and CmeDEF in conferring antimicrobial resistance and maintaining cell viability in *Campylobacter jejuni*. *J Antimicrob Chemother* 57:52–60.

6. Lin J, Michel LO, Zhang Q (2002) CmeABC functions as a multidrug efflux system in *Campylobacter jejuni*. *Antimicrob Agents Chemother* 46:2124–2131.

7. Pumbwe L, Piddock LJ (2002) Identification and molecular characterization of CmeB, a *Campylobacter jejuni* multi-drug efflux pump. *FEMS Microbiol Lett* 206:185–189.

8. Cagliero C, Mouline C, Payot S, Cloeckaert A (2005) Involvement of the CmeABC efflux pump in the macrolide resistance of *Campylobacter coli*. *J Antimicrob Chemother* 56:948–950.

9. Tseng TT, Gratwick KS, Kollman J, Park D, Nies, DH, Goffeau A, Saier, MH Jr (1999) The RND permease superfamily: an ancient, ubiquitous and diverse family that includes human disease and development proteins. *J Mol Microbiol Biotechnol* 1:107–125.

10. Schweizer HP (2003) Efflux as a mechanism of resistance to antimicrobials in *Pseudomonas aeruginosa* and related bacteria: unanswered questions. *Genet Mol Res* 2:48–62.

11. Luo N, Sahin O, Lin J, Michel LO, Zhang Q (2003) In vivo selection of *Campylobacter* isolates with high levels of fluoroquinolone resistance associated with gyrA mutations and the function of the CmeABC efflux pump. *Antimicrob Agents Chemother* 47:390–394.

12. Lin J, Cagliero C, Guo B, Barton YW, Maurel MC, Payot S, Zhang Q (2005) Bile salts modulate expression of the CmeABC multidrug efflux pump in *Campylobacter jejuni. J Bacteriol* 187:7417–7424.

13. Lin J, Akiba M, Sahin O, Zhang Q (2005) CmeR functions as a transcriptional repressor for the multidrug efflux pump CmeABC in *Campylobacter jejuni*. *Antimicrob Agents Chemother* 49:1067–1075.

14. Grkovic S, Brown MH, Skurray RA (2002) Regulation of bacterial drug export systems. *Microbiol Mol Biol Rev* 66:671–701.

15. Ramos JL, Martinez-Bueno M, Molina-Henares AJ, Teran W, Watanabe K, Zhang XD, Gallegos MT, Brennan R, Tobes R (2005) The TetR family of transcriptional repressors. *Microbiol Mol Biol Rev* 69:326–356.

16. Gu R, Su C-C, Shi F, Li M, McDermott G, Zhang Q, Yu EW (2007) Crystal Structure of the transcriptional regulator CmeR from *Campylobacter jejuni. J Mol Biol* 372:583–593.

17. Routh MD, Su C-C, Zhang Q, Yu EW (2009) Structures of CmeR and AcrR: insight into the mechanisms of transcriptional repression and multi-drug recognition in the TetR family of regulators. *Biochim Biophys Acta* 1794:844–851.

18. Schumacher MA, Miller MC, Brennan RG (2001) Structural mechanisms of QacR induction and multidrug recognition. *Science* 294:2158–2163.

19. Schumacher MA, Miller MC, Brennan RG (2004) Structural mechanism of the simultaneous binding of two drugs to a multidrug-binding protein. *EMBO J* 23: 2923–2930.

20. Alekshun MN, Levy SB, Mealy TR, Seaton BA, Head JS (2001) The crystal structure of MarR, a regulator of multiple antibiotic resistance, at 2.3 Å resolution. *Nature Struct Biol* 8:710–714.

21. Alguel Y, Meng C, Tera´n W, Krell T, Ramos JL, Galle- gos M-T, Zhang X (2007)

Crystal structures of multi- drug binding protein TtgR in complex with antibiotics and plant antimicrobials. *J Mol Biol* 369:829–840.

22. Su C-C, Rutherford DJ, Yu EW (2007) Characterization of the multidrug efflux regulator AcrR from *Escherichia coli*. *Biochem Biophys Res Commun* 361:85–90.

23. Li M, Gu R, Su C-C, Routh MD, Harris KC, Jewell ES, McDermott G, Yu EW (2007) Crystal structure of the transcriptional regulator AcrR from *Escherichia coli*. *J Mol Biol* 374:591–603.

24. Guazzaroni M-E, Krell T, Felipe A, Ruiz R, Meng C, Zhang X, Gallegos M-T, Ramos JL (2005) The multidrug efflux regulator TtgV recognizes a wide range of structurally different effectors in solution and complexed with target DNA. *J Biol Chem* 280:20887–20893.

25. Lewinson O, Bibi E (2001) Evidence for simultaneous binding of dissimilar substrates by the *Escherichia coli* mulitdrug transporter MdfA. *Biochemistry* 40: 12612–12618.

26. Brooks BE, Piro KM, Brennan RG (2007) Multidrug- binding transcription factor QacR binds the bivalent aromatic diamidines DB75 and DB359 in multiple positions. *J Am Chem Soc* 129:8389–8395.

27. Murray DS, Schumacher MA, Brennan RG (2004) Crystal structures of QacR-diamidine complexes reveal additional multidrug-binding modes and a novel mechanism, of drug charge neutralization. *J Biol Chem* 279: 14365–14371.

28. Su C-C, Shi F, Gu R, Li M, McDermott G, Yu EW, Zhang Q (2007) Preliminary structural studies of the transcriptional regulator CmeR from *Camplobacter jejuni*. *Acta Crystallog F* 63:34–36.

29. Otwinowski Z, Minor M (1997) Processing of X-ray diffraction data collected in oscillation mode. *Methods Enzymol* 276:307–326.

30. Afonine PV, Grosse-Kunstleve RW, Adams PD (2005) The Phenix refinement framework. *CCP4 Newsletter* 42: Contribution 8.

31. McCoy AJ, Grosse-Kunstleve RW, Adams PD, Winn MD, Storoni LC, Read RJ (2007) Phaser crystallographic software. *J Appl Crystallog* 40:658–674.

32. Emsley P, Cowtan K (2004) Coot: Model-building tools for molecular graphics. *Acta Crystallog D* 60:2126–2132.

33. Bru¨nger AT, Adams PD, Clore GM, DeLano WL, Gros P, Grosse-Kunstleve RW, Jiang JS, Kuszewski J, Nilges M, Pannu NS, Read RJ, Rice LM, Simonson T, Warren GL (1998) Crystallography & NMR system: a new software suite for macromolecular structure determination. *Acta Crystallog D* 54:905–921.

34. Laskowski RA, MacArthur MW, Moss DS, Thornton JM (1993) PROCHECK: a program to check the stereochemical quality of protein structures. *J Appl Crystallog* 26:283–291.

Figures And Captions

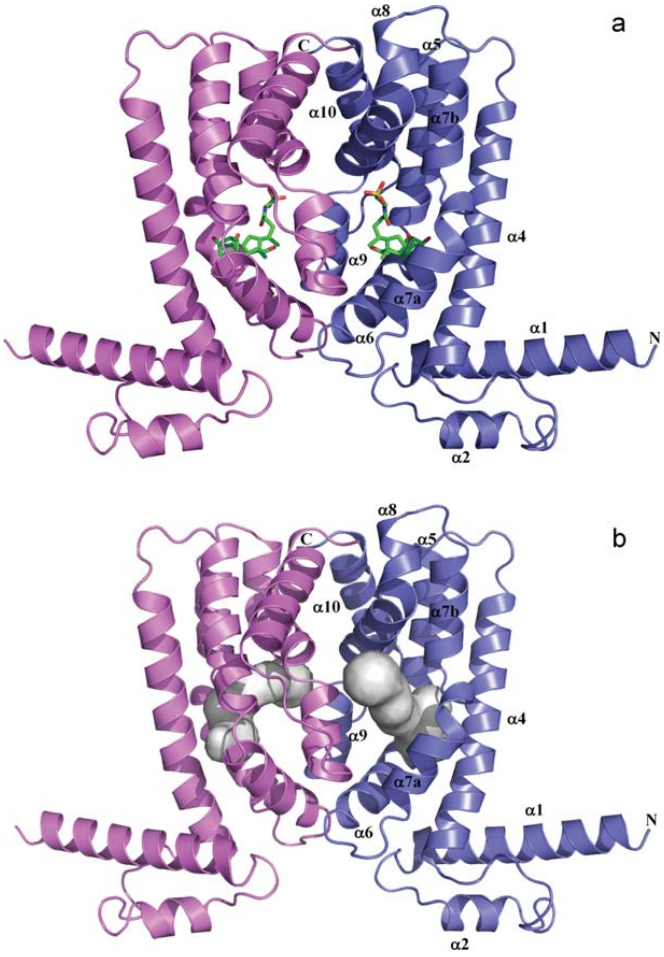

Figure 1. Structure of a CmeR-ligand complex. (a) Ribbon diagram of the taurocholate-bound CmeR homodimer generated by crystallographic symmetry. The taurocholate is shown as a stick model (green, carbon; blue, nitrogen; red, oxygen). (b) The hydrophobic binding tunnel of CmeR. This tunnel was calculated using the program CAVER (http://www.caver.cz), utilizing the position of residue A108 as a starting point. The binding tunnel on each subunit of CmeR is colored gray.

Table I. *Crystallographic Data and Refinement Statistics*

	CmeR-Tch	CmeR-Chd
A. Data collection		
Wavelength (Å)	0.9792	0.9792
Space group	$P2_12_12$	$P2_12_12$
Cell constants (Å)	$a = 94.0$, $b = 37.8$, $c = 57.6$	$a = 94.0$, $b = 37.4$, $c = 57.8$
Resolution (Å)	2.20 (2.28-2.20)	2.35 (2.43-2.35)
Completeness (%)	99.8 (99.2)	98.4 (99.2)
Total no. of reflections	227,441	286,493
No. of Unique reflections	11,011	8,984
Redundancy	4.7	3.2
R_{merge} (%)[a]	4.5 (22.5)	6.3 (42.1)
$\langle I/\sigma(I)\rangle$	36.4 (5.0)	17.9 (2.1)
B. Refinement		
R_{work} (%)	22.2	20.0
R_{free} (%)	28.4	26.3
⟨B⟩		
Overall (Å^2)	45.6	43.6
Protein (Å^2)	45.0	43.1
Ligand (Å^2)	73.1	57.8
Water (Å^2)	43.9	40.9
No. of ligands	1	1
No. of waters	54	60
Rms deviations		
Bond angles (°)	1.0	1.3
Bond length (Å)	0.006	0.009
Ramachandran analysis		
Most favored regions (%)	93.5	93.0
Allowed regions (%)	6.5	7.0
Generously allowed regions (%)	0.0	0.0
Disallowed regions (%)	0.0	0.0

$R_{\text{merge}} = \frac{\sum_{hkl}\sum_j |I_{hkl,j} - \langle I_{hkl}\rangle|}{\sum_{hkl}\sum_j I_{hkl,j}}$, where $I_{hkl,j}$ is the jth intensity measurement of reflection hkl and $\langle I_{hkl}\rangle$ is the average intensity from multiple observation.

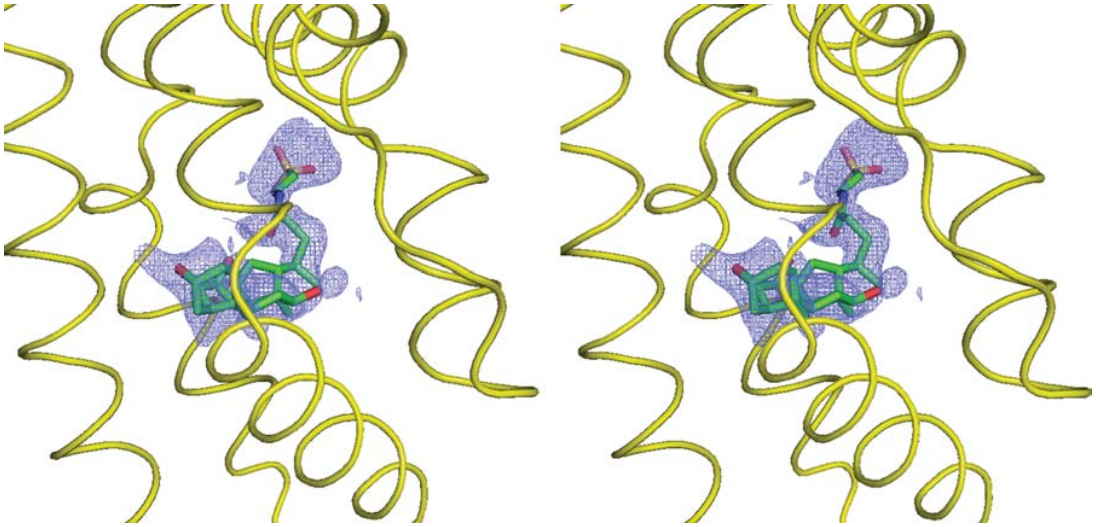

Figure 2. Stereo view of the simulated annealing electron density map of the bound taurocholate. The bound taurocholate in the left subunit of dimeric CmeR (the orientation corresponds to Fig. 1) is shown as a stick model (green, carbon; blue, nitrogen; red, oxygen). The 2Fo-Fc simulated annealing omit map is contoured at 1.2 σ (blue mesh). The electron density for the surrounding protein has been deleted. The surrounding secondary structural elements are shown as yellow ribbons.

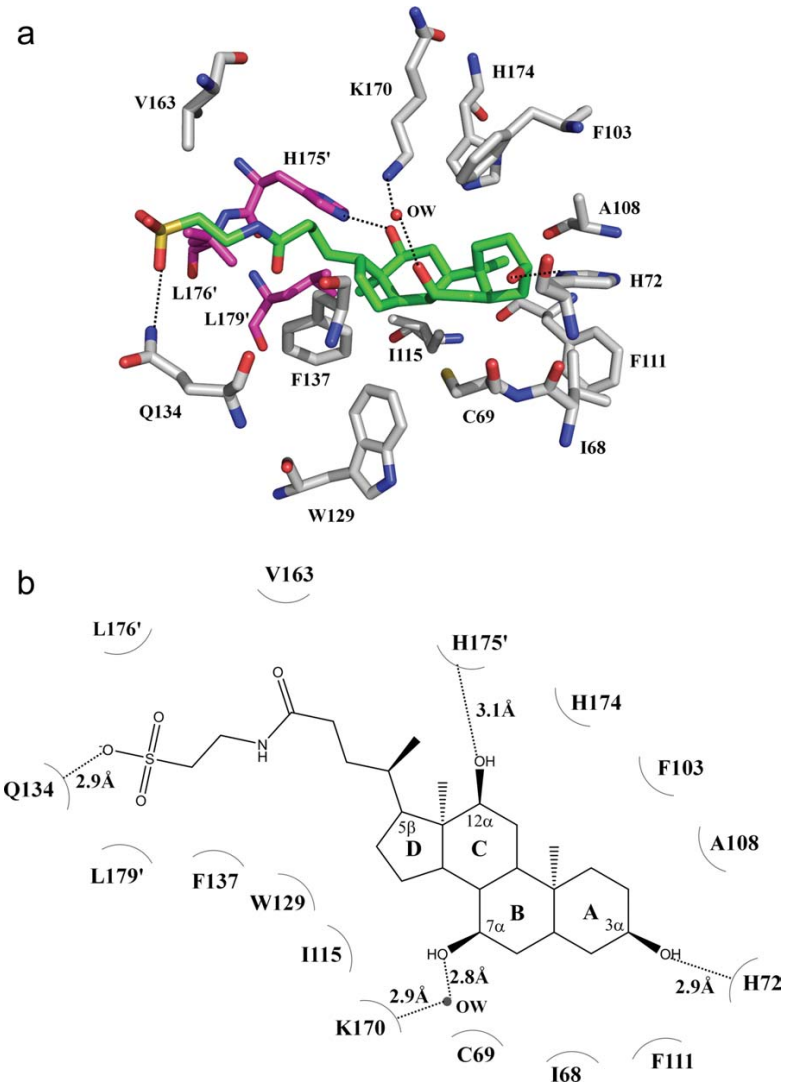

Figure 3. The taurocholate binding site. (a) Amino acid residues within 4.2 Å from the bound taurocholate (green, carbon; blue, nitrogen; red, oxygen; orange, sulfur). The side chains of selected residues are shown as gray sticks (gray, carbon; blue, nitrogen; red, oxygen). Residues from the next subunit of CmeR are shown as magenta sticks (magenta, carbon; blue, nitrogen; red, oxygen). A water molecule (OW) hydrogen-bonded with the bound taurocholate is shown as red sphere. (b) Schematic representation of the CmeR and taurocholate interactions shown in panel a. Dotted lines depict the hydrogen bonds. The hydrogen-bonded distances are also indicated in this figure.

Table II. *CmeR-ligand Contacts Contacts Within 4.2 Å of Any Ligands are Listed*

	Distance (Å)		
CmeR residues	Taurocholate	Cholate	Glycerol
L65		3.5	
I68	4.1		
C69	4.0		
H72	2.9		
F99			3.7
F103	3.2	3.7	3.4
A108	3.5	3.0	
F111	4.1	3.9	
G112		3.4	
I115	4.0	4.0	
W129	3.6	3.3	
Q134	2.9		
F137	4.0	3.6	3.8
S138			3.1
Y139		4.0	3.3
C166		2.9	4.0
V163	3.8		
K170			4.2
H174	4.0		
P172′		3.8	
H175′	3.1	3.0	
L176′	4.0		
L179′	4.0	4.2	
V163···OW/OW···Gol			3.0/2.9
T167···OW/OW···Gol			3.2/2.9
C69···OW/OW···Tch/Chd		3.0/2.9	
K170···OW/OW···Tch/Chd	2.9/2.8	2.9/3.1	
H174···OW/OW···Tch/Chd		2.7/3.0	

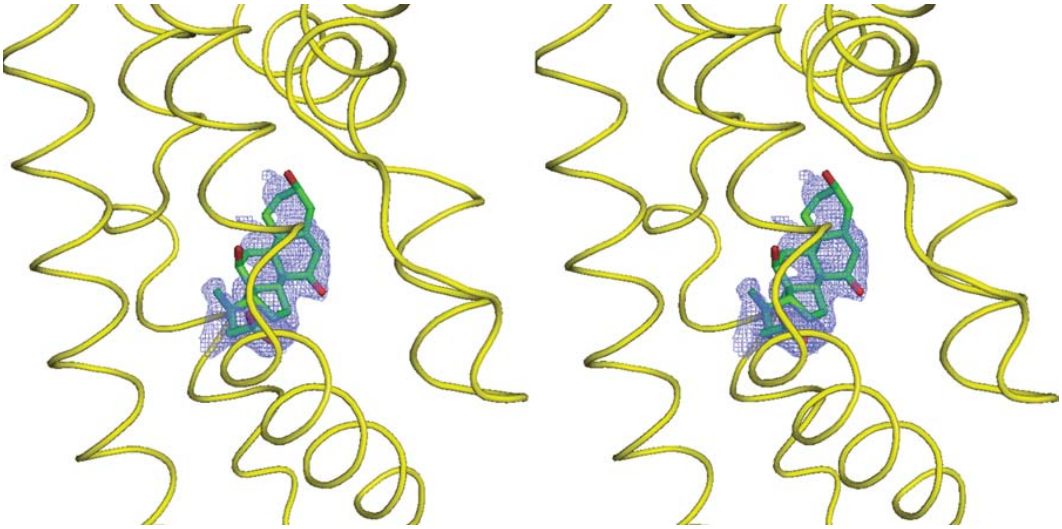

Figure 4. Stereo view of the simulated annealing electron density map of the bound cholate. The bound cholate in the left subunit of dimeric CmeR (the orientation corresponds to Fig. 1) is shown as a stick model (green, carbon; blue, nitrogen; red, oxygen). The 2Fo-Fc simulated annealing omit map is contoured at 1.2 σ (blue mesh). The electron density for the surrounding protein has been deleted. The surrounding secondary structural elements are shown as yellow ribbons.

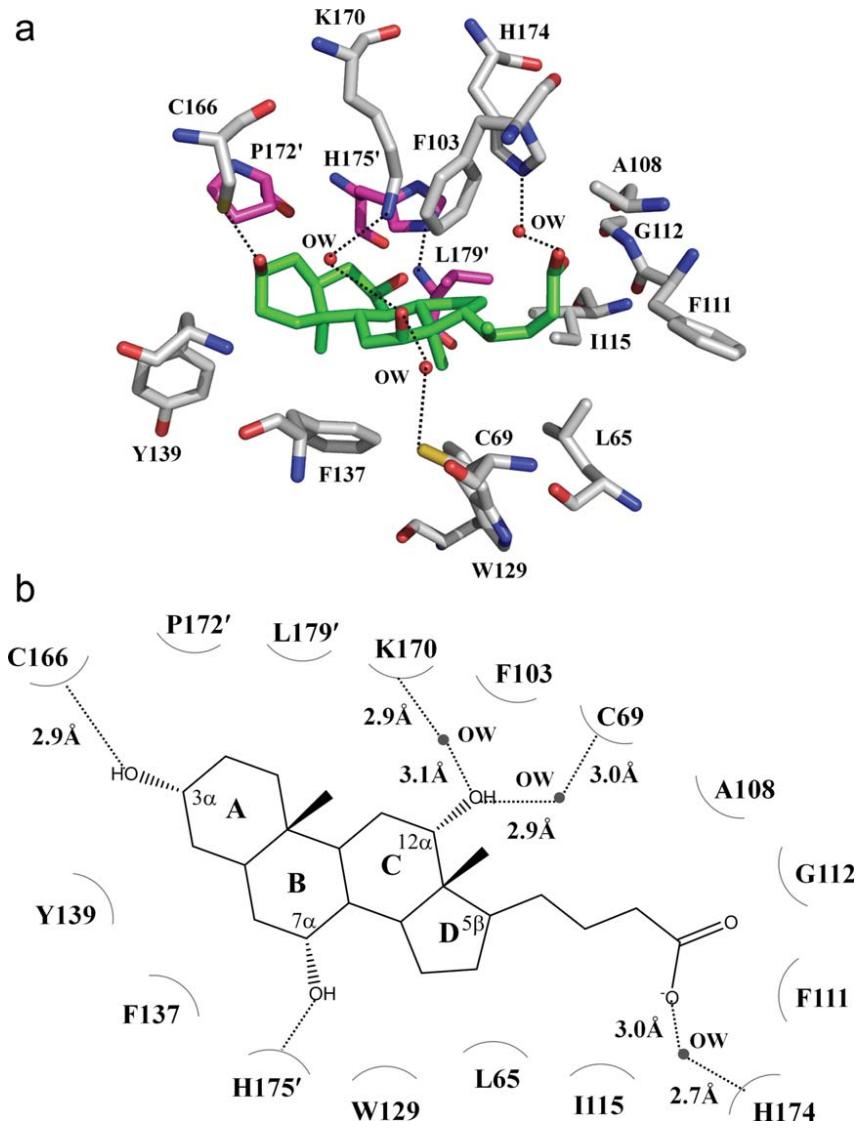

Figure 5. The cholate binding site. (a) Amino acid residues within 4.2 Å from the bound cholate (green, carbon; blue, nitrogen; red, oxygen). The side chains of selected residues are shown as gray sticks (gray, carbon; blue, nitrogen; red, oxygen). Residues from the next subunit of CmeR are shown as magenta sticks (magenta, carbon; blue, nitrogen; red, oxygen). (b) Schematic representation of the CmeR and cholate interactions shown in panel a. Dotted lines depict the hydrogen bonds. The hydrogen-bonded distances are also indicated in this figure.

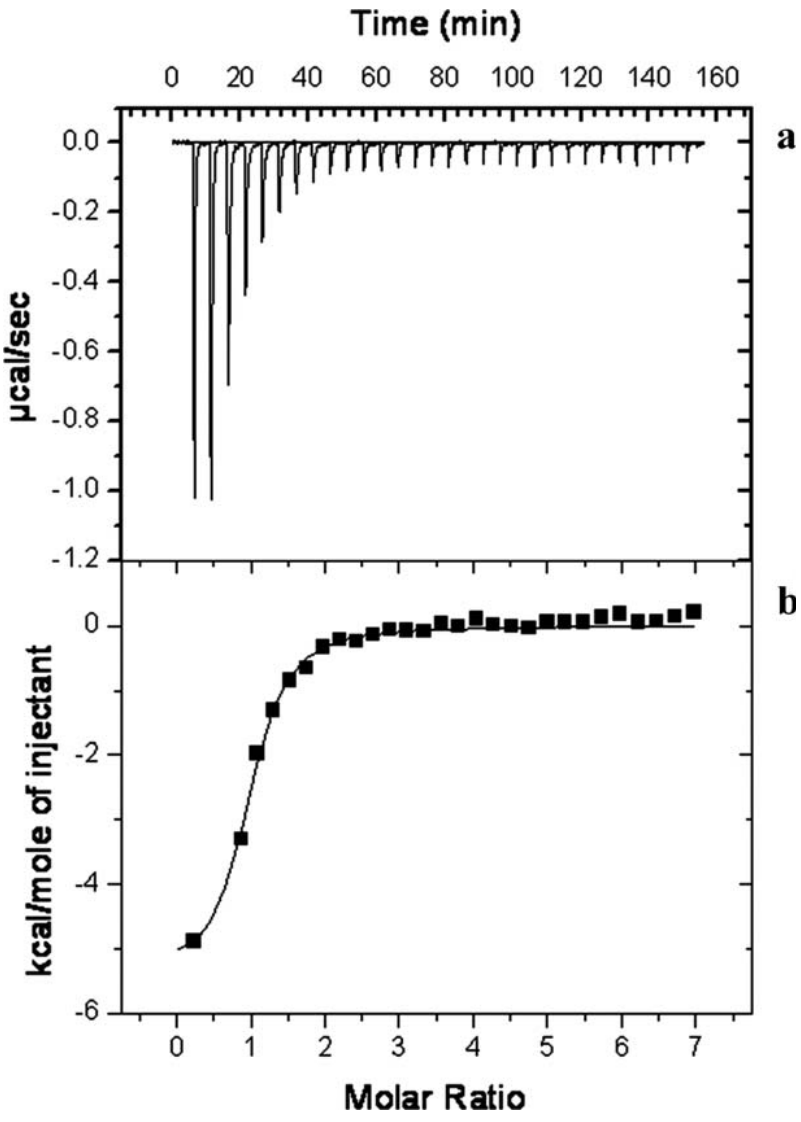

Figure 6. Representative isothermal titration calorimetry for the binding of taurocholate to CmeR. (a) Each peak corresponds to the injection of 10 µL of 0.5 mM Tch in buffer containing 10 mM Na-phosphate (pH 7.2) and 100 mM NaCl into the reaction containing 20 µM CmeR in the same buffer. (b) Cumulative heat of reaction is displayed as a function of the injection number. The solid line is the least-square fit to the experimental data, giving a KD of 1.5 ± 0.1 µM.

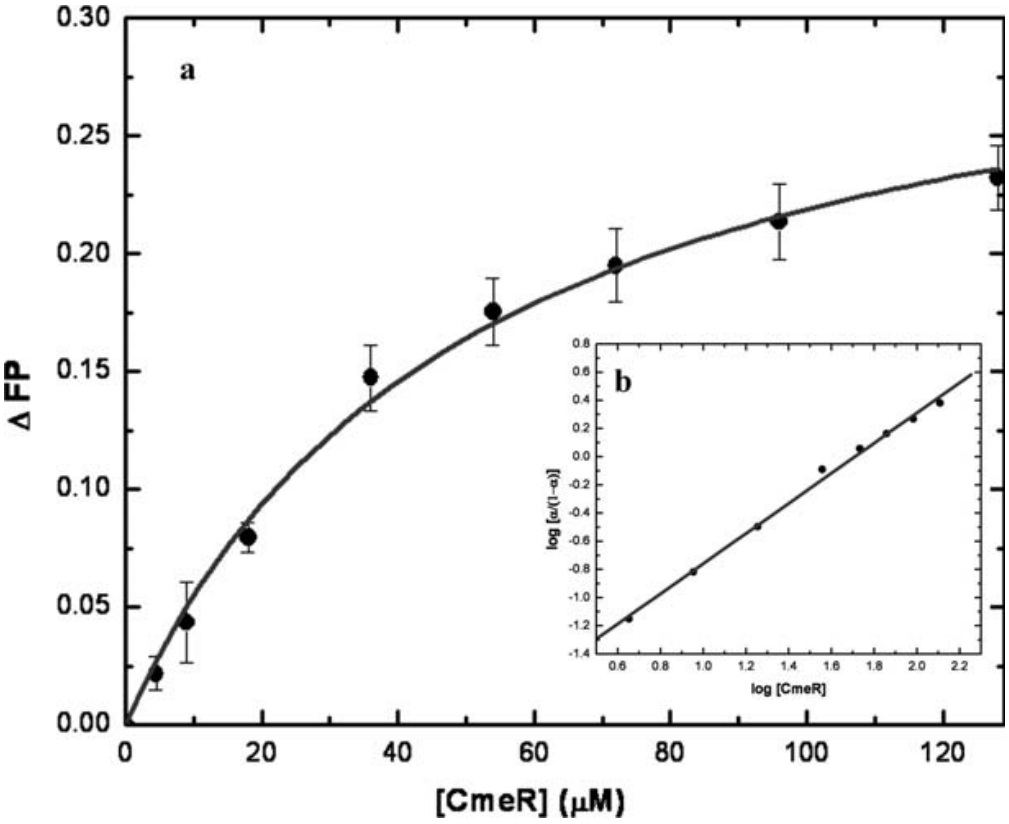

Figure 7. Fluorescence polarization of CmeR with cholyl-lysyl-fluorescein. (a) Binding isotherm of CmeR with cholyl-lysyl-fluorescein, showing a K_D of 50.2 ± 0.4 μM, in buffer containing 10 mM Na-phosphate (pH 7.2) and 100 mM NaCl. (b) Hill plot of the data obtained for cholyl-lysyl-fluorescein binding to CmeR. a corresponds to the fraction of bound cholyl-lysyl-fluorescein. The plot gives a slope of 1.07 ± 0.03, indicating a simple binding process with no cooperativity. The interception of the plot provides a K_D of 51.1 ± 7.7 μM for the cholyl-lysyl-fluorescein binding.

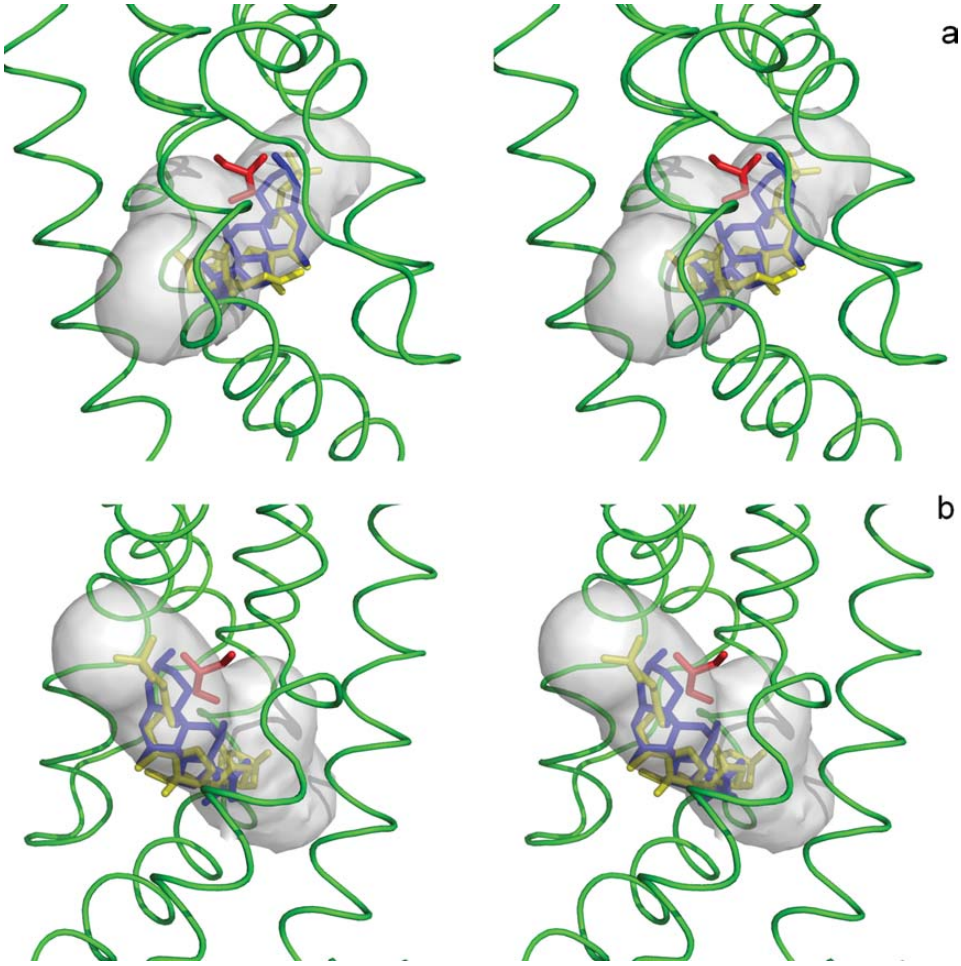

Figure 8. Stereo view of the bile acid and glycerol-binding sites of CmeR. This is a composite figure showing the locations of the bound ligands in the ligand binding tunnel of the (a) left and (b) right subunits of the CmeR dimer. The ligands shown in stick models are taurocholate (yellow), cholate (blue) and glycerol (red). The hydrophobic binding tunnel is colored gray. The surrounding secondary structural elements, based on the structure of the CmeR-glycerol complex, are shown as green ribbons.

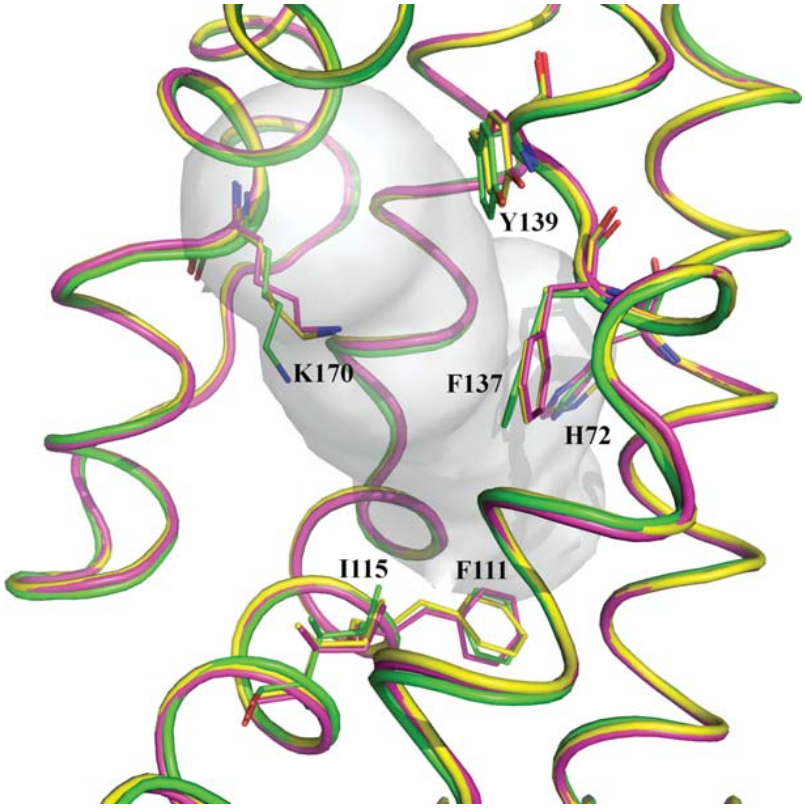

Figure 9. The change in conformation of the binding residues. This is a composite figure showing the conformational change of the side chains H72, F111, I115, F137, Y139, and K170 to accommodate ligand binding. The structural elements of CmeR-glycerol, CmeR-Tch and CmeR-Chd are colored green, yellow and pink, respectively.

CHAPTER 3. CRYSTAL STRUCTURES OF CUSC REVIEW CONFORMATIONAL CHANGES ACCOMPANYING FOLDING AND TRANSMEMBRANE CHANNEL FORMATION

A paper published in Journal of Molecular Biology, 2014, 426, 403–411

Hsiang-Ting Lei, Jani Reddy Bolla, Nicholas R. Bishop, Chih-Chia Su and Edward W. Yu

Abstract

Gram-negative bacteria, such as *Escherichia coli*, frequently utilize tripartite efflux complexes in the RND (resistance–nodulation–cell division) family to expel diverse toxic compounds from the cell. These complexes span both the inner and outer membranes of the bacterium via an α-helical, inner membrane transporter; a periplasmic membrane fusion protein; and a β-barrel, outer membrane channel. One such efflux system, CusCBA, is responsible for extruding biocidal Cu(I) and Ag(I) ions. To remove these toxic ions, the CusC outer membrane channel must form a β-barrel structural domain, which creates a pore and spans the entire outer membrane. We here report the crystal structures of wild-type CusC, as well as two CusC mutants, suggesting that the first N-terminal cysteine residue plays an important role in protein–membrane interactions and is critical for the insertion of this channel protein into the outer membrane. These structures provide insight into the mechanisms on CusC folding and transmembrane channel formation. It is found that the interactions between CusC and membrane may be crucial for controlling the opening and closing of this β-barrel, outer membrane channel.

Introduction

Integral membrane proteins are very hydrophobic and cannot be dissolved in aqueous solution. These proteins can be divided into two distinct structural classes: α-helical bundles and β-barrels. The β-barrel membrane proteins are often found in the outer membranes of Gram-negative bacteria and mitochon- dria, whereas the α-helical membrane proteins are commonly located in the inner membranes of bacteria and in plasma membranes. Approximately, one-third of all proteomes accounted for are embedded in biological membranes [1].

Efflux pumps of the RND (resistance–nodulation– cell division) superfamily are ubiquitous in bacteria, archaea and eukaryotes. In Gram-negative bacteria, these RND pumps play major roles in the intrinsic and acquired tolerance of antibiotics and toxic compounds [2,3]. They are the key components utilized by Gram-negative pathogens in overcoming toxic environments that are otherwise unfavorable for their survival. An RND-type efflux pump [4–11] is an α-helical, inner membrane protein. It typically works with a periplasmic membrane fusion protein [12–18] and a β-barrel, outer membrane channel to form a functional tripartite protein complex [19,20]. The resulting efflux complex spans both the inner and outer membranes of Gram-negative bacterium to export substrates directly from the cell [2,3]. This process is driven by proton import, which is catalyzed by the inner membrane RND efflux pump.

Escherichia coli CusA is a large α-helical, inner membrane RND-type, heavy-metal efflux pump that is responsible for extruding the biocidal Cu(I) and Ag(I) ions [21,22]. CusA operates with a periplasmic membrane fusion protein (CusB) and a β-barrel, outer membrane

channel (CusC) to form a functional protein complex. The resulting CusCBA three-part efflux system spans the entire cell envelope and confers resistance to Cu(I) and Ag(I) by exporting these metal ions directly out of the cell [21,22].

The crystal structures of each individual component of this tripartite complex system have been deter- mined. The structure of CusA suggests that this RND pump exists as a homotrimer [11]. Each subunit of CusA consists of 12 transmembrane α-helices (TM1–TM12) and a large periplasmic domain formed by two periplasmic loops between TM1 and TM2 and between TM7 and TM8, respectively. The periplasmic domain of CusA can be divided into a pore domain (comprising sub-domains PN1, PN2, PC1 and PC2) and a CusC docking domain (containing sub-domains DN and DC). The structures indicate that this transporter utilizes methionine pairs and clusters to bind and export Cu(I) and Ag(I) ions [11].

Overall, the structure of CusB demonstrates that this adaptor protein is folded into a four-domain elongated structure, ~120 Å long and ~40 Å wide [16]. The first three domains (domains 1–3) of the protein are mostly β-strands. However, the fourth domain (domain 4) is all α-helices and is folded into a three-helix-bundle structure.

Interestingly, the co-crystal structure of the CusBA adaptor–transporter reveals that the trimeric CusA pump associates with six CusB molecules to form the CusB6–CusA3 complex [23,24]. Thus, the entire tripartite efflux assembly is expected to be in the form of CusC3–CusB6–CusA3, which span both the inner and outer membranes of E. coli to export Cu(I) and Ag(I) ions. This assemblage is indeed in good agreement with the predicted 3:6:3 polypeptide ratios of these tripartite complexes [25,26].

Recently, the crystal structure of the CusC channel has also been resolved [20], suggesting that the architecture of this protein resembles those of TolC [19] and OprM [27]. The trimeric CusC channel consists of a membrane-anchoring β-barrel domain and an elongated periplasmic α-helical tunnel [20]. The periplasmic tunnel is ~100 Å long with an outermost diameter of ~ 35 Å at the tip of the tunnel.

It is interesting to note that the N-terminal end of CusC forms an elongated loop. This loop extends from the membrane surface and leads down to the middle section (equatorial domain) of the α-helical periplasmic domain. The first N-terminal residue of CusC is a cysteine (Cys1). It has been observed that this residue is covalently linked to the lipid elements at the inner leaflet of the outer membrane. We reasoned that this Cys1 residue may play an important role in protein–membrane interaction and could be critical for the insertion of this channel protein into the outer membrane. We thus removed the Cys1 residue of CusC to form the ΔC1 mutant. We also replaced this residue by a serine to create the C1S mutant channel. Here we report the crystal structures of the wild-type CusC outer membrane channel, as well as the ΔC1 and C1S mutant channels. In comparison with these three structures, it is suggested that the Cys1 residue indeed plays a crucial role in anchoring the trans- membrane β-barrel onto the outer membrane. These structures also indicate that the ΔC1 and C1S mutants should represent the unstructured intermediate state of these β-barrel channel proteins.

Results

Crystal structure of the wild-type CusC channel protein

We cloned, expressed and purified the wild-type, ΔC1 and C1S CusC proteins. Each of these proteins contains a 6×His at the C-terminus. We obtained crystals of all these three channels using vapor diffusion.

Data collection and refinement statistics of these CusC crystals are summarized in Table 1. The crystal structure of the wild-type CusC channel was resolved to a resolution of 2.09 Å (Fig. 1a). The final structure is nearly identical with the structure of CusC (PDB code: 3PIK) [20] determined by Kulathila et al. Superimposition of these two structures results in an RMSD of 0.28 Å for 429 Cα atoms. CusC exists as a homotrimer that forms an ~ 130-Å-long α/β barrel. Each subunit of CusC contains four β-strands (contributing to the 12-stranded outer membrane β-barrel) and nine α-helices (forming the elongated periplasmic α-barrel) (Figs. 1b and S1 and S2). The trimeric CusC channel creates a large cylindrical internal cavity of ~28,000 Å [3]. Like the previous crystal structure of CusC [20], our X-ray structure suggests that the N-terminal Cys1 residue is covalently linked to the outer membrane via a thioester bond. Thus, the trimeric CusC channel is most likely triacylated through the Cys1 residue to secure the anchoring of this protein onto the outer membrane.

Crystal structure of the ΔC1 CusC mutant

The crystal structure of the ΔC1 CusC channel was determined to a resolution of 2.53 Å (Figs. 1c and S3). The final ΔC1 mutant model consists of the complete mature protein sequence, with the exception of the disordered residues 21–31 and 99–129. Intriguingly, the overall structure of the ΔC1 mutant is very distinct from that of wild-type CusC. Superim-position of a protomer of these two structures gives a high RMSD of 22.49 Å (for 378 Cα atoms), suggesting highly significant differences between these two channels (Fig. 2). In ΔC1

CusC, the amino acids that form the four transmembrane β-strands in the wild-type structure adopt a dramatically different conformation. The majority of these residues appear to be unstructured and form two large random loops. Residues 290–326, which form the transmembrane β-strands S3 and S4 in the wild-type structure, are found to flip down to the outermost surface of the periplasmic α-helical tunnel. In addition, the top portion of the vertical periplasmic α-helices, H7 and H8, make substantial changes and are found to bend downward to accommodate for the change in conformation. Residues N276 of H7 and N334 of H8 appear to form hinges for the bending.

Interestingly, the drastic changes in conformation described above are accompanied by the structural changes of residues 84–116, which form the transmembrane β-strands S1 and S2 of the wild-type CusC channel. In the ΔC1 mutant, the electron density map in the region between residues 82 and 111 is very unclear, suggesting that the majority of the secondary structure of this area is disordered. Thus, this region, located at the innermost surface of the periplasmic α-helical tunnel, also creates a large random loop in the ΔC1 mutant. Similar to the case of helices H7 and H8, the top portion of the vertical periplasmic α-helices, H3 and H4, also bend downward and the hinges are found in nearby residues N76 and T137. Excluding these areas, the remaining tertiary fold of the ΔC1 CusC monomer is very similar to that of a promoter of the wild-type CusC. However, ΔC1 crystallized as a monomer with two molecules in the asymmetric unit (Figs. S3 and S4). The structure suggests that the ΔC1 mutant is monomeric. This monomeric ΔC1 CusC mutant is mostly α-helical, forming an ~95-Å-long secondary structure.

Crystal structure of the C1S CusC mutant

The crystal structure of the C1S mutant was determined to a resolution of 2.69 Å (Figs. 1d and S5). Overall, the structural model of the C1S mutant is nearly identical with that of the ΔC1 CusC channel. Like ΔC1, gel filtration suggests that the C1S mutant is also monomeric in nature (Fig. S6). Superimposition of these two structures gives an overall RMSD of 0.37 Å (for 381 Cα atoms). Again, the monomer's four-stranded antiparallel β-sheet, which packs against one another to form the 12-stranded transmembrane β-barrel of the wild-type trimeric CusC channel, does not seem to exist in this mutant structure. Similar to the ΔC1 mutant, the residues that are supposed to form the four-stranded β-sheet contribute to two independent random loops. One of these loops is found at the position that is supposed to form the upper portion of the innermost core of the periplasmic α-helical tunnel. Another loop is located at the outermost core of the upper portion of this periplasmic tunnel.

The structural difference between wild-type CusC and ΔC1 or C1S suggests that the α-helical tunnels of the wild type and these mutant channels are in different conformational states. Superimposition of the periplasmic α-helical domains of wild-type CusC and ΔC1 indicates that the conformations of helices H8 and H9 on these two structures are significantly different. It is found that helices H8 and H9 shift their positions in the ΔC1 mutant in comparison to those of the wild type. When each protomer of the wild-type CusC trimer is superimposed with the ΔC1 mutant, the change in conformation between the wild-type and ΔC1 proteins can be interpreted as an outward swing of H8 and H9 at the periplasmic tip of the α-helical tunnel from the structure of the wild-type CusC trimer to adopt the conformational state of ΔC1 (Fig. 2). This conformational shift results in the opening of the channel of the periplasmic tunnel. As the structure of the wild-type CusC trimer represents a closed form of the channel [20], the conformation of the α-helical tunnel of the ΔC1 and C1S

mutants may correspond to the open state of the channel. If this is the case, then the interaction between the β-barrel residues and outer membrane may be critical for controlling the opening and closing of the CusC channel.

Discussion

In our protein expression system, a CusC signaling peptide was included at the N-terminus of each target protein. Thus, each protein, including the wild-type CusC and mutants ΔC1 and C1S, should secrete to the periplasm. To ensure that the harvested CusC proteins were attached to or anchored to the E. coli outer membrane, and not the inner membrane, we performed a pre-extraction procedure using 0.5% sodium lauroyl sarcosinate [28] to selectively dissolve and remove proteins of the inner membrane (see Materials and Methods). The undissolved outer membrane constituents, containing the corresponding CusC outer membrane proteins, were then collected by ultracentrifugation before protein extraction. As all of our CusC proteins were extracted from the outer membrane pellets, with the use of detergents, these proteins should be associated with the outer membrane, viz., peripheral outer membrane proteins. In comparison with the structural differences between the monomeric ΔC1 and C1S CusC mutants, as well as trimeric wild-type CusC channel, these structural data provide molecular detail into the mechanisms of assembly and folding of this outer membrane channel (Fig. 3). In the case of the OmpA outer membrane protein [29], in vitro studies have demonstrated that the insertion and folding of this protein into the lipid bilayer occur spontaneously without the need of accessory proteins, including the β-barrel assembly machinery complex [30,31]. In the aqueous phase, OmpA is unstructured and does not have any β-signature. It encounters the inner leaflet of the outer membrane from the

periplasm to form an intermediate I_{MI} [32]. At this state, the protein is still disordered and does not yet appear to have any β-structure. Upon membrane association, two more sequential intermediates, including molten disk (I_{M2}) and molten global (I_{M3}), are formed prior to the completion of the mature folded β-barrel channel [32]. Some fractions of the β-structure have been found to develop in the I_{M2} intermediate state. However, these structures appear to localize on the membrane surface, and no correct tertiary β-contact or penetration into the membrane has yet been made. In the I_{M3} molten globule state, the β-hairpin loops have partially translocated into the lipid bilayer. This intermediate is more globular, but the correct tertiary fold is needed to complete the formation of the native structure. Finally, the native structure is achieved through an extensive rearrangement of side-chain contacts and formation of backbone hydrogen bonds between strands to form a transmembrane β-channel [31], spanning the outer membrane.

In this respect, the monomeric ΔC1 and C1S structures should correspond to the unstructured I_{M1} intermediate of the β-channel membrane proteins. As we isolated these two mutant proteins from the membrane fractions, they should interact with the membrane even though they failed to form a fully inserted β-barrel. This may support the idea that the unstructured I_{M1} intermediate of CusC is associated with inner leaflet of the outer membrane.

Interestingly, the architecture of the α-helical secondary structures of the periplasmic domain of this channel has already been achieved at this state. It has been proposed that the monomeric LukF structure [33], containing a partial β-strand signature, represents the molten disk form of the α-hemolysin heptamer [34]. Thus, the next step for CusC folding may be the formation of a monomeric molten disk (mono-I_{M2}) intermediate, where a partial β-strand conformation has been established at this state (Fig. 3). Upon oligomerization at the interface

of the inner leaflet of the outer membrane, the subsequent step may be the transition to the trimeric molten disk (tri-I_{M2}) intermediate, where the β-hairpins of each monomer are still localized at the membrane interface and have not yet penetrated into the membrane. Then, the next step should well be the formation of a trimeric I_{M3} molten globule intermediate, in which the β-hairpins have been inserted into the membrane and the partial β-barrel has been achieved. Finally, the native state of trimeric CusC should be formed and the mature β-barrel channel should be completed, allowing the β-structural elements to span the entire outer membrane.

Although the phenomenon of outer membrane protein folding has been studied extensively using fluorescence methods, the three-dimensional structures of these unfolded intermediates are difficult to obtain by X-ray crystallography and NMR because of their intrinsically unstructured and disordered nature. This study provides a snapshot of the conformation of these outer membrane channel proteins in their unstructured form. The structures of CusC have allowed us to unmask the sequential transition of conformations leading to the folding and membrane insertion of this channel. During the course of channel formation, it is believed that specific protein–protein and protein–lipid interactions play a critical role in the assembly of this trimeric transmembrane β-barrel channel.

Materials And Methods

Cloning, expression and purification of the CusC, C1S and ΔC1 channel proteins

Briefly, the full-length CusC membrane protein containing a 6×His tag at the C-terminus was overproduced in *E. coli* C43(DE3)/pBAD22bΩcusC cells. Cells were grown in 12 L of LB medium with 100 μg/ml ampicillin at 37 °C. When the OD600 reached 0.5, the culture was

cooled down to 20 °C and then treated with 0.2% arabinose to induce cusC expression. Cells were harvested after shaking for 16 h at 20 °C. The collected bacteria were resuspended in buffer containing 20 mM Na–Hepes (pH 7.5), 300 mM NaCl and 1 mM phenylmethylsulfonyl fluoride (PMSF) and were then disrupted with a French pressure cell. The membrane fraction was collected by ultracentrifugation, followed by a pre-extraction procedure by incubating in buffer containing 0.5% sodium lauroyl sarcosinate, 20 mM Na–Hepes (pH 7.5) and 50 mM NaCl for 0.5 h at room temperature. The membrane was collected and washed twice with buffer containing 20 mM Na–Hepes (pH 7.5) and 50 mM NaCl. The membrane protein was then solubilized in 2% (w/v) n-dodecyl-β-D-maltoside (DDM). Insoluble material was removed by ultracentrifugation at 100,000g. The extracted protein was purified with a Ni^{2+}- affinity column. The purity of the CusC protein (> 95%) was judged using 10% SDS-PAGE stained with Coomassie Brilliant Blue. The purified protein was then dialyzed and concentrated to 15 mg/ml in buffer containing 20 mM Na-Hepes (pH 7.5), 200 mM NaCl and 0.05% DDM.

The C1S CusC protein that contains a 6×His tag at the C-terminus was overproduced in *E. coli* C43(DE3) cells using the pBAD22bΩcusC(C1S) expression vector. The procedures for expressing and purifying the C1S mutant channel were identical with those of 6×His CusC. The purified C1S protein was concentrated to 15 mg/ml in buffer containing 20 mM Na–Hepes (pH 7.5), 200 mM NaCl and 0.05% DDM for crystallization.

The ΔC1 CusC protein containing a 6×His tag at the C-terminus was overproduced in *E. coli* C43(DE3) cells/ pBAD22bΩcusC(ΔC1). The procedures for cell growth and protein expression were identical with those of 6×His CusC. For protein purification, the procedures were nearly identical with those of the 6×His CusC channel, except that the extracted outer

membrane was solubilized in 2% (w/v) 6-cyclohexyl-1-hexyl-β-D-maltoside (Cymal-6). Insoluble material was removed by ultracentrifugation at 100,000g. The ΔC1 protein was purified with a Ni^{2+}-affinity column. The purity of the ΔC1 protein (>95%) was judged using 10% SDS-PAGE stained with Coomassie Brilliant Blue. The purified ΔC1 protein was then dialyzed and concentrated to 15 mg/ml in buffer containing 20 mM Na–Hepes (pH 7.5), 200 mM NaCl and 0.05% Cymal-6.

For 6×His SeMet-ΔC1 (SeMet, selenomethionine), the protein was expressed in *E. coli* BL21Star(DE3) cells possessing pET15bΩcusC(ΔC1). In brief, a 10-ml LB broth overnight culture containing *E. coli* BL21star(DE3)/pET15- bΩcusC(ΔC1) cells was transferred into 120 ml of LB broth containing 100 μg/ml ampicillin and grown at 37 °C. When the OD600 value reached 1.2, cells were harvested by centrifugation at 6000 rpm for 10 min and then washed two times with 20 ml of M9 minimal salt solution. The cells were resuspended in 120 ml of M9 media and then transferred into a 12-L pre-warmed M9 solution containing 100 μg/ml ampicillin. The cell culture was incubated at 37 °C with shaking. When the OD600 reached 0.4, 100 mg/l of lysine, phenylalanine and threonine; 50 mg/l of isoleucine, leucine and valine; and 60 mg/l of L-SeMet were added. The culture was induced with 1 mM isopropyl-β-D-thiogalactopyranoside (IPTG) after 15 min. Cells were then harvested within 3 h after induction. The collected bacteria were resuspended in low-salt buffer containing 100 mM sodium phosphate (pH 7.2), 10% glycerol and 1 mM PMSF and were then disrupted with a French pressure cell. The membrane fraction was collected and washed twice with high-salt buffer containing 20 mM sodium phosphate (pH 7.2), 2 M KCl, 10% glycerol, 1 mM ethylenediaminetetraacetic acid and 1 mM PMSF and once with 20 mM Na–Hepes buffer (pH 7.5) containing 1 mM PMSF. The membrane protein was then solubilized in 2%

(w/v) Cymal-6. Insoluble material was removed by ultracentrifugation at 100,000g. The extracted protein was purified with a Ni^{2+}-affinity column. The purity of the SeMet-ΔC1 protein (>95%) was judged using 10% SDS-PAGE stained with Coomassie Brilliant Blue. The purified protein was then dialyzed and concentrated to 20 mg/ml in a buffer containing 20 mM Na–Hepes (pH 7.5), 200 mM NaCl and 0.05% Cymal-6.

Crystallization of the CusC, ΔC1 and C1S proteins

Crystals of the 6×His CusC were obtained using sitting-drop vapor diffusion. The CusC crystals were grown at room temperature in 24-well plates with the following procedures. A 2-µl protein solution containing 15 mg/ml CusC protein in 20 mM Na–Hepes (pH 7.5), 200 mM NaCl and 0.05% (w/v) DDM was mixed with a 2-µl reservoir solution containing 8% polyethylene glycol (PEG) 3350, 0.05 M sodium acetate (pH 4.0), 0.2 M $(NH4)_2SO_4$, 1% JM 600 and 2% OG. The resultant mixture was equilibrated against 500 µl of the reservoir solution. Crystals of CusC grew to a full size in the drops within 2 weeks. Typically, the dimensions of the crystals were 0.2 mm × 0.2 mm × 0.2 mm. Cryoprotection was achieved by raising the glycerol concentration stepwise to 30% with a 5% increment in each step. Crystals of the 6×His ΔC1 mutant were obtained using sitting-drop vapor diffusion. Briefly, a 2-µl protein solution containing 15 mg/ml ΔC1 protein in 20 mM Na–Hepes (pH 7.5), 200 mM NaCl and 0.05% (w/v) Cymal-6 was mixed with a 2-µl reservoir solution containing 10% PEG 2000, 0.1 M Na–Hepes (pH 7.5) and 0.1 M KSCN. The resultant mixture was equilibrated against 500 µl of the reservoir solution. Crystals of ΔC1 grew to a full size in the drops within 3 days with the dimensions 0.2 mm × 0.2 mm × 0.2 mm. Cryoprotection was achieved by raising the glycerol concentration stepwise to 30% with a 5% increment in each

step.

The crystallization conditions for SeMet-ΔC1 were the same as those for the native ΔC1 protein. The procedures for crystallizing the 6×His C1S mutant were nearly identical with those of 6×His CusC. The reservoir solution used to crystallize C1S contained 12% PEG 3350, 0.1 M sodium citrate (pH 6.5), 0.1 M sodium acetate and 15% butane-2,3-diol. Crystals of C1S also grew to a full size in the drops within 2 weeks. Cryoprotection was achieved by raising the glycerol concentration stepwise to 30% with a 5% increment in each step.

Data collection, structural determination and refinement

All diffraction data were collected at 100 K at beamline 24ID-C located at the Advanced Photon Source, using an ADSC Quantum 315 CCD-based detector. Diffraction data were processed using DENZO and scaled using SCALE- PACK [35]. Crystals of 6×His CusC belong to space group R32 (Table S1). Based on the molecular mass of CusC (49.3 kDa), there is a single molecule per asymmetric unit with a solvent content of 67.8%. The structure of the CusC channel protein was phased using molecular replacement, utilizing the published CusC structure (PDB code: 3PIK) as the search model. Structural refinement was then performed using PHENIX [36] and CNS [37] by refining the model against our 2.09-Å-resolution diffraction data (Table 1).

Crystals of 6×His ΔC1 took a space group P21 (Table 1). In the asymmetric unit, two molecules of ΔC1 were found with a solvent content of 47.1%. Single anomalous dispersion phasing using the program Phaser [38] was employed to obtain experimental phases. Phases were then subjected to density modification and phase extension to 2.53 Å resolution using

the program RESOLVE [39]. The ΔC1 CusC protein contains six methionine residues, and five selenium sites per ΔC1 molecule (10 selenium sites per asymmetric unit) were identified. The SeMet data not only augmented the experimental phases but also helped in tracing the molecules by anomalous difference Fourier maps where we could ascertain the proper registry of SeMet residues. After tracing the initial model manually using the program Coot [40], we refined the model against the native data at 2.53 Å resolution using PHENIX [36] and CNS [37]. The conformations of the two ΔC1 molecules in the asymmetric unit are very similar. Superimposition of these two molecules gives an overall RMSD of 1.0 Å (for 372 Cα atoms). Crystals of 6×His C1S CusC belong to space group P21 (Table 1). Two molecules per asymmetric unit were found in the crystal with a solvent content of 47.3%. The structure of the C1S protein was phased using molecular replacement, utilizing the ΔC1 structure as the search model. The model was then refined against the C1S data at 2.69 Å resolution using the same procedures for the full-length CusC and ΔC1 structures. The structures of the two C1S molecules in the asymmetric unit are nearly identical with each other. Superimposition of these two molecules gives an overall RMSD of 0.9 Å (for 350 Cα atoms).

Gel filtration

A protein liquid chromatography Superdex 200 16/60 column (Amersham Pharmacia Biotech) with a mobile phase containing 20 mM Na–Hepes (pH 7.5), 200 mM NaCl and 0.05% DDM was used in the gel-filtration experiments. Blue dextran (Sigma-Aldrich) was used to determine the column void volume, and proteins for use as gel-filtration molecular weight standards were cytochrome C (Mr, 12,400), carbonic anhydrase (Mr, 29,000),

albumin bovine serum (Mr, 66,000), alcohol dehydrogenase (Mr, 150,000) and β-amylase (Mr, 200,000). All these standards were purchased from Sigma-Aldrich. The molecular weights of the experimental samples were determined following the protocols supplied by the manufacturers.

Data deposition

Atomic coordinates and structure factors have been deposited in the Protein Data Bank under codes 4K7R (wild-type CusC), 4K7K (ΔC1) and 4K34 (C1S).

Supplementary data to this article can be found online at http://dx.doi.org/10.1016/j.jmb.2013.09.042.

Acknowledgements

This work is supported by a National Institutes of Health Grant R01GM086431 (E.W.Y.). This work is based upon research conducted at the Northeast- ern Collaborative Access Team beamlines of the Advanced Photon Source, supported by award RR-15301 from the National Center for Research Resources at the National Institutes of Health. Use of the Advanced Photon Source is supported by the U.S. Department of Energy, Office of Basic Energy Sciences, under Contract No. DE-AC02-06CH11357. N.R.B. was supported through a Science Undergrad- uate Laboratory Internship (SULI) from the DOE.

References

[1] Wallin E, von Heijine G. Genome-wide analysis of integral membrane proteins from eubacterial, archaean, and eukary- otic organisms. Protein Sci 1998;7:1029–38.

[2] Tseng TT, Gratwick KS, Kollman J, Park D, Nies DH, Goffeau A, et al. The RND permease superfamily: an ancient, ubiquitous and diverse family that includes human disease and develop- ment protein. J Mol Microbiol Biotechnol 1999;1:107–25.

[3] Nies DH. Efflux-mediated heavy metal resistance in prokary- otes. FEMS Microbiol Rev 2003;27:313–39.

[4] Murakami S, Nakashima R, Yamashita E, Yamaguchi A. Crystal structure of bacterial multidrug efflux transporter AcrB. Nature 2002;419:587–93.

[5] Yu EW, McDermott G, Zgruskaya HI, Nikaido H, Koshland DE. Structural basis of multiple drug binding capacity of the AcrB multidrug efflux pump. Science 2003;300:976–80.

[6] Murakami S, Nakashima R, Yamashita E, Matsumoto T, Yamaguchi A. Crystal structures of a multidrug transporter reveal a functionally rotating mechanism. Nature 2006;443: 173–9.

[7] Seeger MA, Schiefner A, Eicher T, Verrey F, Dietrichs K, Pos KM. Structural asymmetry of AcrB trimer suggests a peristaltic pump mechanism. Science 2006;313:1295–8.

[8] Sennhauser G, Amstutz P, Briand C, Storchengegger O, Grütter MG. Drug export pathway of multidrug exporter AcrB revealed by DARPin inhibitors. PLoS Biol 2007;5:e7.

[9] Yu EW, Aires JR, McDermott G, Nikaido H. A periplasmic drug- binding site of the AcrB multidrug efflux pump: a crystallo- graphic and site-directed mutagenesis study. J Bacteriol 2005;187:6804–15.

[10] Sennhauser G, Bukowska MA, Briand C, Grütter MG. Crystal structure of the multidrug exporter MexB from Pseudomonas aeruginosa. J Mol Biol 2009;389:134–45.

[11] Long F, Su C-C, Zimmermann MT, Boyken SE, Rajashankar KR, Jernigan RL, et al. Crystal structures of the CusA efflux pump suggest methionine-mediated metal transport. Nature 2010;467:484–8.

[12] Higgins MK, Bokma E, Koronakis E, Hughes C, Koronakis V. Structure of the periplasmic component of a bacterial drug efflux pump. Proc Natl Acad Sci USA 2004;101:9994–9.

[13] Akama H, Matsuura T, Kashiwag S, Yoneyama H, Narita S, Tsukihara T, et al. Crystal structure of the membrane fusion protein, MexA, of the multidrug transporter in Pseudomonas aeruginosa. J Biol Chem 2004;279:25939–42.

[14] Mikolosko J, Bobyk K, Zgurskaya HI, Ghosh P. Conforma- tional flexibility in the multidrug efflux system protein AcrA. Structure 2006;14:577–87.

[15] Symmons M, Bokma E, Koronakis E, Hughes C, Koronakis V. The assembled structure of a complete tripartite bacterial multidrug efflux pump. Proc Natl Acad Sci USA 2009;106: 7173–8.

[16] Su C-C, Yang F, Long F, Reyon D, Routh MD, Kuo DW, et al. Crystal structure of the membrane fusion protein CusB from Escherichia coli. J Mol Biol 2009;393:342–55.

[17] Yum S, Xu Y, Piao S, Sim S-H, Kim H-M, Jo W-S, et al. Crystal structure of the periplasmic component of a tripartite macrolide-specific efflux pump. J Mol Biol 2009;387: 1286–97.

[18] De Angelis F, Lee JK, O'Connell JD, Miercke LJW, Verschueren KH, Srinivasan V, et al. Metal-induced confor- mational changes in ZneB suggest an active role of membrane fusion proteins in efflux resistance systems. Proc Natl Acad Sci USA 2010;107:11038–43.

[19] Koronakis V, Sharff A, Koronakis E, Luisi B, Hughes C. Crystal structure of the bacterial membrane protein TolC central to multidrug efflux and protein export. Nature 2000;405:914–9.

[20] Kulathila R, Kulathila R, Indic M, van den Berg B. Crystal structure of Escherichia coli CusC, the outer membrane component of a heavy-metal efflux pump. PLoS One 2011;6: e15610.

[21] Franke S, Grass G, Nies DH. The product of the ybdE gene of the Escherichia coli chromosome is involved in detoxification of silver ions. Microbiology 2001;147:965–72.

[22] Franke S, Grass G, Rensing C, Nies DH. Molecular analysis of the copper-transporting efflux system CusCFBA of Escherichia coli. J Bacteriol 2003;185:3804–12.

[23] Su C-C, Long F, Zimmermann MT, Rajashankar KR, Jernigan RL, Yu EW. Crystal structure of the CusBA heavy-metal efflux pump of Escherichia coli. Nature 2011;467:484–8.

[24] Su C-C, Long F, Lei H-T, Bolla JR, Do SV, Rajashankar KR, Yu EW. J Mol Biol 2012;422:429–41.

[25] Rensing C, Pribyl T, Nies DH. New functions for the three subunits of the CzcCBA cation-proton antiporter. J Bacteriol 1997;179:6871–9.

[26] Stegmeier JF, Polleichtner G, Brandes N, Hotz C, Andersen C. Importance of the adaptor (membrane fusion) protein hairpin domain for the functionality of multidrug efflux pumps. Biochemistry 2006;45:10303–12.

[27] Akama H, Kanemaki M, Yoshimura M, Tsukihara T, Kashiwag T, Yoneyama H, et al. Crystal structure of the drug discharge outer membrane protein, OprM, of Pseudomonas aeruginosa: dual modes of membrane anchoring and occluded cavity end. J Biol Chem 2004;279:52816–9.

[28] Filip C, Fletcher G, Wulff JL, Earhart CF. Solubilization of the cytoplasmic membrane of Escherichia coli by the ionic detergent sodium-lauryl sarcosinate. J Bacteriol 1973;115: 717–22.

[29] Pautsch A, Schulz GE. Structure of the outer membrane protein A transmembrane domain. Nat Struct Biol 1998;5: 1013–7.

[30] Kleinschmidt JH, Tamm LK. Folding intermediates of a beta- barrel membrane protein. Kinetic evidence for a multi-step membrane insertion mechanism. Biochemistry 1996;35: 12993–3000.

[31] Tamm LK, Arora A, Kleinschmidt JH. Structure and assembly of β-barrel membrane proteins. J Biol Chem 2001;276:32399–402.

[32] Tamm LK, Hong H, Liang B. Folding and assembly of beta- barrel membrane proteins. Biochim Biophys Acta 2004;1666: 250–63.

[33] Olson R, Nariya H, Yokota K, Kamio Y, Gouaux E. Crystal structure of staphylococcal LukF delineates conformational changes accompanying formation of a transmembrane channel. Nat Struct Biol 1999;6:134–40.

[34] Song L, Hobaugh MR, Shustak C, Cheley S, Bayley H, Gouaux JE. Structure of staphylococcal alpha-hemolysin, a heptameric transmembrane pore. Science 1996;274:1859–66.

[35] Otwinowski Z, Minor M. Processing of X-ray diffraction data collected in oscillation mode. Methods Enzymol 1997;276: 307–26.

[36] Adams PD, Grosse-Kunstleve RW, Hung LW, Ioerger TR, McCroy AJ, Moriarty NW, et al. PHENIX: building new software for automated crystallographic structure determination. Acta Crystallogr Sect D Biol Crystallogr 2002;58:1948–54.

[37] Brünger AT, Adams PD, Clore GM, DeLano WL, Gros P, Grosse-Kunstleve RW, et al. Crystallography & NMR system: a new software suite for macromolecular structure determination. Acta Crystallogr Sect D Biol Crystallogr 1998;54:905–21.

[38] McCoy AJ, Grosse-Kunstleve RW, Adams PD, Winn MD, Storoni LC, Read RJ. Phaser crystallographic software. J Appl Crystallogr 2007;40:658–74.

[39] Terwilliger TC. Maximum-likelihood density modification using pattern recognition of structural motifs. Acta Crystallogr Sect D Biol Crystallogr 2001;57:1755–62.

[40] Emsley P, Cowtan K. Coot: model-building tools for molecular graphics. Acta Crystallogr Sect D Biol Crystallogr 2004;60:2126–32.

Figures And Captions

Table 1. Data collection, phasing and structural refinement statistics of the CusC, ΔC1 and C1S proteins.

	CusC (WT)	ΔC1	ΔC1 (SeMet)	C1S
Data collection				
Space group	*R*32	*P*21	*P*21	*P*21
Cell dimensions				
a, *b*, *c* (Å)	88.49, 88.49, 474.72.60	62.02, 104.47, 72.03	61.93, 104.41, 71.95	61.88, 105.03, 72.36
α, β, γ (°)	90, 90, 120	90, 101.03, 90	90, 101.03, 90	90, 101.06, 90
Wavelength (Å)	0.979	0.979	0.979	0.979
Resolution (Å)	50–2.09 (2.17–2.09)	50–2.53 (2.63–2.53)	50–2.8 (2.90–2.80)	50–2.69 (2.84–2.69)
R_{sym} (%)	8.3 (40.4)	6.9 (41.7)	11.6 (45.9)	10.2 (30.4)
Average $I/\sigma I$	12.7 (1.8)	12.1 (1.7)	10.5 (2.16)	9.3 (3.4)
Completeness (%)	97.3 (97.2)	94.0 (91.6)	99.9 (99.8)	98.5 (95.0)
Redundancy	2.4 (2.4)	2.1 (2.0)	2.8 (2.8)	3.8 (3.7)
Total reflections	640,300	426,465	654,832	94,904
Unique reflections	43,397	30,236	22,466	24,874
Phasing				
Number of sites			10	
Figure of merit (acentric/centric)			0.821/0.797	
Refinement				
Resolution (Å)	50–2.09	50–2.53		50–2.69
Number of reflections	54,129	31,197		24,838
R_{work}/R_{free} (%)	20.60/23.50	20.77/26.71		19.08/24.61
B-factors (Å^2)				
Protein chain A	30.6	43.7		46.3
Protein chain B		50.7		51.8
RMSD				
Bond lengths (Å)	0.007	0.008		0.009
Bond angles (°)	0.924	1.105		1.143
Ramachandran				
Most favored	96.4	93.4		92.8
Additional allowed	3.6	6.6		6.2
Generously allowed	0	0		0.7
Disallowed	0	0		0.3

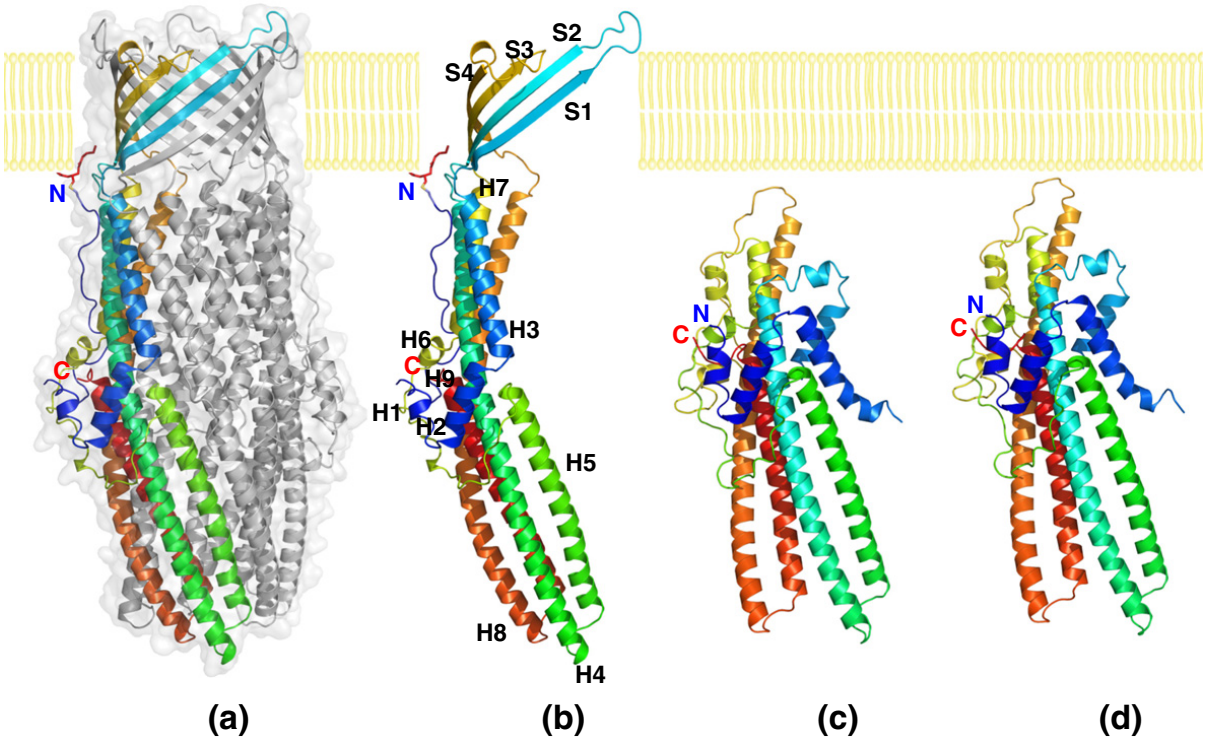

Fig. 1. Structures of the CusC channel proteins. (a) Side view of the trimeric CusC channel. One of the protomers of CusC is in rainbow colors. The other two molecules of CusC are colored gray. (b) Ribbon diagram of the structure of a CusC protomer. The CusC protomer is acylated (red sticks) through the Cys1 residue to anchor onto the outer membrane. (c) Ribbon diagram of the structure of a protomer of the ΔC1 mutant. (d) Ribbon diagram of the structure of a protomer of the C1S mutant. The molecules are colored using a rainbow gradient from the N-terminus (blue) to the C-terminus (red).

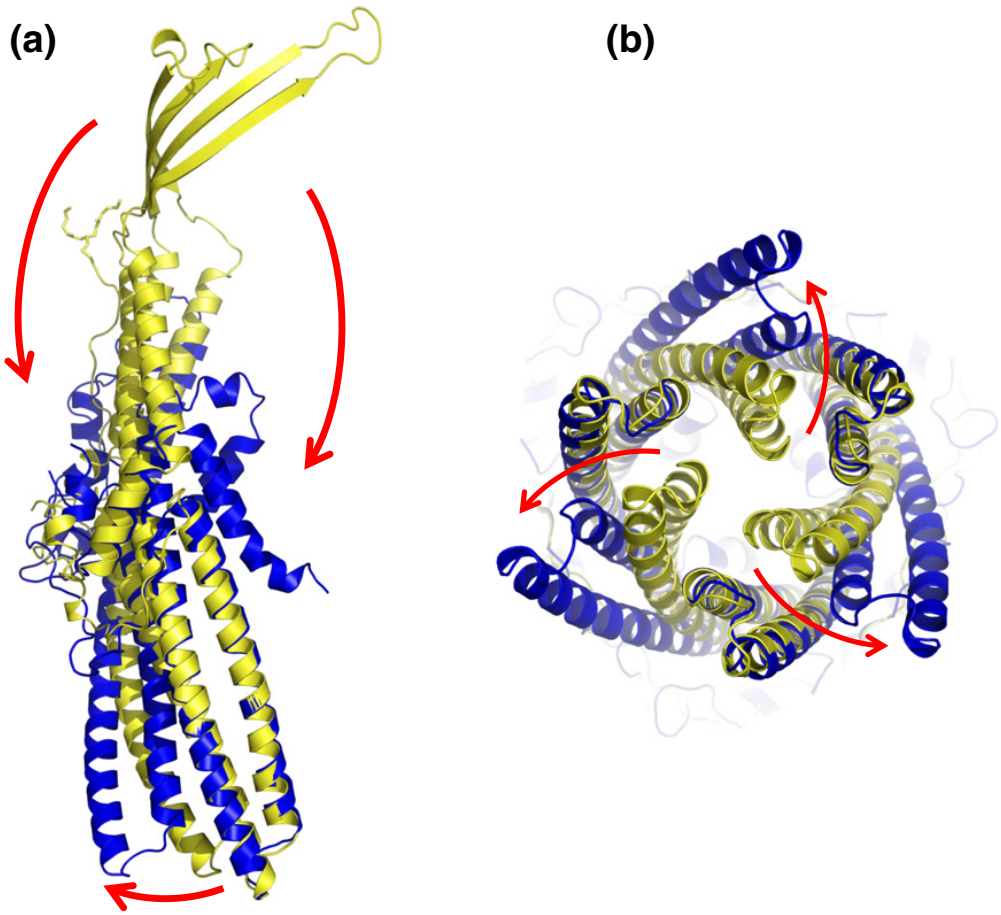

Fig. 2. Comparison of the conformations of wild-type CusC and ΔC1. (a) Superimposition of a monomer of wild-type CusC onto that of the ΔC1 mutant. The structures of the wild-type CusC and ΔC1 protomers are colored yellow and blue, respectively. The arrows indicate the drastic changes in positions and secondary structures when comparing the conformations of the wild-type and ΔC1 CusC. (b) Superimposition of each protomer of the wild-type CusC trimer with the ΔC1 mutant. Each arrow indicates the shift in the positions of H8 and H9 in each protomer when comparing the wild-type and ΔC1 structures.

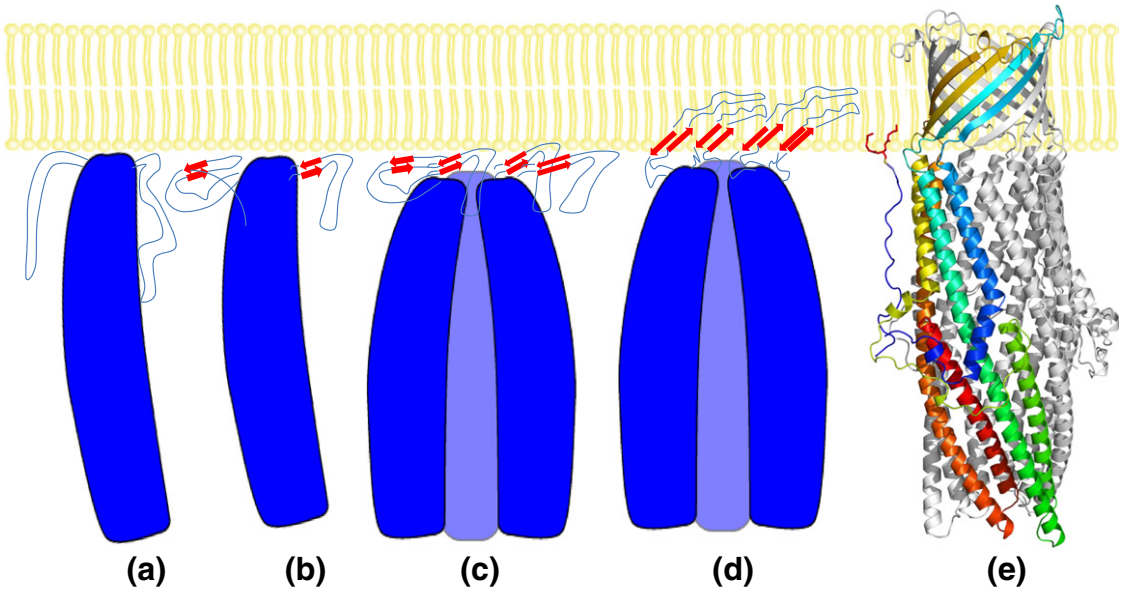

Fig. 3. Model of folding and membrane insertion of the CusC channel protein. This includes the (a) unstructured I_{M1} intermediate, (b) monomeric molten disk (mono-I_{M2}) intermediate, (c) trimeric molten disk (tri-I_{M2}) intermediate, (d) trimeric I_{M3} molten globule intermediate and (e) mature trimeric CusC protein.

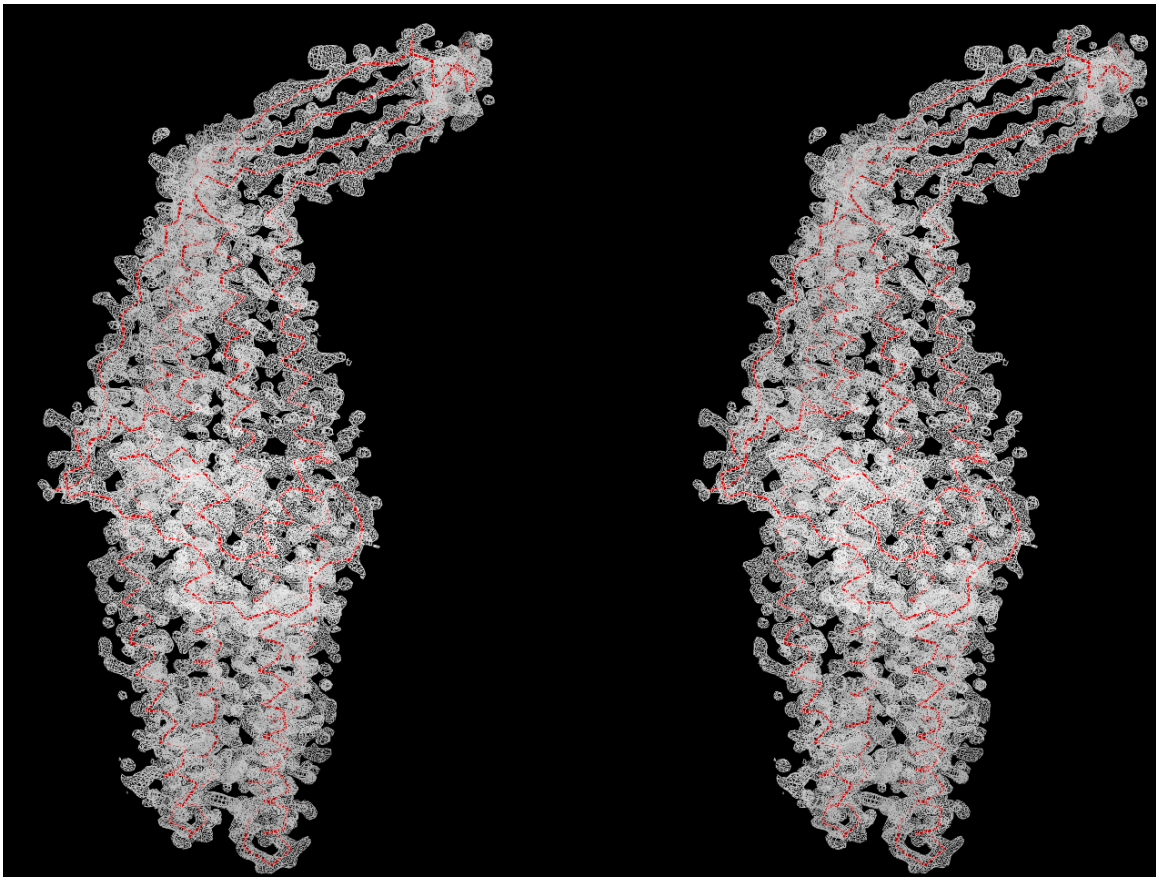

Fig. S1.

Stereo view of the electron density map of the full-length CusC channel at a resolution of 2.09 Å. This is a 2Fo − Fc electron density map (white mesh) contoured at 1.2 σ. The Cα traces of CusC are colored red.

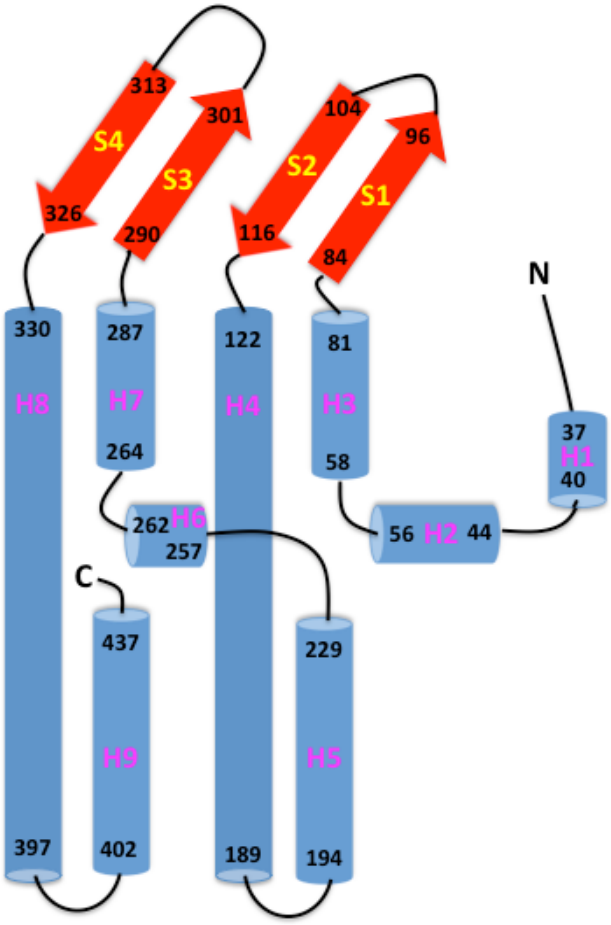

Fig. S2.

Secondary structural topology of the CusC monomer. The topology was constructed based on the crystal structure of CusC. The α-helices and β-strands are colored blue and red, respectively.

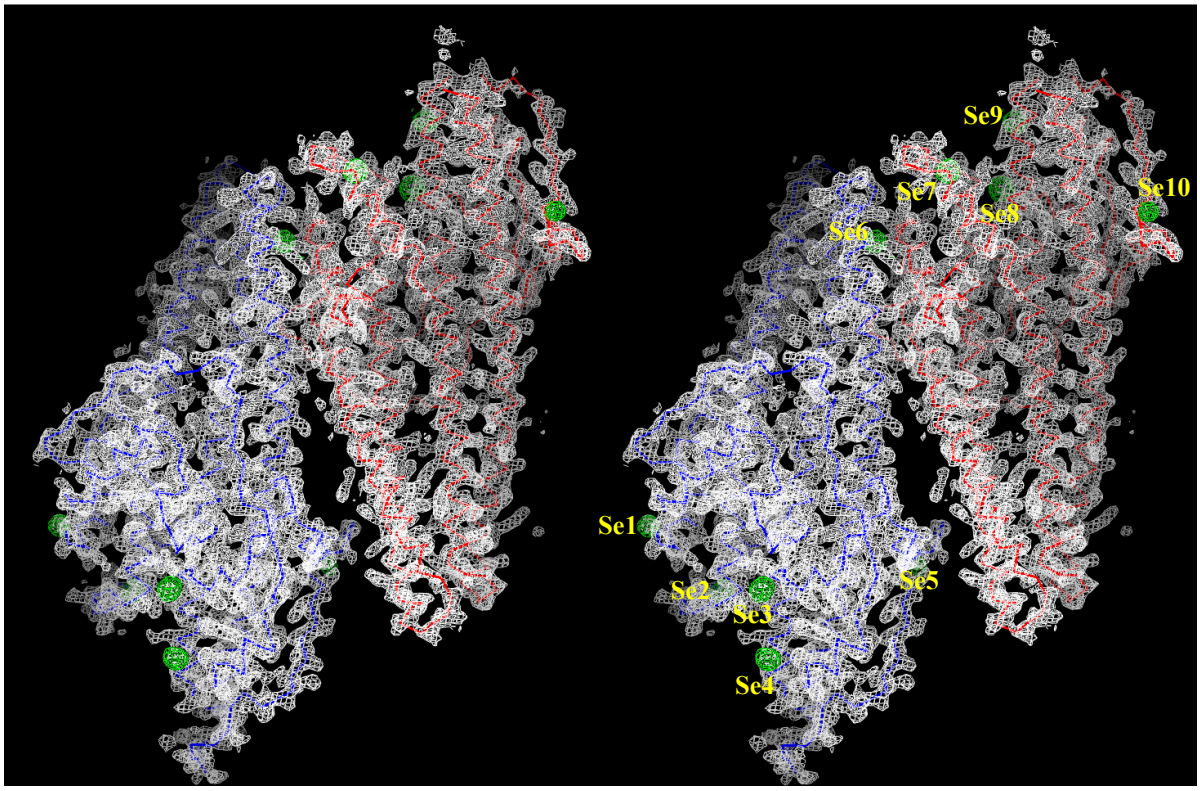

Fig. S3.

Stereo view of the experimental electron density map of the ΔC1 mutant at a resolution of 2.53 Å. Anomalous maps of the 10 selenium sites (contoured at 3 σ), corresponding to the five methionines from each protomer, are colored green. The electron density (colored white) is contoured at the 1.2 σ level and superimposed with the Cα traces of the two ΔC1 protomers (red and blue) in the asymmetric unit.

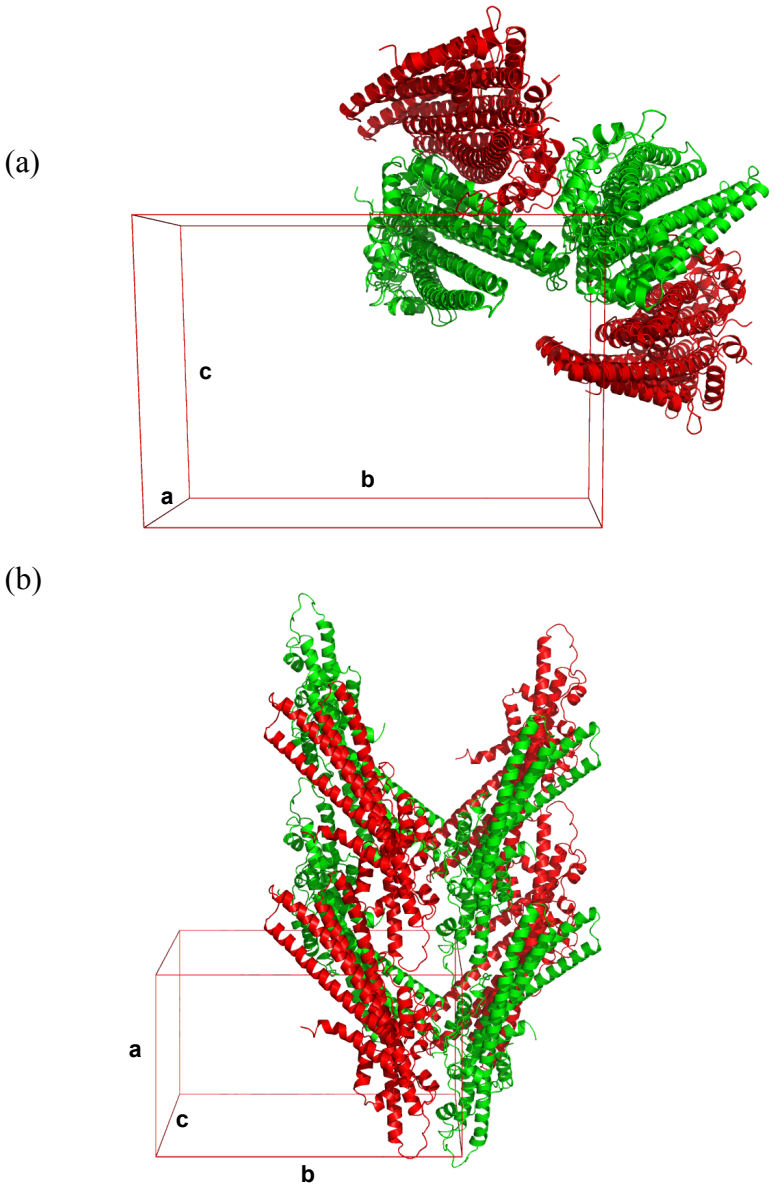

Fig. S4.

Crystal packing of ΔC1. Packing diagram of ΔC1viewed along the (a) a-axis. (b) Packing diagram of ΔC1viewed orthogonal to (a). The ΔC1 molecules are colored red and green.

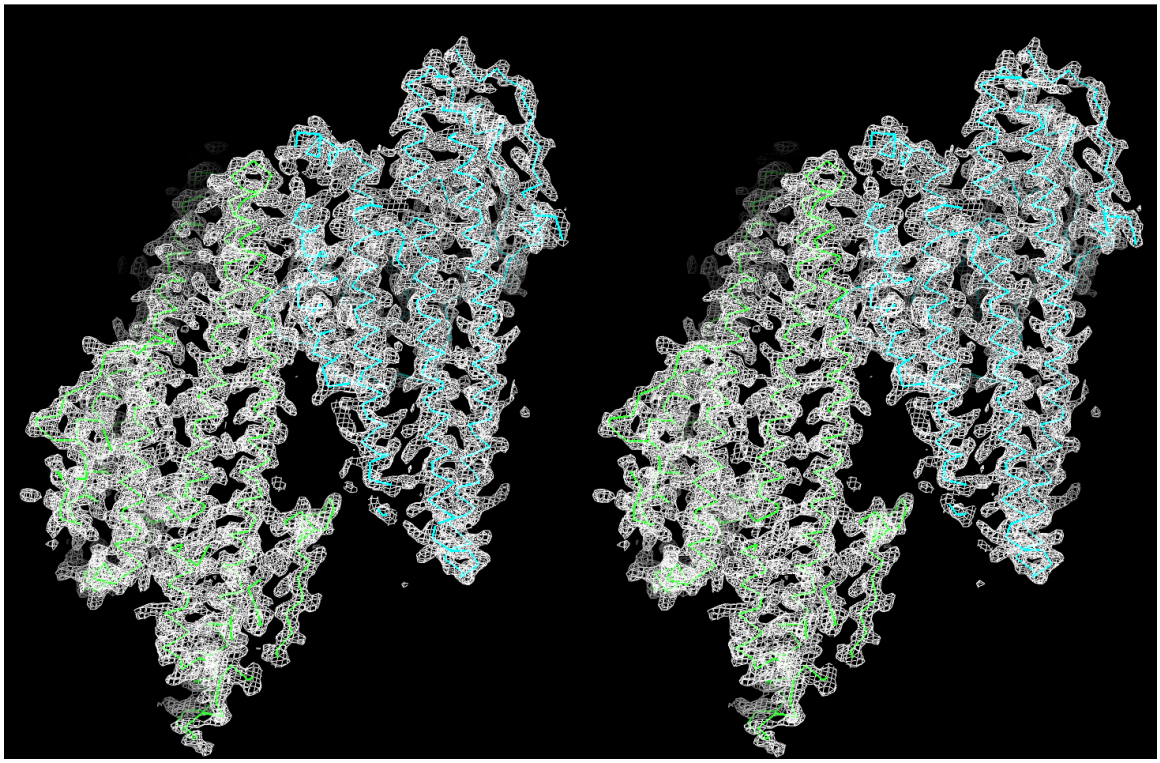

Fig. S5.

Stereo view of the electron density map of the C1S CusC mutant at a resolution of 2.69 Å. The electron density (colored white) is contoured at the 1.2 σ level and superimposed with the Cα traces of two C1S protomers (blue and green) in the asymmetric unit.

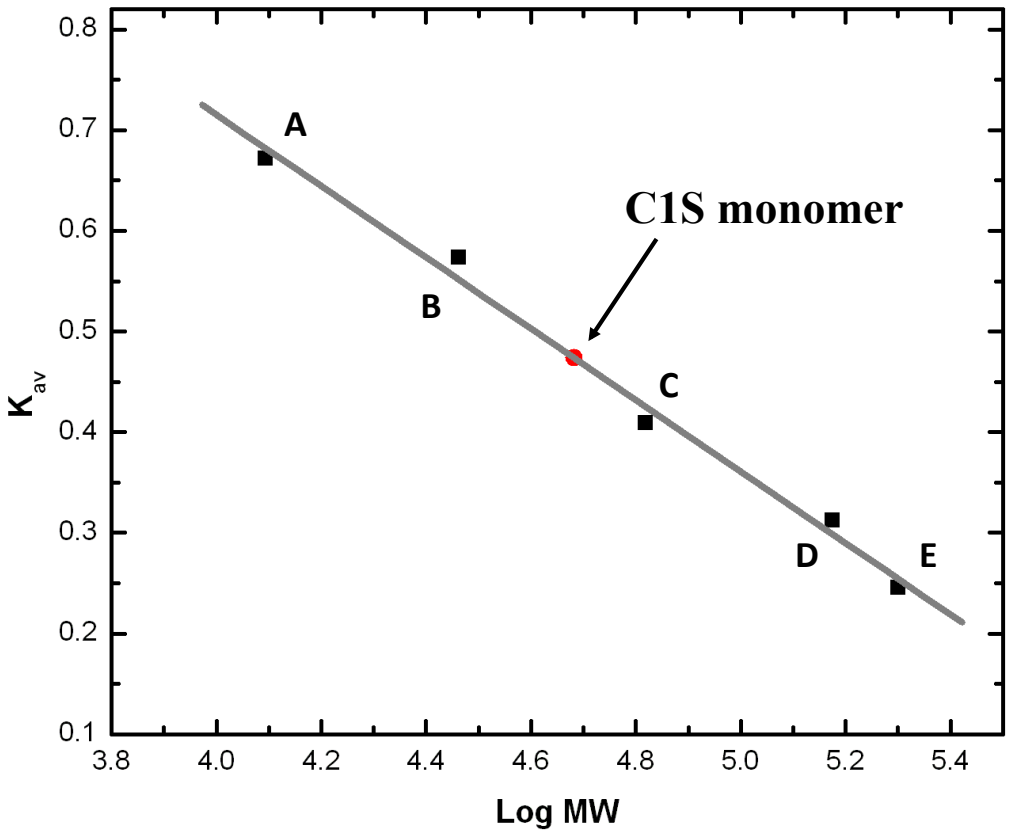

Fig. S6.

Representative gel-filtration experiment. The experiment demonstrated that the C1S mutant is monomeric. The y-axis values were defined as follows: Kav = (Ve − V0)/(VT − V0), where VT, Ve and V0 are the total column volume, elution volume and void volume of the column, respectively. Standards used were as follows: A, cytochrome C (Mr, 12,400); B, carbonic anhydrase (Mr, 29,000); C, albumin bovine serum (Mr, 66,000); D, alcohol dehydrogenase (Mr, 150,000); and E, β-amylase (Mr, 200,000). The void volume was measured using blue dextran (Mr, 2,000,000). The experiment suggested an average molecular mass of 48.1 ± 4.0 kDa for the C1S mutant. This value is in good agreement with the theoretical value of 48.4 kDa for one C1S molecule, indicating that the C1S mutant is monomeric in form.

CHAPTER 4. CRYSTAL STRUCTURE OF THE OPEN STATE OF THE *NEISSERIA GONORRHOEAE* MTRE OUTER MEMBRANE CHANNEL

A paper accepted by PLoS One doi: 10.1371/journal.pone.0097475.

Hsiang-Ting Lei, Tsung-Han Chou, Chih-Chia Su, Jani Reddy Bolla, Nitin Kumar, Abhijith Radhakrishnan, Feng Long , Jared A. Delmar, Sylvia V. Do, Kanagalaghatta R. Rajashankar, William M. Shafer, and Edward W. Yu

Abstract

Active efflux of antimicrobial agents is one of the most important strategies used by bacteria to defend against antimicrobial factors present in their environment. Mediating many cases of antibiotics resistance are transmembrane efflux pumps, composed of one or more proteins. The *Neisseria gonorrhoeae* MtrCDE tripartite multidrug efflux pump, belonging to the hydrophobic and amphiphilic efflux resistance-nodulation-cell division (HAE-RND) family, spans both the inner and outer membranes of *N. gonorrhoeae* and confers resistance to a variety of antibiotics and toxic compounds. We here describe the crystal structure of *N. gonorrhoeae* MtrE, the outer membrane component of the MtrCDE tripartite multidrug efflux system. This trimeric MtrE channel forms a vertical tunnel extending down contiguously from the outer membrane surface to the periplasmic end, indicating that our structure of MtrE depicts an open conformational state of this channel.

Introduction

Neisseria gonorrhoeae is a Gram-negative diplococcus, which is found only in humans and causes the sexually transmitted disease gonorrhea. Gonorrhea is one of the oldest described diseases, however, it remains a significant global problem with more than 100 million cases reported annually worldwide and antibiotic resistance is a major concern [1]. Since *N. gonorrhoeae* is a strictly human pathogen and can colonize both male and female genital mucosal surfaces and other sites, it has developed mechanisms to overcome antimicrobial systems of the host's innate defense. One major mechanism that this bacterium uses to repel antimicrobial agents is the expression of multidrug efflux pumps that recognize and actively export a variety of structurally unrelated toxic compounds from the bacterial cell, including antibacterial peptides, long-chain fatty acids, and several clinically important antibiotics [2-5].

The best characterized and most clinically important efflux system in *N. gonorrhoeae* is the MtrCDE tripartite multidrug efflux system [6-8], which belongs to the hydrophobic and amphiphilic efflux resistance-nodulation-cell division (HAE-RND) family. In Gram-negative bacteria, efflux systems of the HAE-RND family play major roles in the intrinsic and acquired tolerance of antibiotics and toxic compounds [9]. They represent key components for Gram-negative pathogens to use in overcoming toxic environments unfavorable for their survival. Typically, an RND efflux pump [10-16] works in conjunction with a periplasmic membrane fusion protein [17-20], and an outer membrane channel to form a functional protein complex [21,22]. The resulting tripartite efflux system spans the inner and outer membranes of Gram-negative bacterium to export substrates directly out of the cell [9].

For the MtrCDE tripartite efflux system, MtrD [7,23] is a large proton-motive-force dependent inner membrane HAE-RND efflux pump composed of 1,067 amino acids. MtrE [24,25] is a 447 amino acid protein that forms an outer membrane channel. The membrane fusion protein MtrC [25,26], containing 412 amino acids, bridges between MtrD and MtrE to form the tripartite efflux complex MtrCDE. This powerful efflux complex spans the entire cell envelope of *N. gonorrhoeae* and mediates the export of hydrophobic antimicrobial agents, such as antibiotics, nonionic detergents, antibacterial peptides, bile salts and gonadal steroidal hormones [2,7,27,28].

Currently, there are only two crystal structures of HAE-RND efflux pumps resolved by crystallography. These efflux pumps are the *Escherichia coli* AcrB [10-15] and *Pseudomonas aeruginosa* MexB [16] multidrug transporters. The crystal structures of the other components of these tripartite complex systems have also been determined. These include the outer membrane channels, *E. coli* TolC [21] and *P. aeruginosa* OprM [22] as well as the periplasmic membrane fusion proteins, *E. coli* AcrA [19] and *P. aeruginosa* MexA [20-22]. In Gram-negative bacteria, several other crystal structures of outer membrane channels, such as VceC of *Vibro choleria* [29] and CusC of *E. coli* [30,31] have also been reported.

Thus far, there is no structural information available for any protein component of the MtrCDE tripartite complex system. However, it has been reported that individual protein components of this tripartite system are able to interact between each other, suggesting that the tripartite MtrCDE pump is assembled in the form of $MtrD_3$-$MtrC_6$-$MtrE_3$ [25]. It is important to note that this result is indeed in good agreement with the CusAB transporter-

adaptor co-crystal complex [32,33] of the CusABC efflux system [30,31,34-37] where the stoichiometry is 3:6 transporter-to-adaptor molar ratio [32,33].

Here we present the crystal structure of the outer membrane MtrE channel, which represents an open conformational state of this multidrug efflux protein. The structure suggests that the interior surface of the channel protein forms a continuous, elongated tunnel, which extends from the outer membrane surface and leads down to the tip of the α-helical periplasmic domain. In addition, an aspartate ring created by six aspartates is found at the tip of the periplasmic tunnel, presumably participating as a selectivity gate of the channel.

Results And Discussion

Overall structure of the *N. gonorrhoeae* MtrE outer membrane channel

We cloned, expressed, and purified the full-length MtrE outer membrane channel containing a 6xHis tag at the C-terminus. We obtained crystals of this membrane protein using vapor diffusion. We then used molecular replacement, utilizing the structure of *P. aeruginsa* OprM (pdb code: 1WP1) [22] to determine the three-dimensional structure of MtrE. The diffraction data were indexed to the space group $P6_322$. Data collection and refinement statistics are summarized in Table 1. The resulting electron density maps (Fig. 1) reveal that the asymmetric unit consists of one protomer. The crystal structure of the full-length MtrE outer membrane channel protein was then determined to a resolution of 3.29 Å (Table 1). The final model comprises 99% of the total amino acids (residues 1-445) (Fig. 2a). The final structure is refined to R_{work} and R_{free} of 24.1% and 29.4%, respectively. Superimposition of the final structure of MtrE with that of OprM (pdb code: 1WP1) [22] results in a RMSD of 18.2 Å over 445 C^{α} atoms, suggesting highly significant difference in the overall tertiary

structures between these two channel proteins (Fig. S1).

Like TolC [21] and OprM [22], MtrE exists as a homotrimer that forms a ~130 Å long α/β barrel (Fig. 2b). Each subunit of MtrE contains four β-strands (contributing to the 12-stranded outer membrane β-barrel) and eight α-helices (forming the elongated periplasmic α-barrel) (Fig. 3). These four β-strands (S1, S2, S3 and S4) constitute the β-barrel domain and are organized in an antiparallel fashion, spanning the outer membrane. In contrast, the elongated periplasmic tunnel of MtrE contains six α-helices. Similar to the structure of TolC, two long helices (H3 and H7) are found to extend across the entire length of the periplasmic α-helical tunnel. The α-helical tunnel of MtrE also includes two pairs of shorter α-helices, (H2 and H4) and (H6 and H8). These two pairs of shorter helices stack end-to-end to form pseudocontinuous helices, which contribute coiled-coil interactions with the two long helices. The equatorial domain of MtrE is composed of two helices (H1, H5) and the remaining elements at this domain are mostly unstructured. The periplasmic tunnel of MtrE is ~100 Å long with an outermost diameter of ~35 Å at the tip of the tunnel.

The crystal structure of MtrE shows that the internal surface of the protein forms a continuous channel

In view of the crystal structure of MtrE, it is found that the internal surface of the protein forms a continuous channel. This channel is completely open and fully accessible through both the periplasmic end and outer membrane surface, suggesting that the MtrE channel is at its open conformational state. To date, most of the available structures of outer membrane channels, including TolC [21], OprM [22] and CusC [30,31] are closed at one or both sides. However, several structures of the TolC mutants, which led to the opening of the TolC exit

dust, have been reported [38,39]. These structures also indicate how important residues interact with one another to control the opening and closing of the periplasmic end of this channel. Nonetheless, our crystal structure of the wild-type MtrE channel indicates that this channel is in its open conformational state (Fig. 4). The widest section of the channel is located at the surface of the outer membrane, with the internal diameter of ~22 Å. The volume of the continuous channel formed by the internal surface of the MtrE trimer is ~45,000 $Å^3$.

In addition, all available structures of outer membrane channel proteins, such as TolC [21], OprM [22] and CusC [30,31] indicate that the interior surfaces of these channels are highly electronegative. However, MtrE is distinct in that its internal surface does not have extensive positively or negatively charge patches (Fig. 5). On the contrary, the charge distribution of the outside surface of MtrE is very similar to other outer membrane channels, in which the outside surfaces of all these channels have no extensive charged patches.

The interior aspartate ring

Like the TolC channel, an aspartate ring is found at the periplasmic entrance of the interior of the MtrE channel. Each protomer of MtrE contributes D402 and D405 to form two concentric circles of negative charges in the inner cavity of the trimeric MtrE channel (Fig. 6). Thus, this interior aspartate ring is composed of six aspartate residues. In TolC, the corresponding aspartate ring creates a selectivity gate for this channel and this ring can be blocked by large cations. Fig. S2 illustrates the alignment of protein sequences of the MtrE and TolC channels. The internal diameter of the MtrE aspartate ring is ~12 Å, which creates the narrowest region of the tunnel. It is likely that this aspartate ring is responsible for the

selectivity of the channel, similar to the case of TolC [40]. Indeed, it has been demonstrated that the aspartate ring of MtrE can be blocked by the large positively charged hexamminecobalt (III) complex [25].

In comparison with the TolC structures, it appears that the apparent dilation of our MtrE structure is higher than any reported structures of the open state of TolC. For example, the longest distances between D374 residues of the three TolC protomers in the $TolC^{WT}$, $TolC^{RS}$ and $TolC^{YFRS}$ structures, measured between the side chain O(δ2) atoms, are 6.2, 6.2 and 9.9 Å [39]. The longest distances between the Cα atoms of D374 residues within these TolC trimers are 11.7, 12.3 and 15.4 Å [39]. In the MtrE trimer, the corresponding distance between the side chain O(δ2) atoms of D405 residues becomes 11.8 Å. Additionally, the distance between the Cα atoms of these aspartates is 16.0 Å. It is suspected that the open conformational state of MtrE reflects the low-pH form of this channel, as we crystallized this channel at low pH which would neutralize the aspartate ring.

During the course of substrate import or export, the aspartate ring may need to dilate and increase its internal diameter to allow substrate to pass through the channel. Although our structure indicates that MtrE is capable of opening this channel by itself, it has been suggested that the dilation and constriction of the aspartate ring may be controlled by the MtrC periplasmic membrane fusion protein [24]. In addition, it has been observed that the MtrE channel is able to allow the large vancomycin molecule to enter the cell [24]. However, it only does so in response to the binding of MtrC [24], presumably enhancing the degree of dilation of the MtrE channel. It appears that the opening and closing of the MtrE channel may be induced by the change in conformation of the MtrC membrane fusion protein, which propagates the progressive motion of the MtrD multidrug efflux pump within

the transport cycle to the MtrE channel. As MtrD is a proton motive force-dependent pump, this may imply that active proton translocation within the MtrD inner membrane efflux pump provides the energy to open and close the MtrE outer membrane channel.

The exterior intra- and inter-protomer grooves

The outermost surface of the periplasmic domain of the MtrE trimer forms three intra-protomer and three inter-protomer grooves. These grooves are likely to provide interaction sites for the MtrC membrane fusion protein. There is a chance that the α-helical coiled-coil domain of MtrC could fit into these grooves and contact MtrE to function. Based on the co-crystal structure of the CusAB transporter-adaptor complex [32,33], the β-barrel domains of the elongated MtrC membrane fusion protein should interact with the periplasmic domain of the MtrD pump, bridging the gap between the MtrD and MtrE membrane proteins. This suggests that MtrC could relay conformational changes from the MtrD pump to MtrE channel, allowing these two efflux proteins to communicate between each other. In turn, this relay network may control the opening and closing of MtrE.

Several surface-exposed residues, including E161, R168, E407, E414 and Q421, are found at the intra-protomer groove of MtrE. Interestingly, many of these residues are charged amino acids. Likewise, a number of charged and polar residues, such as Q167, N178, E198, E202, R215 and R219, also line the surface of the inter-protomer groove of MtrE. These charged and polar residues may be critical for MtrE-MtrC interaction. Indeed, it has been identified that residues E414 and Q421 (found in the intra-protomer groove) as well as N178 (located at the inter-protomer groove) are important for the function of the MtrCDE tripartite efflux pump [24].

The α-helical hairpin of the MtrC membrane fusion protein may directly engage to contact the inter- and intra-protomer grooves of the MtrE channel to form a complex. Thus, these surface-exposed charged and polar residues, found within the inter- and intra-protomer grooves of MtrE, may be crucial for the binding of MtrC to the MtrE channel. Exactly how MtrC and MtrE interact must await confirmation by elucidation of the crystal structure of the MtrC membrane fusion protein.

It is well established that overexpression of RND multidrug efflux pumps leads to a resistant phenotype in pathogenic organisms. Because of the fact that these multidrug efflux pumps are able to respond to a wide spectrum of substrates, pathogenic bacteria that overexpress them can be selected for by many different agents. Thus, it is very important to understand the molecular mechanism as well as detailed structural information of these efflux pumps in order to combat infectious diseases. The control of gonorrhea has been compromised by the increasing proportion of infections due to antibiotic-resistant strains, which are growing at alarming rate. The availability of the crystal structure of the MtrE efflux channel may allow us to rationally design agents that block its function and eventually heighten the sensitivity of *N. gonorrhoeae* to antimicrobials.

Materials And Methods

Cloning, expression and purification of the outer membrane MtrE channel

Briefly, the full-length MtrE membrane protein containing a 6xHis tag at the C-terminus was overproduced in *E. coli* C43(DE3) cells possessing the expression vector pBAD22bΩ*mtrE*. Cells were grown in 12 L of LB medium with 100 μg/ml ampicillin at 37°C. When the OD_{600} reached 0.5, the culture was cooled down to 25°C and then treated with 0.2% (w/v)

arabinose to induce *mtrE* expression. Cells were harvested after shaking for 16 h at 25°C. The collected bacteria were resuspended in buffer containing 20 mM Na-HEPES (pH 7.5), 300 mM NaCl and 1 mM PMSF, and then disrupted with a French pressure cell. The membrane fraction was collected by ultracentrifugation, followed by a pre-extraction procedure by incubating in buffer containing 0.5% (w/v) sodium lauroyl sarcosinate, 20 mM Na-HEPES (pH 7.5) and 50 mM NaCl for 0.5 h at room temperature. The outer membrane was collected and washed twice with buffer containing 20 mM Na-HEPES (pH 7.5) and 50 mM NaCl. The MtrE membrane protein was then solubilized in 2% (w/v) n-dodecyl β-D-maltoside (DDM). Insoluble material was removed by ultracentrifugation at 100,000 x g. The extracted protein was purified with a Ni^{2+}-affinity column. The purity of the MtrE protein (>95%) was judged using 12% SDS-PAGE stained with Coomassie Brilliant Blue. The purified protein was then dialyzed and concentrated to 15 mg/ml in buffer containing 20 mM Na-HEPES (pH 7.5), 200 mM NaCl and 0.05% (w/v) DDM.

Crystallization of MtrE

Crystals of the 6xHis MtrE were obtained using sitting-drop vapor diffusion. A 2 μl protein solution containing 15 mg/ml MtrE protein in 20 mM Na-HEPES (pH 7.5), 200 mM NaCl and 0.05% (w/v) DDM was mixed with a 2 μl of reservoir solution containing 20% PEG 400, 0.2 M sodium acetate (pH 4.6), 0.25 M $MgSO_4$ and 2% (w/v) n-octyl-β-D-glucoside (OG). The resultant mixture was equilibrated against 500 μl of the reservoir solution at room temperature. Crystals of MtrE grew to a full size in the drops within two weeks. Typically, the dimensions of the crystals were 0.2 mm x 0.2 mm x 0.2 mm. Crystals were flash-cooled, using solution containing 30% PEG 400, 0.2 M sodium acetate (pH 4.6), 0.25 M $MgSO_4$,

0.05% DDM and 2% OG, as a cryoprotectant before data collection.

Data collection, structural determination and refinement

All diffraction data were collected at 100K at beamline 24ID-C located at the Advanced Photon Source, using an ADSC Quantum 315 CCD-based detector. Diffraction data were processed using DENZO and scaled using SCALEPACK [41].

Crystals of the MtrE channel protein belong to the space group $P6_322$ (Table 1) and the best crystal diffracted x-ray to a resolution of 3.29 Å. Analysis of Matthew's coefficient indicated the presence of one MtrE protomer (49.29 kDa) per asymmetric unit, with a solvent content of 75.8%.

The structure of MtrE was phased using molecular replacement, utilizing the structure of OprM (pdb id: 1WP1) [22] as a search model. After tracing the initial model manually using the program Coot [42] the model was refined against the data at 3.29 Å-resolution using TLS refinement techniques adopting a single TLS body as implemented in PHENIX [43] leaving 5% of reflections in Free-R set. Iterations of refinement using PHENIX [43] and CNS [44] and model building in Coot [42] lead to the current model, which contains 455 amino acids with excellent geometrical characteristics (Table 1).

Accession code

Atomic coordinates and structure factors have been deposited with the Protein Data Bank under the accession code 4MT0.

Acknowledgements. This work was supported by NIH Grants R37AI021150 (W.M.S.) and R01GM086431 (E.W.Y.) and a VA Merit Award (W.M.S.) from the Medical Research Service of the Department of Veterans Affairs. W.M.S. is the recipient of a Senior Research Career Scientist from the Medical Research Service of the Department of Veterans Affairs. This work is based upon research conducted at the Northeastern Collaborative Access Team beamlines of the Advanced Photon Source, supported by an award GM103403 from the National Institutes of General Medical Sciences. Use of the Advanced Photon Source is supported by the U.S. Department of Energy, Office of Basic Energy Sciences, under Contract No. DE-AC02-06CH11357.

References

1. Tapsall J (2006) Antibiotic resistance in *Neisseria gonorrhoeae* is diminishing available treatment options for gonorrhea: some possible remedies. Expert Review of Anti-infective Therapy 4:619-628.

2. Shafer WM, Qu XD, Waring AJ, Lehrer RI (1998) Modulation of *Neisseria gonorrhoeae* susceptibility to vertebrate antibacterial peptides due to a member of the resistance/nodulation/division efflux pump family. Proc Natl Acad Sci USA 95:1829-1833.

3. Lee EH, Shafer WM (1999) The *far*AB-encoded efflux pump mediates resistance of gonococci to long-chained antibacterial fatty acids. Mol Microbiol 33:7753-7758.

4. Shafer WM, Veal WL, Lee EH, Zarentonelli L, Balthazar JT, Rouquette C (2001) Genetic organization and regulation of antimicrobial efflux systems possessed by *Neisseria gonorrhoeae* and *Neisseria meningitides*. J Mol Microbiol Biotechnol 3:219-225.

5. Rouquette-Loughlin C, Dunham SA, Kuhn M, Balthazar JT, Shafer WM (2003) The NorM efflux pump of by *Neisseria gonorrhoeae* and *Neisseria meningitides* recognizes antimicrobial cationic compounds. J Bacteriol 185:1101-1106.

6. Warner DM, Shafer WM, Jerse AE (2008) Clinically relevant mutations that cause derepression of the Neisseria gonorrhoeae MtrC-MtrD-MtrE efflux pump system confer different levels of antimicrobial resistance and in vivo fitness. Mol Microbiol 70:462-478.

7. Hagman KE, Lucas CE, Balthazar JT, Snyder LA, Nilles M, Judd RC, Shafer WM (1997) The MtrD protein of *Neisseria gonorrhoeae* is a member of resistance/nodulation/division protein family constituting part of an efflux system. Microbiology 143:2117-2125.

8. Lucas CE, Hagman KE, Levin JC, Stein DC, Shafer WM (1995) Importance of lipooligosaccharide structure in determining gonococcal resistance to hydrophobic antimicrobial agents resulting from the *mtr* efflux system. Mol Microbiol 16:1001-1009.

9. Tseng TT, Gratwick KS, Kollman J, Park D, Nies DH, Goffeau A, Saier MH, Jr. (1999) The RND permease superfamily: an ancient, ubiquitous and diverse family that includes human disease and development protein. J Mol Microbiol Biotechnol 1:107-125.

10. Murakami S, Nakashima R, Yamashita E, Yamaguchi A (2002) Crystal structure of bacterial multidrug efflux transporter AcrB. Nature 419:587-593.

11. Yu EW, McDermott G, Zgurskaya HI, Nikaido H, Koshland DE, Jr. (2003) Structural basis of multiple drug binding capacity of the AcrB multidrug efflux pump. Science 300:976-980.

12. Yu EW, Aires JR, McDermott G, Nikaido H (2005) A periplasmic-drug binding site of the AcrB multidrug efflux pump: a crystallographic and site-directed mutagenesis study. J Bacteriol 187:6804-6815.

13. Murakami S, Nakashima R, Yamashita E, Matsumoto T, Yamaguchi A (2006) Crystal structures of a multidrug transporter reveal a functionally rotating mechanism. Nature 443:173-179.

14. Seeger MA, Schiefner A, Eicher T, Verrey F, Dietrichs K, Pos KM (2006) Structural asymmetry of AcrB trimer suggests a peristaltic pump mechanism. Science 313:1295-1298.

15. Sennhauser G, Amstutz P, Briand C, Storchenegger O, Grütter MG (2007) Drug export pathway of multidrug exporter AcrB revealed by DARPin inhibitors. PLoS Biol 5:e7.

16. Sennhauser G, Bukowska MA, Briand C, Grütter MG (2009) Crystal structure of the multidrug exporter MexB from *Pseudomonas aeruginosa*. J Mol Biol 389:134-145.

17. Higgins MK, Bokma E, Koronakis E, Hughes C, Koronakis V (2004) Structure of the periplasmic component of a bacterial drug efflux pump. Proc Natl Acad Sci USA 101:9994-9999.

18. Akama H, Matsuura T, Kashiwag S, Yoneyama H, Narita S, Tsukihara T, Nakagawa A, Nakae T (2004) Crystal structure of the membrane fusion protein, MexA, of the multidrug transporter in *Pseudomonas aeruginosa*. J Biol Chem 279:25939-25942.

19. Mikolosko J, Bobyk K, Zgurskaya HI, Ghosh P (2006) Conformational flexibility in the multidrug efflux system protein AcrA. Structure 14:577-587.

20. Symmons M, Bokma E, Koronakis E, Hughes C, Koronakis V (2009) The assembled structure of a complete tripartite bacterial multidrug efflux pump. Proc Natl Acad Sci USA 106:7173-7178.

21. Koronakis V, Sharff A, Koronakis E, Luisi B, Hughes C (2000) Crystal structure of the bacterial membrane protein TolC central to multidrug efflux and protein export. Nature 405:914-919.

22. Akama H, Kanemaki M, Yoshimura M, Tsukihara T, Kashiwag T, Yoneyama H, Narita S, Nakagawa A, Nakae T (2004) Crystal structure of the drug discharge outer membrane protein, OprM, of *Pseudomonas aeruginosa*. J Biol Chem 279:52816-52819.

23. Maness MJ, Sparling PF (1973) Multiple antibiotic resistance due to a single mutation in *Neisseria gonorrhoeae*. J Infect Dis 128:321-330.

24. Janganan TK, Zhang L, Bavro VN, Matak-Vinkovic D, Barrera NP, Burton MF, Steel PG, Robinson CV, Borges-Walmsley MI, Walmsley AR (2011) Opening of the outer

membrane protein channel in tripartite efflux pumps is induced by interaction with the membrane fusion partner. J Biol Chem 286:5484-5493.

25. Janganan TK, Bavro VN, Zhang L, Borges-Walmsley MI, Walmsley AR (2013) Tripartite efflux pumps: energy is required for dissociation, but not assembly or opening of the outer membrane channel of the pump. Mol Microbiol 88:590-602.

26. Veal WL, Yellen A, Balthazar JT, Pan W, Spratt BG, Shafer WM (1998) Loss-of-function mutations in the *mtr* efflux system of *Neisseria gonorrhoeae*. Microbiology 144:621-627.

27. Hagman KE, Pan W, Spratt BG, Balthazar JT, Judd RC, Shafer WM (1995) Resistance of *Neisseria gonorrhoeae* to anitmicrobial hydrophobic agents is modulated by the *mtrRCDE* efflux system. Microbiology 141:611-622.

28. Delahay RM, Robertson BD, Balthazar JT, Ison CA (1997) Involvement of the gonococcal MtrE protein in the resistance of *Neisseria gonorrhoeae* to toxic hydrophobic agents. Microbiology 143:2127-2133.

29. Federici L, Du D, Walas F, Matsumura H, Fernandez-Recio J, McKeegan KS, Borges-Walmsley MI, Luisi BF, Walmsley AR (2005) The crystal structure of the outer membrane protein VceC from the bacterial pathogen Vibrio cholerae at 1.8 Å resolution. J Biol Chem 280:15307-15314.

30. Kulathila R, Kulathila R, Indic M, van den Berg B (2011) Crystal structure of *Escherichia coli* CusC, the outer membrane component of a heavy-metal efflux pump. PLoS One 6:e15610.

31. Lei HT, Bolla JR, Bishop NR, Su CC, Yu EW (2014) Crystal structures of CusC review conformational changes accompanying folding and transmembrane channel formation. J Mol Biol 426:403-411.

32. Su CC, Long F, Zimmermann MT, Rajashankar KR, Jernigan RL, Yu EW (2011) Crystal Structure of the CusBA Heavy-Metal Efflux Complex of *Escherichia coli*. Nature 470:558-562.

33. Su CC, Long F, Lei HT, Bolla JR, Do SV, Rajashankar KR, Yu EW (2012) Charged Amino Acids (R83, E567, D617, E625, R669, and K678) of CusA Are Required for Metal Ion Transport in the Cus Efflux System. J Mol Biol 422:429-441.

34. Franke S, Grass G, Nies DH (2001) The product of the *ybdE* gene of the *Escherichia coli* chromosome is involved in detoxification of silver ions. Microbiology 147:965-972.

35. Franke S, Grass G, Rensing C, Nies DH (2003) Molecular analysis of the copper-transporting efflux system CusCFBA of *Escherichia coli*. J Bacteriol 185:3804-3812.

36. Su CC, Yang F, Long F, Reyon D, Routh MD, Kuo DW, Mokhtari AK, Van Ornam JD, Rabe KL, Hoy JA, Lee YJ, Rajashankar KR, Yu EW (2009) Crystal structure of the membrane fusion protein CusB from *Escherichia coli*. J Mol Biol 393:342-355.

37. Long F, Su CC, Zimmermann MT, Boyken SE, Rajashankar KR, Jernigan RL, Yu EW (2010) Crystal structures of the CusA heavy-metal efflux pump suggest methionine-mediated metal transport mechanism. Nature 467:484-488.

38. Bavro VN, Pietras Z, Furnham N, Pérez-Cano L, Fernández-Recio J, Pei XY, Misra R, Luisi B (2008) Assembly and channel opening in a bacterial drug efflux machine. Mol Cell 30:114-121.

39. Pei XY, Hinchliffe P, Symmons MF, Koronakis E, Benz R, Hughes C, Koronakis V (2011) Structures of sequential open states in a symmetrical opening transition of the TolC exit duct. Proc Natl Acad Sci USA 108:2112-2117.

40. Andersen C, Koronakis E, Hughes C, Koronakis V (2002) An aspartate ring at the TolC tunnel entrance determines ion selectivity and presents a target for blocking by large cations. Mol Microbiol 44:1131-1139.

41. Otwinowski Z, Minor M (1997) Processing of X-ray diffraction data collected in oscillation mode. Methods Enzymol 276:307-326.

42. Emsley P, Cowtan K (2004) Coot: model-building tools for molecular graphics. Acta Cryst D60:2126.

43. Adams PD, Grosse-Kunstleve RW, Hung LW, Ioerger TR, McCroy AJ, Moriarty NW, et al. (2002) PHENIX: building new software for automated crystallographic structure determination. Acta Cryst 58:1948-1954.

44. Brünger AT, Adams PD, Clore GM, DeLano WL, Gros P, Grosse-Kunstleve RW, Jiang JS, Kuszewski J, Nilges M, Pannu NS, Read RJ, Rice LM, Simonson T, Warren GL (1998) Crystallography & NMR system: A new software suite for macromolecular structure determination. Acta Cryst D54:905-921.

Figures And Captions

Table 1. Data collection and refinement statistics.

Data set	MtrE
Data Collection	
Wavelength (Å)	0.98
Space group	$P6_322$
Resolution (Å)	50 – 3.29 (3.41-3.29)
Cell constants (Å)	
a	93.89
b	93.89
c	391.54
α, β, γ (°)	90, 90, 120
Molecules in ASU	1
Redundancy	3.4 (3.3)
Total reflections	287,882
Unique reflections	16,706
Completeness (%)	98.7 (95.6)
R_{sym} (%)	11.8 (43.5)
R_{pim} (%)	7.6 (30.2)
Average I / σ(I)	9.7 (2.4)
Refinement	
Resolution (Å)	50 – 3.29
R_{work}	24.1
R_{free}	29.4
rms deviation from ideal	
bond lengths (Å)	0.009
bond angles (°)	1.249
Ramachandran	
most favoured (%)	96.8
additional allowed (%)	3.2
generously allowed (%)	0.0
disallowed (%)	0.0

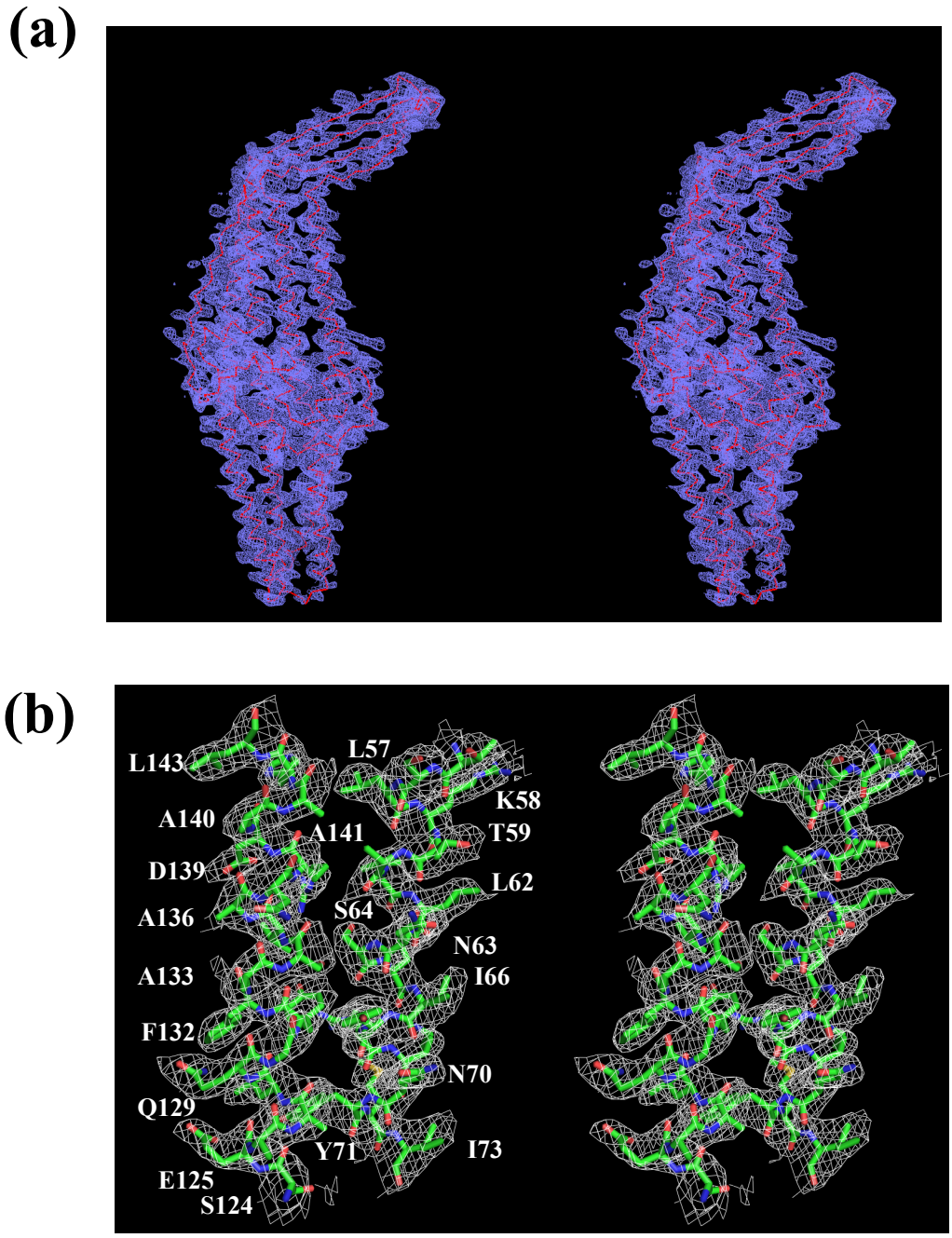

Fig. 1. Stereo view of the composite omit electron density map of the MtrE channel protein at a resolution of 3.29 Å. (a) The composite omit map contoured at 1.2 σ is in blue. The Cα traces of MtrE are in red. (b) Representative section of the electron density at the interface between H2 and H3 of the periplasmic domain of MtrE. The electron density (colored white) is contoured at the 1.2 σ level and superimposed with the final refined model (green, carbon; red, oxygen; blue, nitrogen).

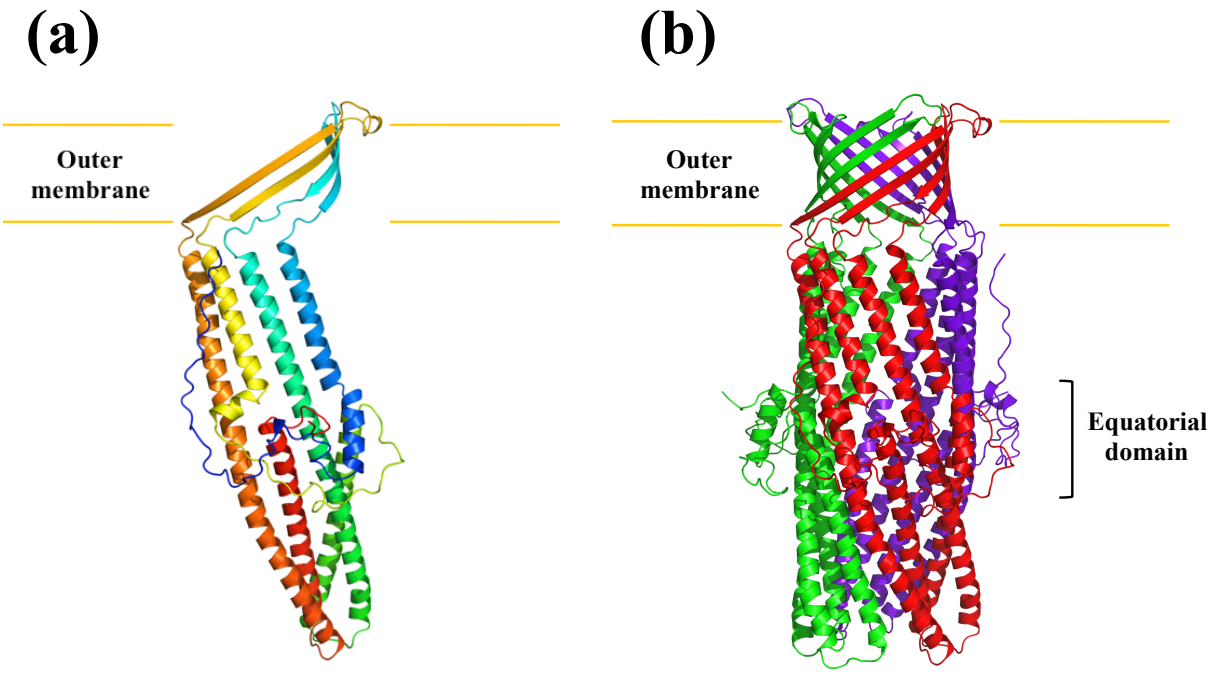

Fig. 2. Structure of the *N. gonorrhoeae* MtrE channel protein. (a) Ribbon diagram of a protomer of MtrE viewed in the membrane plane. The molecule is colored using a rainbow gradient from the N-terminus (blue) to the C-terminus (red). (b) Ribbon diagram of the MtrE trimer viewed in the membrane plane. Each subunit of MtrE is labeled with a different color.

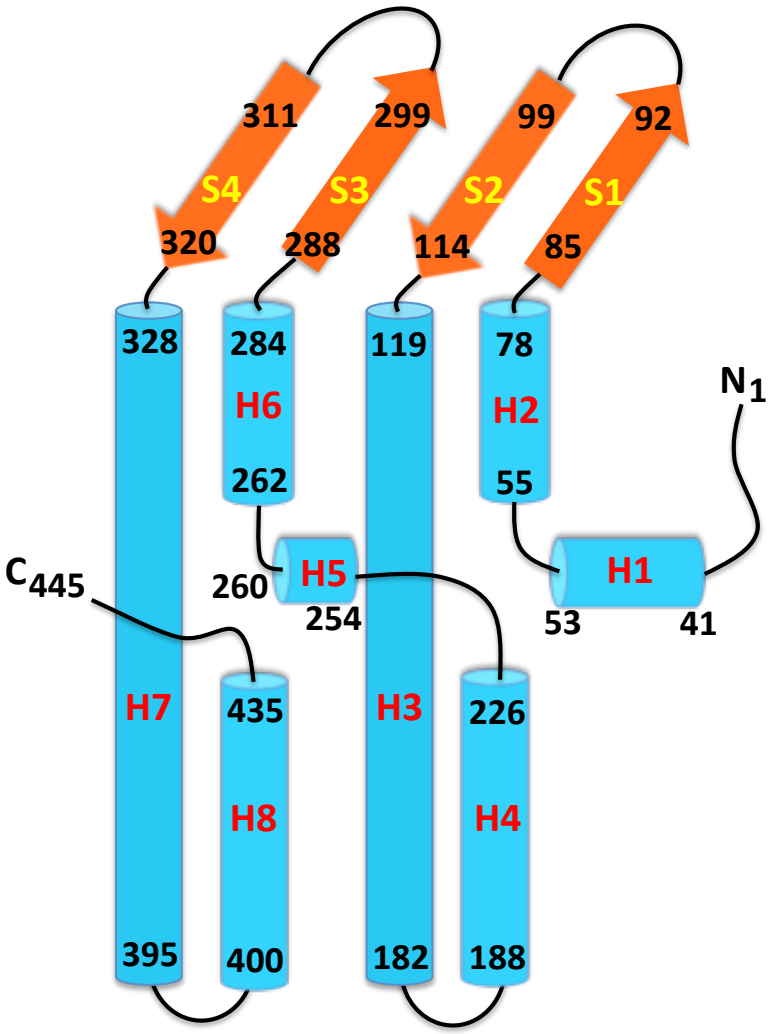

Fig. 3. Secondary structural topology of the MtrE monomer. The topology was constructed based on the crystal structure of MtrE. The α-helices and β-strands are colored cyan and orange, respectively.

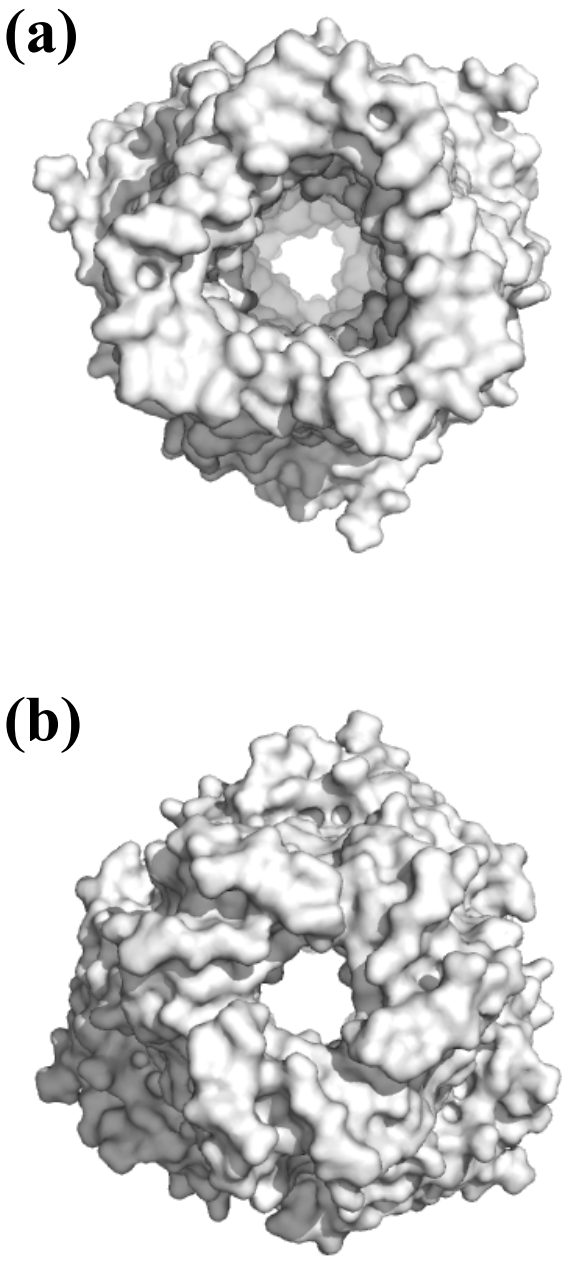

Fig. 4. Surface representations of the trimeric MtrE channel. The views from both the (a) extracellular and (b) periplasmic sides suggest that the MtrE channel is in its open form.

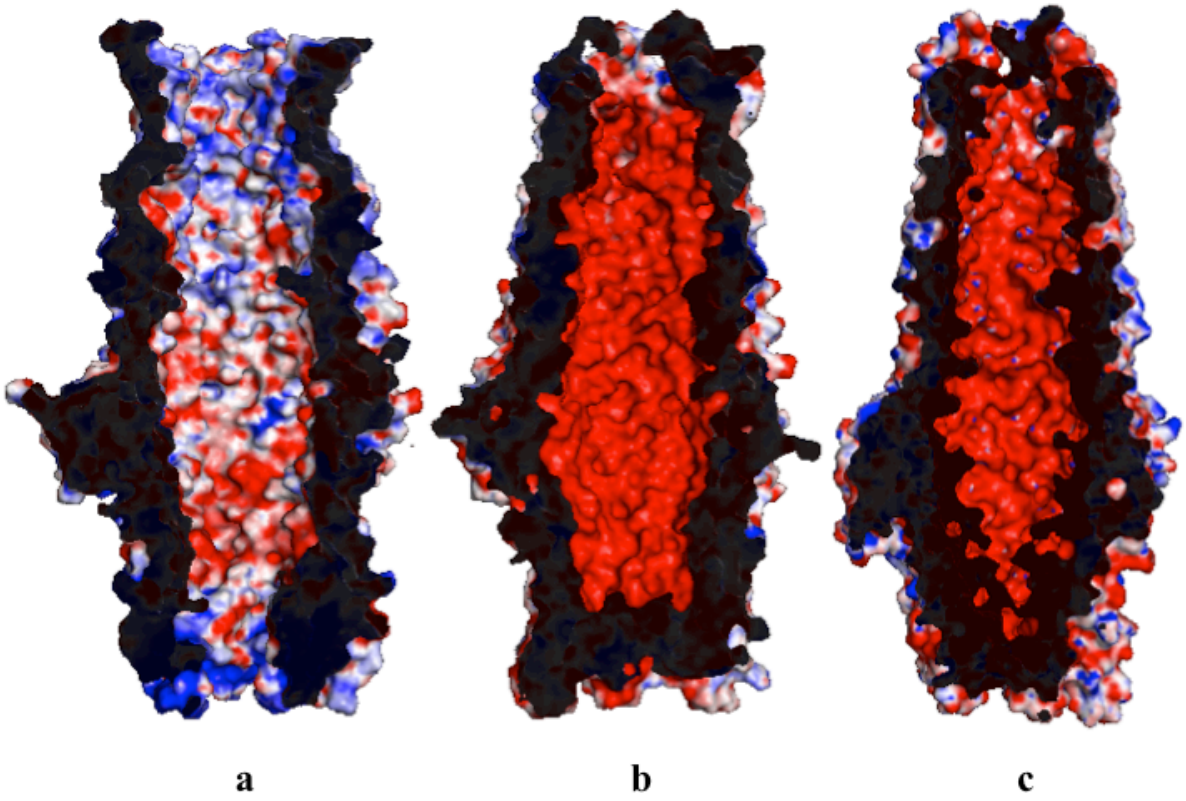

Fig. 5. Electrostatic surface potentials of MtrE, TolC and OprM. Surface representations of the inside of the (a) MtrE, (b) TolC (pdb id: 1EK9) [21] and (c) OprM (pdb id: 1WP1) [22] channels colored by charge (red; negative -15 kT/e, blue; positive +15 kT/e).

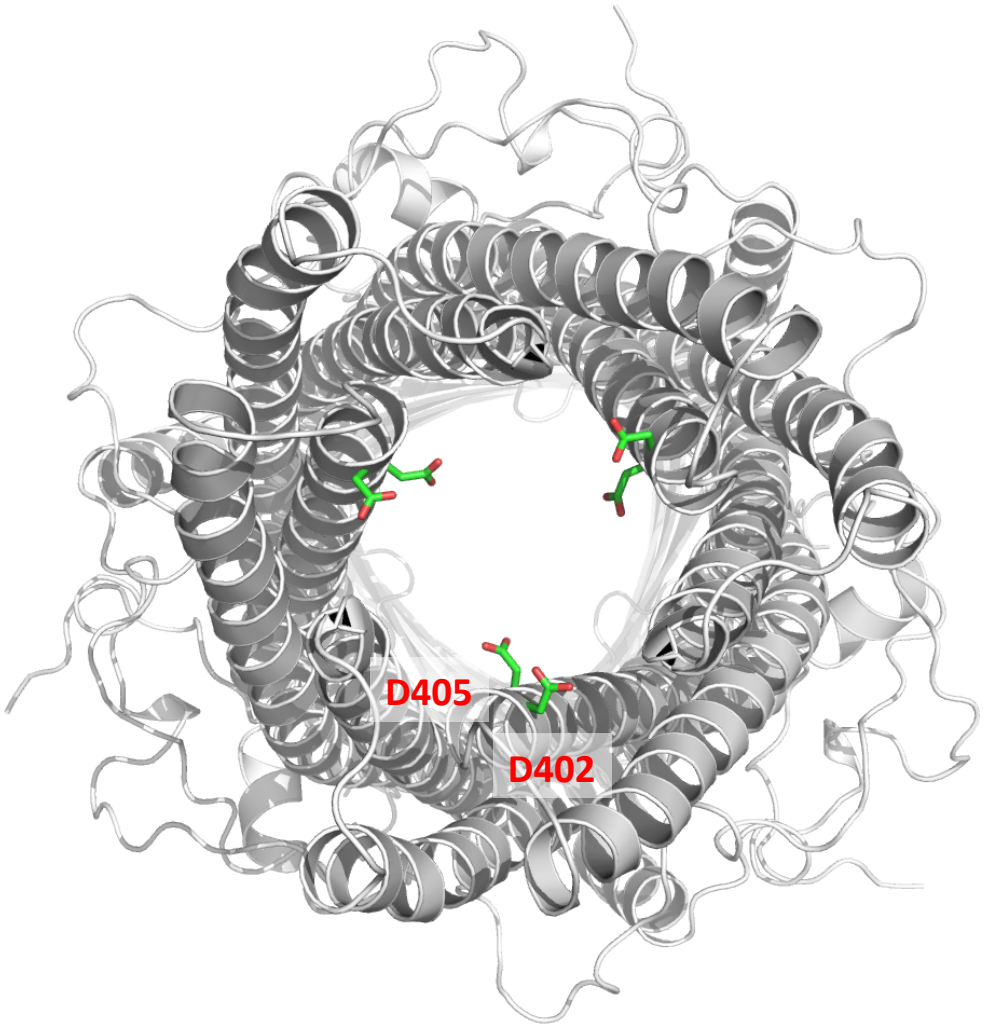

Fig. 6. The periplasmic aspartate ring. Viewed from the periplasmic side, this aspartate ring (formed by D402 and D405 of each protomer) is found at the periplasmic entrance of the interior of the MtrE channel. It is likely that this ring is responsible for the selectivity of channel.

Fig. S1. Comparison of the structures of the MtrE and OprM channels. This is a superimposition of a subunit of MtrE (red) onto that of OprM (blue), indicating that the structures of these two efflux pumps are quite distinct.

```
MtrE      1 CTMIPQYEQPKVEVAETFQNDTSVSSIRAVDLGWHDYFADPRLQKLIDIALERNTSLRTA 60
TolC      1 ENLMQVYQQARLSNPE--LRKSAADR----------------------DAAFEKINEARSP 37
             .::  *:*.::. .*   ..::..                        * *:*: .. *:.

MtrE     61 VLNSEIYRKQYMIERNNLLPTLAANANGSRQGSLSGGNVSSSYNVGLGAASYELDLFGRV 120
TolC     38 LLPQLGLGADYTYS----------NGYRDANGINSNATSAS-LQLTQSIFDMSKWRAL 84
            :* .     :*  .           ** *:..  ..*.:*:  : *  : :::. :  :

MtrE    121 RSSSEAALQGYFASVANRDAAHLSLIATVAKAYFNERYAEEAMSLAQR----VLKTREET 176
TolC     85 TLQEKAAG----IQDVTYQTDQQTLILNTATAYFNVLNAIDVLSYTQAQKEAIYRQLDQT 140
             ..:**      . .. :: : :** ..*.****   * :.:* :*     : :  ::*

MtrE    177 YNAVRIAVQGRRDFRRRPAPAEALIESAKADYAHAARSREQARNALATLINRPIPEDLPA 236
TolC    141 TQRFNVGLVAITDVQNARAQYDTVLANELTARNNLDNAVEQLRQITGNYYPELAALNVEN 200
             : ..:.: .  *.:.  *  :::: .  :   :  .: ** *:  ..   .  . ::

MtrE    237 GLPLDKQFFVEKLPAGLSSEVLLDRPDIRAAEHALKQANANIGAARAAFFPSIRLTGSVG 296
TolC    201 -FKTDKPQPVNALLKEAEKRNLS----LLQARLSQDLAREQIRQAQDGHLPTLDLTASTG 255
             :  **   *: *    ... *     :  *. : . *. :*  *: ..:*:: **.*.*

MtrE    297 TGSVELGG----------LFKSGTGVWAFAPSITLPIFTWGTNKANLDVAKLRQQAQIVA 346
TolC    256 ISDTSYSGSKTRGAAGTQYDDSNMGQNKVGLSFSLPIYQGGMVNSQVKQAQYNFVGASEQ 315
             .... .*           .*. *   .. *::***:  *  ::::. *: .  .

MtrE    347 YESAVQSAFQDVANALAAREQLDKAYDALSKQSRASKEALRLVGLRYKHGVSGALDLLDA 406
TolC    316 LESAHRSVVQTVRSSFNNINASISSINAYKQAVVSAQSSLDAMEAGYSVGTRTIVDVLDA 375
             *** :*..* * .::   :   .: :* .:   :::.:*  :   *. *.   :*:***

MtrE    407 ERSSYSAEGAALSAQLTRAENLADLYKALG----------GGLKRDTQTGK- 447
TolC    376 TTTLYNAKQELANARYNYLINQLNIKSALGTLNEQDLLALNNALSKPVSTNPE 428
             : *.*:    .*: .   *  :: .***           ..*.: ..*.
```

Fig. S2. Alignment of the amino acid sequences of the MtrE and TolC channels. The alignment was done using CLUSTAL W. *, identical residues; :, >60% homologous residues. Sequence alignment indicates that these two outer membrane channels share 16.7% identity.

CHAPTER 5. GENERAL CONCLUSIONS AND FUTURE DIRECTIONS

The development of new classes of antibiotics seems halted since 1970 [1]. In response to the need for addressing the problem of drug resistant Gram-negative bacterial pathogens, the "10 x'20 Initiative" was launched in 2010. Much effort was put on the inactivation of β-lactamases, protein synthesis inhibition and peptide mimetics [2]. In recent years, the multidrug efflux pumps have been characterized extensively, and could become an ideal target for broadening the antibacterial activity of the common β-lactam-based antibiotics.

Among the efflux pumps, RND-type transporters such as CmeABC and MtrCDE are particularly involved in the drug-resistance of infectious pathogens [3][4]. The transcriptional regulator CmeR has been identified as the local repressor which has the ability to bind the promoter region of the *cmeABC* operon [5]. The crystal structure of CmeR allows us to see the large ligand-binding pocket and the two-helices DNA binding domain as the distinguishable aspects from other TetR-type transcriptional regulators [6][7].

In Chapter 2, CmeR is separately liganded with two large amphiphilic molecules: taurocholic acid and cholic acid, which are abundant in intestinal tracts of animals. Although the overall structure of the CmeR-bile acid complex is similar to the first discovered glycerol-bound CmeR, the interaction between each bile acid-conjugate and the residues in the binding pocket is interesting. It is worth noting that several polar or charged residues stabilize the four-ring hydrophobic region on the hydroxyl groups of the bile salts, in cooperation with the hydrophobic tunnel. The diverse binding coordination and multiple sub-binding sites, as shown in the binding cavity in the structural analysis of Chapter 2, lead to

the capability of multi-ligand derepression of efflux pump expression indicated by the conformation of the DNA binding motif. The formation of the α3-helix upon binding to DNA is likely to occur. The structure of CmeR-IR complex should give support to the previous studies regarding the DNA-induced α-helical formation [8].

In Chapter 3, the outer membrane channel CusC from CusCBA, the only HME-RND transporter in *E. coli,* is discussed. The wild-type and mutated CusC have been cloned, expressed and crystallized. The Cys1 residue at the N-termini is evidently important in the presented structures of the Cys1 mutants of CusC. It is surprising to see the partially formed α-helices as dilated coiled-coils when superimposed to the trimeric CusC channel in contrast to the completely unstructured β-strands due to the single amino acid mutation at the Cys1 residue. Comparison of the wild type and the mutant three-fold oligomers directs the proposed mechanism of the folding sequence of the outer membrane channel. Although the structure of unfolded β-barrel has been found, more evidence is needed to establish the subsequent steps in the folding process, such as the structure of intermediate state as a trimeric bundle without the transmembrane β-barrel domain.

In Chapter 4, the wild-type MtrE from MtrCDE efflux system has been cloned, expressed and crystallized. The findings of the first native open-state of the outer membrane channel protein from the structure of MtrE highlights the group of charged residues that could possibly control the size of the periplasmic entrance and promote the interaction between different components. The studies based on the efflux system AcrAB-TolC have suggested that the recruitment of the outer membrane channel is transient [9]. Assembled in the periplasm, the outer membrane channel in RND-type efflux systems is likely to cycle through repeated recruitment by the inner membrane transporter [9]. As a hollow tube, MtrE

should rely on the guidance from the membrane fusion protein MtrC to accept substrates from the pump MtrD [10]. The enhanced interaction between MtrC and MtrE should allow us to obtain a co-crystal of the MFP-OMP complex for further structural analysis.

In this dissertation, the proteins that confer drug resistance to Gram-negative bacteria and the regulation of their expression have been studied. In addition to the transcriptional regulator-bile salt complex of CmeR, the outer membrane proteins CusC and MtrE have been purified and crystallized for the purpose of obtaining crystal structures using X-ray crystallography. The depicted structures of CmeR-bile salt explain the ligand recognition that is commonly used by the TetR protein family of repressors [7]. The disclosure of the structures of CusC mutants stresses the importance of the Cys1 residue and leads to the proposed folding sequence that the outer membrane protein associates with the membrane to become multiple intermediates and create a passage for substrates of the RND efflux pump through the outer membrane. After the discussion of outer membrane channel formation, the topic is shifted to the conformational state of the outer membrane channel MtrE. As indicated by the crystal structure of MtrE and other studies of its interactions with the membrane fusion protein MtrC [10], the change of states of OMPs could be inducible by the presence of a working partner or a change in pH. The change of states of OMPs could be further studied using single channel conductance. In particular, results should show the increased conductance of MtrE in the open state compared with the closed state. The transition of the states could be investigated with different experimental conditions such as a pH gradient and the presence of other components in the MtrCDE efflux system.

The characterization of fully assembled RND efflux systems is sill largely incomplete. Although inhibitors could be rationally designed from structures of individual

components, side effects may include the unwanted inhibition of human proteins transporting essential nutrients. Instead of targeting the components separately, breaking down the assembly to disable the pump is another method. The efficiency of RND transporters is due to the close collaboration between each part. Therefore, one can possibly produce drugs that attack the state of cooperation. Knowledge of the exact interactions between these antimicrobial pumps and methods to disrupt them must await elucidation of the structures of the fully assembled efflux complexes.

Reference

[1] Powers, J. H. Antimicrobial drug development-the past, the present, and the future. *Clin. Microbiol. Infect.* **10**, 23–31 (2004).

[2] Boucher, H. W., Talbot, G. H., Benjamin, D. K., Bradley, J., Guidos, R. J., Jones, R. N., Murray, B. E., Bonomo, R. A. & Gilbert, D. 10 x '20 Progress--development of new drugs active against gram-negative bacilli: an update from the Infectious Diseases Society of America. *Clin. Infect. Dis.* **56**, 1685–1694 (2013).

[3] Lin, J., Michel, L. O. & Zhang, Q. CmeABC Functions as a Multidrug Efflux System in *Campylobacter jejuni*. *Antimicrob. Agents Chemother.* **46**, 2124–2131 (2002).

[4] Jerse, A. E., Sharma, N. D., Simms, A. N., Emily, T., Snyder, L. A., Shafer, W. M. & Crow, E. T. A Gonococcal Efflux Pump System Enhances Bacterial Survival in a Female Mouse Model of Genital Tract Infection. *Infect. Immun.* **71,** 5576–5582 (2003).

[5] Lin, J., Akiba, M., Sahin, O. & Zhang, Q. CmeR Functions as a Transcriptional Repressor for the Multidrug Efflux Pump CmeABC in *Campylobacter jejuni*. *Antimicrob. Agents Chemother.* **49**, 1067–1075 (2005).

[6] Gu, R., Su, C.-C., Shi, F., Li, M., Mcdermott, G. & Zhang, Q. Crystal Structure of the Transcriptional Regulator CmeR from *Campylobacter jejuni*. *J Mol Biol*. **372**, 583–593 (2008).

[7] Ramos, J. L., Martı, M., Molina-henares, A. J., Tera, W., Brennan, R. & Tobes, R. The TetR Family of Transcriptional Repressors. *Microbiol. Mol. Biol. Rev*. **69**, 326–356 (2005).

[8] Percipalle, P., Simoncsits, A., Zakhariev, S., Guarnaccia, C., Sánchez, R. & Pongor, S. Rationally designed helix-turn-helix proteins and their conformational changes upon DNA binding. *EMBO J*. **14**, 3200–3205 (1995).

[9] Tikhonova, E. B., Yamada, Y. & Zgurskaya, H. I. Sequential mechanism of assembly of multidrug efflux pump AcrAB-TolC. *Chem. Biol*. **18**, 454–463 (2011).

[10] Janganan, T. K., Zhang, L., Bavro, V. N., Matak-Vinkovic, D., Barrera, N. P., Burton, M. F., Steel, P. G., V Robinson, C., Borges-Walmsley, M. I. & Walmsley, A. R. Opening of the outer membrane protein channel in tripartite efflux pumps is induced by interaction with the membrane fusion partner. *J. Biol. Chem*. **286**, 5484-5493 (2011).

ACKNOWLEDGMENTS

In here I would like to express the most sincere thanks to my advisor, Dr. Edward Yu, for his guidance in the scientific research. He led me through challenges and difficulties in my PhD study. Without his supervision and high-standard expectation, the time over these years couldn't have been meaningful. He has given me the attitude of courage and persistence. His care is always around as a mentor and a friend. I would also like to specially thank him for giving me the chance to begin my research in his lab when I lost my previous advisor Dr. Victor Shang-Yi Lin. He has lightened the road for me to overcome the dark days and cultivate my interest toward chemical and biological sciences.

I am very thankful for having my study committee members: Dr. Drena Dobbs, Dr. Emily Smith, Dr. Ning Fang and Dr. Arthur Winter. Their advice and support have directed me to my best self. I appreciate their time spent with me when I had questions, and their attention for my progress.

I am very fortunate to work with many people who have given me priceless supports and encouragements in these years. I want to give many thanks to Dr. Chih-Chia Su and Dr. Feng Long. I appreciate their opinions and discussions to solve the problems during the experiments. I really enjoyed working with my lab mates, Jani Reddy Bolla, Sylvia Do, Abhijith Radhakrishnan, Nitin Kumar, Tsung-Han (Eric) Chou and Jared Delmar. Without these people, the research life would have been plain. Those many lunches we had together also brought me unforgettable memories.

I would like to thank Dr. Kanagalaghatta R. Rajashankar and all the staff members of NECAT in Advanced Photon Source for their help and assistance during the course of collecting data and data processing.

The collaborative experience with Dr. Qijing Zhang and his lab was remarkable. I would like to give thanks to Dr. Zhang and his group for the work involving the Cme efflux systems and transcriptional regulators. Also, I want to give a lot of thanks to Dr. William Shafer for the work related to the Mtr efflux system.

Last but not least, I would like to give the credits and the best thank you to my family and my friends. As always, they are by my side at all times. My thanks go to especially my mother Su-Tan Chang for her dedication to my brother and me. I would like to thank my father for his support, and my brother for arranging for mother's day during these years when I was away from home. No matter where, I am really blessed to have friends to encourage me through my study. Thank you my fellow classmates Li-Chen Lee, Yijun Guo, Rui Han and Chia-Yu Shen for supporting time and time again during these years.